8-2018

Dead wood and decomposition in a tropical forest : vertical patterns, long-term processes, and the role of lightning.

Evan Matthew Gora
University of Louisville

DEAD WOOD AND DECOMPOSITION IN A TROPICAL FOREST:

VERTICAL PATTERNS, LONG-TERM PROCESSES, AND THE ROLE OF LIGHTNING

By

Evan Matthew Gora
B.S., University of Pittsburgh 2013

A Dissertation
Submitted to the Faculty of the
College of Arts and Sciences of the University of Louisville
in Partial Fulfillment of the Requirements
for the Degree of

Doctor of Philosophy
in Biology

Department of Biology
University of Louisville
Louisville, Kentucky

August 2018

DEAD WOOD AND DECOMPOSITION IN A TROPICAL FOREST:

VERTICAL PATTERNS, LONG-TERM PROCESSES, AND THE ROLE OF LIGHTNING

By

Evan Matthew Gora
B.S., University of Pittsburgh 2013

A Dissertation Approved on

April 26, 2018

By the following Dissertation Committee:

_____
Dissertation Director
Dr. Stephen P. Yanoviak

_____
Dr. Margaret M. Carreiro

_____
Dr. Sarah M. Emery

_____
Dr. Susanna K. Remold

_____
Dr. Phillip M. Bitzer

DEDICATION

This dissertation is dedicated to my parents, Richard Gora and Dr. Alice Gora, who inspired me with their amazing work ethic and their curiosity for the wonder of the natural world. This dissertation also is dedicated to Walter Carson who imparted his passion for ecology and informed me that I could make a career out of it.

ACKNOWLEDGEMENTS

I would first like to thank my major advisor, Steve Yanoviak, for his thoughtful guidance. Any achievements I have made directly reflect his ability and willingness to pass on a great depth of knowledge and wisdom. A special thank you to Jane Lucas for her infinite patience and encouragement, and for her support throughout every aspect of this long process. I thank Oris Acevedo, Melissa Cano, and the rest of the staff at the Smithsonian Tropical Research Institute for logistical support and for making Barro Colorado Island a second home. I would like to thank Paul DeMarco, Terri Norris, and Doris Meadows for their patience in helping me manage my funds and navigate any problems I encountered throughout the degree process. For their comments and stimulating discussions, I thank Egbert Leigh Jr., Joe Wright, Helene Muller-Landau, Allen Herre, Mike Kaspari, Matteo Detto, and Edmund Tanner. I also thank my advisory committee, Margaret Carreiro, Sarah Emery, Susanna Remold, and Phillip Bitzer, for their support, technical knowledge, and comments that were crucial to this dissertation and my approach to science. Thank you Susanna Remold and Jeff Bara for welcoming me into your discussions of evolution and generously providing laboratory support. For field assistance, I thank Max Adams, Jane Lucas, Amanda Winters, Rogelio Luque, Oldemar Valdez, Cesar Guitierrez, Francisco Valdez, Noah Gripshover, and DaniRae Block. In particular, I thank Riley Kneale for going above and beyond during two field seasons in Panama. Comments from Max Adams, Jane Lucas, Alyssa Stark, Jelena Bujan, and Riley Kneale improved this dissertation substantially. Finally, for the funding that made all of this work possible, I thank the Smithsonian Tropical Research Institute, the National Science Foundation, and the National Geographic Society.

ABSTRACT

DEAD WOOD AND DECOMPOSITION IN A TROPICAL FOREST:

VERTICAL PATTERNS, LONG-TERM PROCESSES, AND THE ROLE OF LIGHTNING

Evan M. Gora

April 26, 2018

This dissertation investigates the distribution, production, and decomposition of dead wood (or woody debris) in a lowland tropical forest within the Barro Colorado Nature Monument in Panama. Although the importance of woody debris is widely accepted, information describing components of WD pools and fluxes is generally separated in both time and space, particularly in understudied tropical forests. Here I provide a comprehensive inventory of woody debris in a lowland tropical forest (Chapter 1). Woody debris is highly aggregated and difficult to quantify, and this study demonstrates that historic estimates of woody debris pools and fluxes underestimate their uncertainty. In a separate collaboration, I quantified how soil nutrient availability regulates wood decomposition using a 15-year litter manipulation experiment (Chapter 2). Wood decomposition rates decreased with reduced nutrient availability in the litter removal treatments, but did not change relative to controls in the litter addition

treatments. The first chapter also showed that ca. 50% of woody debris stocks were not in contact with the ground; however, information regarding the factors that regulate wood decomposition comes exclusively from the forest floor. Consequently, I quantified differences in decomposition rates, microclimate, and microbial community structure (prokaryotes and fungi) along a vertical gradient from the ground and the canopy of this tropical forest (Chapter 3). Decomposition rates varied predictably based on microclimate conditions and fungal composition along this vertical gradient. Decomposition rates also vary substantially with species-specific wood traits, and thus the relative contributions of each tree species to woody debris inputs is important to carbon cycling. Large trees contribute disproportionately to dead wood pools and lightning is one of the primary agents of large tree mortality in tropical forests. I used empirical measurements of tree electrical properties and lightning characteristics to model lightning damage parameters (heating and power) for trees of different species and size classes (Chapter 4). These damage parameters differ substantially among species, suggesting that increased lightning frequency will change inputs of woody debris. These studies improve our understanding of woody debris dynamics and tropical forest carbon cycling so that we can better predict future patterns in a changing world.

TABLE OF CONTENTS

Page

LIST OF TABLES

TABLE PAGE

LIST OF FIGURES

FIGURES PAGE

CHAPTER I

INTRODUCTION

Tropical forests influence global carbon dynamics more than any other terrestrial biome. These forests contain 25% of terrestrial biomass and account for c. 40% of the terrestrial carbon sink (Feldpausch et al., 2012; Pan et al., 2011). Wood is particularly important to the role these forests play in carbon cycling as the majority of aboveground carbon in tropical forests is sequestered in wood (Rice et al., 2004) and this carbon is released via the decomposition of woody debris. Indeed, actively decomposing woody debris accounts for as much as 20% of above-ground carbon and 15% of CO2 emissions in tropical forests (Chambers et al., 2004; Palace, Keller, and Silva, 2008; Rice et al., 2004).

Dead wood also is crucial as a habitat and food resource for a variety of forest taxa (reviewed by Harmon et al. 1986). Detritivores, such as fungi and invertebrates, rely on woody debris as a source of nutrition. These decomposers serve as prey items for many primary consumers, some of which inhabit woody debris alongside their prey. Apart from organisms that directly and indirectly rely on woody debris for food, a number of other animals (e.g., birds and mammals) nest within woody debris as a key part of their life history. Ultimately, a tremendous diversity of organisms use dead wood during the lifespan and thus the amount and distribution of woody debris is important to their ecology.

Although many aspects of woody debris have been quantified (reviewed by Palace et al. 2012), relevant information is recorded at coarse scales and is generally separated in both time and space. Woody debris is typically recorded in two size classes

(coarse or fine) and three methodologically-derived groupings called "pools:" 1) downed woody debris, 2) standing woody debris (i.e., standing dead trees), and 3) suspended woody debris (Swift et al. 1976, Harmon and Sexton 1996). The relevance of these pools to the function of woody debris (e.g., decomposition rate or habitat characteristics) remains unclear. Wood traits also are important to decomposition rates (Cornwell et al. 2009, Zanne et al. 2015), yet factors related to these traits, such as tree species and wood types (e.g., liana wood or tree trunk wood), are rarely recorded. To understand woody debris dynamics and develop proper sampling procedures, it also is necessary to quantify patterns of aggregation and variation for all types of woody debris stocks and fluxes (Kral et al. 2014).

The distribution of dead wood is also important to our understanding of decomposition and carbon cycling. Models of global carbon cycling rely on the contemporary understanding of wood decomposition across multiple spatial scales (Adair et al. 2008, Bradford et al. 2014). It is widely accepted that abiotic factors control decomposition at continental scales, whereas biotic factors (wood traits and decomposer organisms) regulate decomposition at smaller spatial scales (Parton et al. 2007, Adair et al. 2008, Cornwell et al. 2009, Bradford et al. 2014, Zanne et al. 2015). However, evidence for these patterns comes almost entirely from measurements of ground-level decomposition whereas, at any given time, approximately half of all dead wood is decomposing above the forest floor (Ovington and Madgwick 1959, Christensen 1977, see Chapter 1). Consequently, our understanding of the factors that regulate wood decomposition locally is incomplete.

Patterns of woody debris inputs (i.e., tree and branch death) ultimately determine the ecosystem-wide distribution of wood traits that regulate rates of decomposition (Cornwell et al. 2009, Cornelissen et al. 2012). Large trees are disproportionately important to carbon cycling (Carlson et al. 2017) and lightning is one

of the primary agents of large tree mortality in tropical forests (Yanoviak and Gora, unpublished data). Consequently, tree species that are more frequently killed by lightning likely contribute greater amounts of necromass to woody debris pools and fluxes. If lightning frequency increases as projected (Williams 2005, Romps et al. 2014), then the canopy trees that are particularly susceptible to lightning, such as those with high electrical resistivity (Gora and Yanoviak 2015), will become disproportionately represented in pools of woody debris. It is important to quantify these patterns now so that it is possible to project future patterns of tree mortality and carbon sequestration.

ORGANIZATION OF THE DISSERTATION

This dissertation explores the spatiotemporal distribution of woody debris and quantifies factors that regulate the production and decomposition of dead wood. The second chapter includes the most comprehensive inventory of woody debris in tropical forests to date. The third chapter quantifies the role of nutrient limitation during long-term wood decomposition (15 years) in a litter manipulation experiment. The fourth chapter investigates the relative importance of microbial community structure and microclimate to wood decomposition along a vertical gradient from the ground to the canopy within a tropical forest. The fifth chapter uses empirically collected electrical data to model the interactions between lightning strikes and trees to shed light on factors related to wood production. Finally, chapter six summarizes the findings from these projects and explores their implications. Collectively, the investigations described in these chapters make major contributions to our understanding of microbial community ecology, carbon cycling, and biogeochemistry in tropical forests.

CHAPTER II

LONG-TERM STOCKS, FLUXES, AND SPATIOTEMPORAL VARIABILITY OF DEAD WOOD IN A TROPICAL FOREST

SUMMARY

Carbon cycling models rely on accurate and precise estimates of dead wood stocks and fluxes, particularly in tropical forests that disproportionately influence carbon cycling. However, information describing tropical woody debris (WD) is limited. Here we conducted the first comprehensive assessment of WD stocks – downed, standing, and suspended WD – and quantify fluxes, input sources, and spatiotemporal variability over eight years in a neotropical forest (Panama). We also quantified key components of carbon cycling models (e.g., branchfall, liana necromass) and the elevated portion of downed WD. Downed WD constituted the majority of total wood stocks, the contributions of suspended WD (1%) and liana wood (2%) were negligible, and branchfall composed only 17% of total downed WD. However, when considering the elevated sections of downed WD, the majority of WD inputs and ca. 50% of WD stocks were above the forest floor. Carbon cycling models and the contemporary understanding of wood decomposition are based exclusively on ground-level decomposition, and thus

overlook this suspended fraction. Using >100 km of transects and >100 ha of plots, we calculated the sampling efforts necessary to precisely estimate WD stocks and fluxes (>130 km for downed CWD and >500ha for standing CWD). Most previous sampling efforts are far below these thresholds indicating that existing WD estimates are likely inaccurate and their uncertainty is chronically underestimated. This is a major problem because these estimates are important parameters of global carbon inventories and carbon cycling models. Consequently, large-scale forest inventories and investigations into the processes that regulate decomposition above the forest floor are necessary to improve our understanding of carbon cycling.

INTRODUCTION

Tropical forests are currently the largest terrestrial carbon sink (Pan et al. 2011) with most of their aboveground carbon stored in woody tissues. After wood dies, it serves a tremendous variety of ecological roles (reviewed by Harmon et al. 1986) and functions as both a carbon sink (20-40% of aboveground carbon) and source (ca. 15% of total respiration; Harmon and Sexton 1996, Brown 1997, Keller et al. 2004, Palace et al. 2007, Palace et al. 2008). Although many aspects of woody debris (WD) are well described (reviewed by Palace et al. 2012), information describing components of WD pools and fluxes is generally separated in both time and space. Consequently, the spatial and temporal distribution of WD remains poorly understood, particularly in understudied tropical forests (Palace et al. 2012). This is one of the major knowledge gaps impeding global carbon inventories and carbon cycling models (Pan et al. 2011).

Woody debris is categorized by its location (or *pool*) and size (Figure 1). Traditionally, WD is separated into three pools: 1) *downed WD* that is in contact with the ground, 2) *standing WD* composed of standing dead trees (snags), and 3) *suspended WD* that is suspended in or attached to living trees or lianas (Swift et al. 1976, Harmon and

Sexton 1996). The majority of necromass is stored in large pieces of WD (coarse woody debris or CWD) and thus most studies either exclusively monitor CWD or separately record fine woody debris (FWD; Harmon et al. 1986, Palace et al. 2012). Downed WD is typically greater than standing WD in mature forests (Spetich et al. 1999, Sierra et al. 2007), but the total amount of WD and its distribution among pools changes with stand age, forest structure, disturbance regime, and management strategy (Janisch and Harmon 2002, Keller et al. 2004, Sierra et al. 2007, Palace et al. 2012, Gora et al. 2014, Carlson et al. 2017). The few studies of suspended woody debris – all conducted in temperate forests – suggest that this pool may be comparable to or even greater than downed and standing WD pools (Ovington and Madgwick 1959, Christensen 1977, however see (Swift et al. 1976). However, to our knowledge, suspended WD has never been quantified in tropical forests.

The categorization of WD into these three pools is based on methodological rather than functional differences. Although downed WD decomposes more rapidly than standing and suspended WD (Fasth et al. 2011, Song et al. 2017), it is likely that standing and suspended WD decompose similarly (Swift et al. 1976). Even among pieces of downed WD, boles that are partially elevated decompose ca. 40% slower than those with more soil contact (Přívětivý et al. 2016). The elevated sections of downed WD (hereafter *elevated WD*), and even upper sections of partially buried wood, experience different microclimate conditions, available nutrients, and propagule pressures than sections of the same piece that contact the ground (Boddy et al. 2009, Oberle et al. 2017). The associated differences in abiotic conditions and decomposer community composition (Boddy 2001) presumably alters decomposition rates (Boddy et al. 1989, van der Wal et al. 2015). Consequently, a more functionally relevant categorization is if, and how much, WD directly contacts the forest floor.

Apart from the distribution of WD stocks, the relative contributions of different WD inputs reflect important aspects of forest carbon cycling. Each piece of downed WD is either input from treefalls, branchfalls, or lianas. Estimates of branchfall inputs are rare (Chave et al. 2003, Palace et al. 2008, Gurdak et al. 2014, Marvin and Asner 2016), even though the proportion of woody biomass lost to branchfall is – or at least should be -- an important parameter in carbon cycle models of forest vegetation (Clark et al. 2001, Malhi et al. 2011, Cleveland et al. 2015, Doughty et al. 2015, Marvin and Asner 2016). Branchfall is commonly omitted from tree mortality-based estimates of WD inputs (Chambers et al. 2000, Meakem et al. 2017) that inherently underestimate necromass production (Palace et al. 2008). Lianas compose a small fraction of standing biomass (van der Heijden et al. 2013), but their contributions to necromass pools and fluxes remain unknown. Most lianas lack recalcitrant structural components and thus liana wood generally should decompose more rapidly than branch and trunk wood. If liana abundance is increasing (Schnitzer and Bongers 2011), then the reduced size and persistence of liana WD relative to tree WD will magnify the negative effects of lianas on forest carbon sequestration (van der Heijden et al. 2015).

To understand WD dynamics and develop proper sampling procedures, it also is necessary to quantify patterns of WD aggregation and variation. In general, WD inputs and stocks are spatially aggregated at small scales (<50m, Woldendorp et al. 2004) and highly variable in space and time, reflecting the stochasticity (and size) of tree mortality and large branch mortality events that contribute the vast majority of WD. At the continental scale, forests with the same general disturbance history and ecosystem classifications (e.g., moist tropical forest) contain CWD stocks and inputs that differ by up to 2 orders of magnitude (Palace et al. 2012). Even within a single European forest, CWD volume differed by 400% (49 to 402 m^3 ha^{-1}) between nearby 1 ha plots (Král et al. 2010). Accordingly, accurate estimates of necromass require spatially and temporally

intense sampling to characterize the range of possible inputs and stocks, as well as their relative frequencies.

Here we provide a comprehensive inventory of wood necromass in a lowland tropical forest, with a focus on poorly quantified aspects of woody debris stocks and fluxes. This is the first study to quantify the relative contributions of all three woody debris pools - downed, standing, and suspended woody debris - in a tropical forest. Within the downed WD pool, we also estimate the proportion of elevated WD and how this proportion changes during decomposition. We compare sources of downed WD (branchfall, treefall, or liana inputs) along with the relative contributions of branch, trunk, and liana wood. Using a large-scale and long-term (2009-2016) dataset, we evaluate spatial and temporal patterns of CWD variation and aggregation. Finally, we estimate the residence time of downed and standing CWD using both individualized and stand-scale approaches.

METHODS

Study site

Field work was conducted in a 50 ha forest dynamics plot on Barro Colorado Island (BCI) in central Panama (9.152°N, 79.847°W). The forest structure and tree species composition at this site is typical of mature moist lowland tropical forest (Hubbell and Foster 1983). The forest has an average annual temperature of 27°C, mean annual rainfall of 2600mm, and a 4-month dry season (January-April, <100mm monthly rainfall). More detailed descriptions of this forest are available elsewhere (e.g., Leigh 1999).

Plot and transect design

We estimated woody debris (WD) stocks, fluxes, and variability using a combination of line-intercept and area-based approaches (Table 1). The majority of our measurements were performed in 100 40x40m plots (hereafter *dynamics plots*) within a

larger 50 ha forest dynamics plot on BCI (Appendix I: Figure S1). Standing WD was censused in the entire area of each plot (16 ha total), and downed WD along four 40m transects that crossed parallel to and 10m away from each plot edge (16 km total; Appendix I: Figure S1). To investigate patterns of spatial variation and aggregation, these plots were divided into 16 equal-sized areas (10x10m) and transect sections (10m). In 50 of these plots, we also established 10x10m subplots in the four corners to measure WD suspended and attached above the forest floor (hereafter collectively referred to as *suspended woody debris*, Appendix I: Figure S1). In addition to the dynamics plots, we quantified downed WD along long transects within the larger 50 ha plot during 2010, 2014, and 2017 (Appendix I: Figure S2), and along short transects haphazardly distributed across BCI during 2015. Coarse and fine WD (i.e., WD with diameters >20cm or <20cm, respectively) were recorded separately in all cases; the minimum diameter recorded for suspended WD was 5cm whereas the minimum diameter for downed and standing WD was 2cm.

Photogrammetry of suspended and attached woody debris

We estimated the volume of suspended woody debris using methods typical of downed woody debris studies. In addition to fully suspended WD, a minority of this pool exhibits minor contact with the forest floor, but is not typically included in surveys of downed WD. Specifically, this WD was classified as suspended rather than downed if it did not contact the ground with at least three branches or a section of its main stem. We used Newton's formula to estimate the volume of suspended wood:

[1] $$V = l * \frac{(A_{e1} + 4 * A_m + A_{e2})}{6}$$

where V is volume (m^3), A is area (m^2) at each end ($_{e1}$, $_{e2}$) and at the midpoint ($_m$) of the woody debris, and l is the length of the woody debris (m, Harmon and Sexton 1996). Using this formula, we measured suspended WD greater than 5 cm in its maximum diameter in the crown or in resident lianas of any tree with more than half of its basal

area inside the 10x10m subplot. To improve accuracy for irregular branches, we separately measured the diameters and length of each approximately linear subsection. For small terminal branches, we measured their basal diameter and estimated their volume as cones.

In the small minority of cases in which the suspended woody debris was within reach of the ground, we took measurements by hand; in other cases, we estimated dimensions using a combination of photographs and laser-based distance measurements (i.e., photogrammetry). We first took photographs of each branch such that the axis of each diameter measurement was parallel to the x or y axis of the photograph (Powershot ELPH 130IS, Canon, USA). We then used a commercially available laser rangefinder (Disto D5, Leica Geosystems, Austria) to measure distance between the camera and the midpoint of the diameter measurement. Using ImageJ software and known camera characteristics, we then calculated a first estimate of branch diameter, D (in m), as

[2] $$D = \frac{z * l_S}{l_F} * \frac{P_b}{P_a}$$

where z is the distance (m) between the camera and the branch, l_S is the length of the image sensor (mm), l_F is the focal length when taking the photo (mm), P_b is the width of the branch (in pixels), and P_a is the width of the image along the same axis as the branch diameter measurement (in pixels). We confirmed the accuracy and precision of this approach in comparisons with direct measurements by hand (Appendix I: Supplementary Methods).

We estimated branch length using angle and distance measurements. Using the same laser, we measured distance to both ends of the branch or branch subsection, and estimated the angle between the two measurements using a protractor and plumb line. We then calculated branch length using the Law of Cosines (Appendix I: Supplementary Methods).

Downed woody debris

We used line-intercept sampling along long transects to quantify different components of downed woody debris (Table 1, Appendix I: Figure S2). To estimate total stocks, we measured FWD and CWD pieces that intersected long transects (500m) running North to South in the 50ha dynamics plot during 2010 and 2014, and both North to South (500m transects) and East to West (1km transects) during 2017. These transects were divided into 20m transect subsections for resampling and FWD was only recorded in the first 1m of each transect subsection. For each piece of woody debris encountered, we recorded its diameter orthogonally to its longitudinal axis and centered around the intersection with the transect. During 2010 and 2014 (but not 2017), we estimated density in the field using a dynamic penetrometer (Larjavaara and Muller-Landau 2010). In 2017, we categorized downed CWD as (1) elevated or in direct contact with soil, (2) branchfall or treefall, and (3) trunk wood, branch wood, or liana wood.

We also quantified the proportion of downed WD (>10cm DBH) elevated above the forest floor (hereafter *elevated WD*) using 33 short transects in 2015 (100m; Table 1). These transects began every 200m along the trail system on BCI and ran orthogonally to the trails themselves, covering a variety of topographical features. We focused our short transect sampling on this diverse topography because the 50ha forest dynamics plot on BCI is located in large part on a plateau and the proportion of elevated WD is affected by local topography (Přívětivý et al. 2016). Each piece of WD was classified into 1 of 5 decomposition classes (Keller et al. 2004). We measured the average cross-sectional area (i.e., volume over length) and the proportion of elevated WD across the entirety of each piece of WD encountered (N = 177). Volume of each subsection was measured using *equation 2*. We then took a weighted average of the elevated proportion of WD over pieces, weighting by average cross-sectional area, to estimate total elevated proportion of WD at the forest-scale. When possible, we performed paired penetrometer

measurements of adjacent WD subsections that were elevated or in direct contact with the forest floor (N = 78).

To quantify inputs, outputs, and spatiotemporal variability of CWD, we performed line-intercept sampling along the four transects within each dynamics plot. These transects were surveyed from 2009 to 2016 (excluding 2011) and each piece of woody debris encountered was uniquely tagged and assigned a transect subsection (10m) identification number. Diameter and penetrometer-estimated density were recorded yearly for all pieces of CWD with diameters >20cm. During 2015 and 2016, we recorded whether new pieces of CWD were input via branchfall or treefall and whether the treefall inputs were composed of branch wood or trunk wood.

Wood density

We performed destructive sampling of woody debris in 2010 to quantify wood density and describe the relationship between real density and penetration with the dynamic penetrometer. To estimate density of wood cross-sections, we used a disk removal approach that accounted for void space and heterogeneity in wood structure and decomposition. Specifically, we removed a ca. 3cm thick cross-sectional disk from the sample woody debris and returned this disk to the lab. Disk volume was estimated as the diameter multiplied by the average of 5 disk thickness measurements, with the mean edge thickness measurement weighted twice as much as center point thickness. If disks were too large to be returned to the lab, then the entire disk was weighed in the field and a subsection of this disk (200-1000g) was removed. Each section or subsection was weighed while fresh, dried at 60˚C, and then reweighed to estimate dry density. For subsampled disks, we assumed that the proportion of dry density in the subsample was representative of the entire disk and prorated field-measured fresh mass accordingly.

Standing woody debris

We censused standing CWD in the entire dynamics plots each year from 2009 to 2016 (except for 2011). Standing CWD was defined as standing WD with a DBH (diameter at breast height, i.e., 1.3 m height) > 20 cm. We measured the height, penetration using dynamic penetrometer, and DBH of each tree. For buttressed trees, we estimated the DBH using a taper function (Cushman et al. 2014). Previous work suggested the relationship between penetration and wood density was the same for standing and downed CWD (Larjavaara and Muller-Landau 2010), and thus we estimated density with the density-penetration relationship described with destructive sampling in 2010.

We estimated volume differently for relatively intact and mostly decomposed snags. We qualitatively recorded whether standing CWD retained none (<10% of branches), some (10-90% of branches), or all (>90%) of its crown. For standing CWD with some or all of its crown, we estimated necromass using an environment-specific biomass function (Chave et al, 2014):

[3] $$AGB = e^{-1.803-0.976*E+0.976*\ln(\rho)+2.673*\ln(D)-0.0299[\ln(D)^2]}$$

Where AGB is aboveground biomass (kg), E is a region-specific environmental parameter (E = 0.0561 for BCI), D is DBH (m), and ρ is density (kg m^{-3}). We assumed that biomass equaled necromass for trees with intact crowns. For trees with part of their crown missing, we estimated that 50% of branches were lost and, because branch wood is ca. 25% of total biomass, we estimated necromass as 87.5% of original biomass (Falster et al. 2015). For standing CWD that lacked branches, we used a taper function to estimate diameter at the top of the remaining trunk (Cushman et al. 2014) and approximated volume as a truncated cone.

We quantified standing FWD (>2 cm DBH) in a 5m radius subplot (78.5m^2) centered within each dynamics plot. We recorded DBH and height for standing FWD, and estimated volume using the same truncated cone approach described above.

Calculations of stocks and fluxes

We estimated mass and volume of stocks and fluxes similarly across sampling types. For most estimates of downed woody debris, we multiplied sample cross-sectional mass and cross-sectional area by the random angle correction factor ($\pi/2$) to account for the orientation of diameter measurements relative to the piece of CWD rather than the transect itself. For datasets with unidirectional transects (i.e., 2010 and 2014 long transects), we divided cross-sectional mass (or area) by sine of the angle between the longitudinal axis of the piece of WD and the transect itself. We then summed cross-sectional mass and cross-sectional area across all samples, and divided by total transect length. Similarly, standing and suspended woody debris volume and mass were summed across all samples, and divided by total area. For all stocks, fluxes, and proportions, we calculated confidence intervals by bootstrapping over spatial subsamples – either transect sections (10 or 20 m in length) or subplots (10x10 m each). When individual density estimates were not available, we estimated mass by multiplying final volume estimates by average dead wood density from the 2010 long transects (0.271 g mm^{-3}). Throughout the manuscript, we reference the year during which the majority of fluxes occurred; however, we note that pieces of CWD were not surveyed until the first two months of the subsequent year.

CWD inputs and outputs were estimated from the yearly surveys of the dynamics plots. We approximated the residence time of CWD using a steady state model; we divided the aggregate stocks (7 years of estimates) by the aggregate inputs (5 years of estimates). We then estimated the decomposition constant, k, as 1 divided by the residence time. Using the decomposition constant, we accounted for the mass and volume lost between when a sample enters the system and when it is first recorded using the following equation based on instantaneous decomposition rates,

[4] $$V_{i,0} = V_{1,t} \frac{r}{1-e^{-rt}}$$

Where V is the individual sample estimate (volume, mass, cross-sectional area, or cross-sectional mass) at the time it entered (subscript "0") and the time it was recorded (subscript "t"), t is time since the previous census (years – always "1" in our analyses), and r is the decomposition constant ($years^{-1}$). We then iteratively recalculated the total inputs and the decomposition constant until the change in r was less than 1% of its total value.

We also performed alternative calculations of residence times using individualized changes in CWD mass and volume. For CWD that remained in our study across multiple censuses, we calculated absolute changes in the mass and volume and calculated the decomposition constant for each year using an exponential decay model (Appendix I: Supplementary methods). We then calculated minimum and maximum mass loss for pieces of CWD that exited our study in a given year (Appendix I: Table S1). Finally, we used the same boles that exited the study to analyze the sensitivity of the residence time estimates to changes in density and diameter. Specifically, we calculated average decomposition constants with minimum, maximum, and 50% of the possible density and diameter measurements for downed and standing CWD (Appendix I: Table S1).

We calculated the sampling effort necessary to estimate pools and fluxes within 10% of the true value with 95% confidence given the observed variability. Specifically, we determined the total transect length (km) or surveyed area (ha) that would meet these criteria using the coefficient of variation and sample size (Metcalfe et al. 2008; Appendix I: Supplementary methods).

Fitting distributions and other analyses

We performed linear regression analysis between the proportion of downed dead wood in direct contact with the soil and decomposition class, and between penetrometer penetration per hit (mm) and dry density ($kg\ m^{-3}$). For penetrometer penetration

relative to dry density, both variables were log transformed to improve normality and linearity. Because both variables were log transformed, we used a correction factor [exp(squared residual error/2)] to convert from penetration to density in all cases when only penetration was known (Chave et al. 2005). We compared the penetrometer-estimated density of adjacent downed and elevated sections of downed CWD using a paired t-test. Finally, we performed Fisher's exact tests (*Binomial tests*) to determine if inputs were more likely in 10m and 100m^2 subsamples that received inputs in previous years.

We fit the univariate distribution of standing and downed CWD pieces over space at different spatial scales (R package *fitdistrplus*) and explored spatial aggregation of CWD mass, volume, and pieces using semivariograms (R package *GeoR*). We used maximum likelihood estimation to quantify how the distribution of CWD pieces fit Poisson and negative binomial distributions and compared their fits using AIC values (dAIC > 2 considered significant). CWD counts per quadrat or transect section will follow a Poisson distribution if individual pieces are independently distributed, and a negative binomial distribution is better if pieces are non-randomly clumped together. For the negative binomial distribution, the overdispersion "size" parameter characterizes the degree of non-random aggregation; smaller values of this parameter indicate greater aggregation. Because the data were generally overdispersed and included many zeros, we log (x+1) transformed cross-sectional area and cross-sectional mass before creating semivariograms. We generated separate omnidirectional semivariograms for inputs and outputs of downed and standing CWD, using each year as a replicate. Semivariograms were calculated for distances up to to 250 m, half the minimum dimension of the 50 ha plot using 10m bins. All calculations and statistical analyses were performed in the R statistical environment (version 3.4, R Core Team 2017).

RESULTS

Pools and inputs of woody debris

Suspended woody debris comprised a negligible proportion of the total WD pool (Figure 2, Appendix I: Table S2). Specifically, suspended WD only accounted for ca. 1% of total WD stocks (20.6 Mg ha-1), whereas the standing and downed CW pools accounted for ca. 20% and 80% of wood mass, respectively (Figures 2-3 and S3). Unlike standing and downed pools, the FWD component of suspended WD mass was nearly three times greater than CWD component. By contrast, downed CWD mass was approximately three times greater than downed FWD, and the mass of standing CWD stocks was nearly 4000 times greater than standing FWD stocks (Figure 2; Appendix I: Tables S2 and S3). Considering all pools of WD, the majority of dead wood mass is downed and stored in pieces of CWD (Figure 2). This traditional categorization of WD suggests that a minority of CWD mass is elevated or suspended above the ground, but this approach misses a functionally important portion of downed WD.

A large portion of downed WD (> 10cm diameter) is actually elevated above the forest floor (Figure 4). The 2017 long transects found that 23% (CI: 14-34%) of downed WD stocks on the 50 ha plot were elevated above the forest floor, whereas the short transect surveys found 52% of downed WD stocks were elevated (N = 177, CI: 46-57%) in other areas of the island. The actual proportion of elevated WD likely falls between these two estimates because of directionally opposing biases (see Supplementary Information in Appendix I for more details). Small-scale vertical stratification is important because suspended sections of downed WD decompose more slowly than sections in contact with the forest floor; in our study, penetrometer-estimated density was 11% higher for elevated WD sections (0.259 kg m^3) relative to adjacent downed sections of the same bole (0.232 kg m^3; $t = 1.99$, d.f. = 77, $p < 0.001$).

Combining elevated WD with suspended and standing pools demonstrated that the majority of WD inputs, and potentially stocks, were elevated above the forest floor.

Specifically, at least 54-71% of WD inputs (as volume) began decomposing before contacting the forest floor and between 40-63% of total WD stocks were either elevated, suspended, or standing (low and high estimates assume that 23% and 52% of downed CWD is elevated, respectively). The difference between inputs and stocks was caused by the greater ratio of standing to downed CWD for inputs (Figure 2; Appendix I: Tables S2 and S4). Although we did not measure the elevated WD of inputs directly, the proportion of elevated WD was highest at early stages of decomposition and decreased from 83% elevated (N = 16, CI: 68-94%) to 12% elevated (N = 32, CI: 4-22%) as wood decomposed from decay class 1 to class 5 ($F_{1,175} = 44.24$, $p < 0.001$; Figure 4). Consequently, we underestimate the proportion of WD input as either elevated, standing, or suspended WD because we use estimates of elevated WD stocks rather than inputs.

Treefalls and trunk wood were the most prominent components of woody debris (Table 3; Appendix I: Tables S5-S6). Branchfall only accounted for ca. 17% (CI: 11-26%) of total downed WD stocks in 2017 and, because branchfalls were primarily FWD, an even smaller portion of CWD inputs during 2015 and 2016 (Table 13). Correspondingly, branch wood was relatively unimportant to total WD inputs. Branch wood composed only 23% (CI: 14-36%) of downed WD stocks and ca. 10% of CWD treefall inputs (Table 13). Liana wood also was input into the downed WD pool, but it only contributed 2% (CI: 2-4%) of total downed WD volume and liana wood was restricted almost entirely to FWD (12% of total FWD, CI: 6-21%).

Aggregation and spatiotemporal variability of CWD

Downed and standing CWD stocks and inputs were highly spatially variable. The coefficient of variation across 10-m and 100-m^2 sampling units ranged from 600% to 1580%, meaning the standard deviation was up to 16 times greater than the mean for all estimates across all years and spatial scales (Table 2 and S7). This pattern was caused by

rare, exceptionally large inputs and the aggregation of CWD pieces (Figures S4-5). Specifically, standing and downed CWD pieces were non-randomly aggregated within the smallest sampling units (i.e., they fit the negative binomial distribution) in 13 of the 14 occasions that spatial aggregation was recorded (the only exception was standing CWD during 2014). However, there was no spatial structure in WD pools above the scale of our sampling units (10-m and 100-m^2), as demonstrated by semivariogram analyses (Appendix I: Figure S6). This was further confirmed by the predictable scaling of the coefficient of variation with increasing sampling scale (Appendix I: Table S7).

Because of this extreme spatial variability, substantial sampling efforts are necessary to accurately estimate most WD stocks and fluxes. FWD and stocks typically required smaller sampling efforts than CWD and fluxes because they were more frequent and the size range of FWD was constrained (<20 cm, Table 2). By contrast, the size distribution of CWD was strongly right-skewed and thus a huge sampling effort was necessary to characterize the frequency of large, high-leverage inputs (Appendix I: Figure S4). Consequently, small sampling efforts either overestimate or underestimate the frequency of large inputs, leading to chronic underestimation of uncertainty. The size distribution of CWD also causes inaccuracy; small sampling efforts that miss large pieces of CWD will underestimate stocks and fluxes (e.g., CWD from the 2014 long transects; Figure 3), whereas small sampling surveys that encounter large pieces of WD will assume they are too frequent and overestimate. The skewed distribution of WD sizes even inhibits predictions of the sampling efforts necessary for accurate estimates. For example, the target sampling efforts that were estimated with less effort in this study tended to be smaller than those estimated with greater effort (Table 2).

Despite limited spatial structure, CWD inputs were non-randomly aggregated through time. Downed CWD inputs occurred 290%, 250%, and 180% more frequently than expected if a piece of CWD was input on the same 10-m transect section either 1

year (Binomial test: $p < 0.001$), 2 years ($p < 0.001$) and 3 years prior ($p = 0.05$), respectively. This pattern is likely the result of fragmentation as a standing dead tree enters the downed CWD pool over multiple years. However, there was no association with downed inputs 4 years prior (Binomial test: $p = 1.0$). By contrast, standing CWD inputs were not associated with previous inputs at the 100 m^2 (Binomial test: $p = 0.098$) or 1600 m^2 sampling scales (Binomial test: $p = 0.975$). Note that we have low power to detect differences in stocks and fluxes among years. The estimated sample efforts necessary for estimation of CWD stocks and inputs within 10% with 95% confidence were >100 km, many times greater than the annual sample efforts in this study (16 km, Table 3). Consequently, our results should not be interpreted as evidence that CWD stocks and inputs are temporally homogenous; rather, qualitative comparisons of CWD stocks, fluxes, and patterns of aggregation suggest that inputs and stocks can vary year-to-year (Figures 3 and S3, Appendix I: Tables S2-4).

Residence time and decomposition constants

Residence times calculated with a steady state model were greater than individualized estimates (Table 4, Appendix I: Table S1). The average residence time for standing CWD (1.8-2.0 years) was approximately half that of downed CWD (3.4-3.6 years). Correspondingly, this indicates that 2.3 Mg ha^{-1} and 3.5 Mg ha^{-1} of wood necromass are output from the standing and downed CWD pools, respectively. However, residence times estimated with a steady state model were 40-60% longer than even the most conservative individualized estimates (Appendix I: Table S1). Individualized estimates also were slightly more sensitive to changes in diameter than changes in density (Appendix I: Table S1).

DISCUSSION

Accurate estimates of WD pools and their spatiaotemporal dynamics are necessary to understand carbon cycling. Here, we conducted the most comprehensive

survey of WD in a tropical forest. Using the first-ever estimate of elevated WD in any forest type, we show that the majority of wood necromass decomposes above the forest floor. We also demonstrate that tremendous sampling efforts are necessary to accurately estimate WD pools and fluxes due to the highly dispersed nature of CWD. These findings challenge the accuracy and precision of WD estimates in most forests and emphasize the need to consider the vertical distribution of WD *in situ* to better understand decomposition.

The contemporary understanding of decomposition is based on ground-level studies (Adair et al. 2008, Bradford et al. 2014), yet half or more of total WD is decomposing aboveground. Combined standing and suspended WD pools are often greater than downed WD (Ovington and Madgwick 1959, Christensen 1977, Delaney et al. 1998); here we show that an additional 25-50% of downed WD is actually elevated. Decomposition rates differ substantially between the forest floor and standing, suspended, or elevated WD (Fasth et al. 2011, Přívětivý et al. 2016, Song et al. 2017), but the mechanisms underlying these differences (e.g., microclimate and nutrient availability) remain untested. Moreover, information regarding the process of decomposition and models of wood decomposition rely on ground-level studies (Thornton 1998, Liski et al. 2005, Weedon et al. 2009reviewed by Cornwell et al. 2009) and/or experiments that only consider completely downed pieces of WD (i.e., no elevated WD; van Geffen et al. 2010, Cornelissen et al. 2012, Bradford et al. 2014, Zanne et al. 2015). Consequently, the processes regulating wood decomposition and related aspects of carbon cycling will remain poorly understood until this knowledge gap is addressed.

The sampling efforts estimated here indicate that WD stocks and fluxes are exceptionally difficult to quantify. Without bootstrapping over large spatial scales with intense replication (> 130 km or 500 ha), it is impossible to capture the true frequency of

large pieces of WD (Appendix I: Figure S6). Because previous studies lack sufficient sampling efforts, existing estimates of WD underestimate their uncertainty (Clark et al. 2002, Woldendorp et al. 2004, Palace et al. 2012, Carlson et al. 2017). Moreover, many estimates of WD stocks and fluxes are inaccurate; they either underestimate WD because large inputs were not sampled, or overestimate WD because these inputs were recorded and their frequency was overestimated. The problems caused by these high-leverage inputs are known (Palace et al. 2012), but even large-scale studies typically lack sufficient sample sizes for precise estimates (Palace et al. 2008, Carlson et al. 2017). These issues likely plague estimates of residence time as well; for example, the highest measured CWD decomposition rate in tropical forests was measured across only 1.5 ha and could be a statistical outlier rather than representative of the local forest (Delaney et al. 1998, Palace et al. 2012). Existing estimates of WD parameters are useful starting points, but should be interpreted cautiously given their tendency for inaccuracy and imprecision.

Forest dynamics studies offer an alternative method for estimating WD fluxes using tree mortality and branchfall (Meakem et al. 2017). Co-located with our study, Meakem and colleagues (2017) estimated CWD (> 10cm DBH) inputs from tree mortality as 5.4 Mg ha^{-1} yr^{-1} from 1985-2010. Branchfall was not included in this mortality-based estimate, and we see that the difference between our estimate of CWD inputs and Meakam's (9%) nearly equals the proportion of CWD input as branchfall (8%, also see Chave et al. 2003). This confirms that mortality-based estimates can be accurate with the exclusion of branchfall. However, branchfall estimates range from 15-45% of total WD inputs (Malhi et al. 2014, Marvin and Asner 2016) and the reasons for differences in branchfall are unclear. Consequently, tree mortality-based estimates of WD inputs require coordinated branchfall measurements to account for potentially large differences in branchfall inputs among sites.

Although direct comparisons with other forests are difficult, the stocks and fluxes observed in our study appear to be unusual. Residence times for standing CWD were the shortest ever recorded (Odum 1970, Lang and Knight 1979) and downed CWD residence times were shorter than most estimates (Palace et al. 2012). Given the substantial mass of CWD inputs relative to other neotropical forests, the fast rates of decomposition likely caused the relatively low WD stocks. Although we did not test mechanisms of decomposition, previous work concluded that oceanic Na deposition causes faster rates of wood decomposition on BCI than in inland Ecuadorian forest (Kaspari et al. 2009, Clay et al. 2015). The possibility that local abiotic conditions, such as proximity to salt water, can dramatically change decomposition rates emphasizes the need for replicated studies quantifying decomposition across a broad range of forest biomes.

Caveats and recommendations

Despite our attempt to provide a comprehensive assessment of woody debris in a tropical forest, the results revealed some important limitations. Line-intercept sampling is not ideal for spatial analyses as it misses some pieces of WD. Downed WD was spatially autocorrelated in a similar temperate study (Král et al. 2014), and the line-intercept approach potentially inhibited our ability to detect this pattern on BCI. Additionally, the two methods for estimating residence time provided substantially different results. There are two possible explanations for these differences. First, if the estimates are accurate, this suggests that CWD stocks are decreasing as decomposition rates are increasing and/or CWD inputs are decreasing. Second, it is possible that one of the residence time estimates is biased. The most likely source of bias is that individualized measurements treat all boles equally and residence times increase with bole size in some cases (reviewed by Harmon et al. 1986). Finally, we sacrificed a larger sampling scale for more intense sampling across a 50 ha stand of forest, but we found this to be the most effective approach. Bootstrapping methods limited problems with

autocorrelation, and intensive WD sampling at this scale enabled us to conduct the most comprehensive assessment of tropical WD stocks and fluxes to date.

This study provides a framework for the interpretation and design of forest inventory studies. The unusual WD fluxes in this forest emphasize the need for replicated studies in many biomes to better understand WD stocks, inputs, and decomposition. Given the spatial variability of WD, future studies of WD should employ bootstrapping to estimate confidence intervals and substantial sampling efforts to improve their accuracy and precision. Without accurate and precise estimates of WD, it is impossible to quantify the contribution of WD to global carbon cycling (Pan et al. 2011). In a broader context, it is likely that highly variable ecosystem components of all biomes are inaccurately estimated with unknown uncertainties. Addressing these considerations in future studies should increase accuracy and reduce uncertainty in forest inventory studies, thus improving models of global carbon cycling.

TABLES

Table 1: Key characteristics of the field datasets analyzed here. The diameter range is for the diameter at the intersection of the transect in the case of downed WD, and the trunk DBH in the case of standing WD. The total sampling effort denotes the aggregate transect length or plot area surveyed per year. The sampling design provides a brief description of the subsample scale, as well as the distribution of samples.

Sampling method	Woody Debris Pool	Diameter Range	Sampling design	Sampling effort (per year)	Density estimate	Years sampled
Dynamics plots	Downed WD	>20 cm	Four 40 m transects, subsampled every 10 m	16 km	Penetrometer	2009-2016
	Standing WD		100 plots of 1600 m^2, subsampled every 100 m^2	16 ha		
		2-20 cm	5 m radius plots centered in the dynamics plots	0.79 ha	Mean only	
	Suspended WD	>20 cm	200 plots, each 100 m^2	2 ha	Mean only	2015
		5-20 cm				
Long transects	Downed WD	>20 cm	500 m transects, subsampled every 20m	8 km	Penetrometer, Disk-sampling	2010
					Penetrometer	2014
		>10 cm	perpendicular transects of 500 m and 1 km, subsampled every 20 m	15 km	Mean only	2017
		2-20 cm	1 m subsamples every 20m of the 500 m transects	0.4 km	Disk-sampling	2010

			1 m subsamples every 20 m of the 2017 long transects	0.75 km	Mean only	2017
	Downed Lianas	>10 cm	perpendicular transects of 500 m and 1 km, subsampled every 20 m	15 km	Mean only	2017
		2-10 cm	1 m subsamples every 20 m of the 2017 long transects	0.75 km		
Short transects	Downed WD	>10 cm	100 m transects haphazardly distributed across BCI	3.3 km	Penetrometer	2015

Table 2: Sampling effort required to estimate the volume of WD pools and fluxes to within 10% of the true mean with 95% confidence. We present values from the smallest sampling scale in cases where multiple scales were recorded. The coefficient of variation (CV, with 95% CI) is the percent of the standard deviation over the mean of total volume per transect.

Pool	Flux, stock, or sub-pool	Estimate method (unit)	Sampling unit	Actual sampling effort	Year (s)	Coefficient of Variation (%)	Required sampling effort, volume (km or ha)
Downed CWD (>20 cm)	Stocks	Transects (km)	10 m	112 km	2009-2016	601 (468, 769	139 (84, 227)
	Inputs			80 km	2009-2016	1369 (554, 2308	720 (118, 2047)
	Outputs					1683 (577, 3085	1088 (128, 3658)
Downed CWD (>10 cm)	Stocks	Transects (km)	20 m	15 km	2017	693 (149, 1483	370 (17, 1695)
	Suspended above soil					386 (255, 576	115 (50, 256)
	In contact with soil					889 (157, 2231	609 (19, 3836)
	Branchfall					334 (239, 472	86 (44, 172)
	Treefall					777 (165, 1760	465 (21, 2388)
	Liana wood					2020 (0, 7673	3145 (0, 45379)
Downed CWD from treefall	Trunk wood	Transects (km)	20 m	15 km	2017	831 (157, 2041	532 (19, 3211)
	Branch wood					631 (344, 1083	307 (91, 904)
Downed FWD (<10 cm)	Stocks	Transects (km)	1 m	0.75 km	2017	228 (161, 322	2 (1, 4)
	Branchfall					322 (228, 426	4 (2, 7)
	Treefall					664 (360, 1258	17 (5, 61)
	Liana wood					789 (360, 1720	24 (5, 114)
	Trunk wood		1 m	0.75 km	2017	738 (395, 1468	21 (6, 83)

Downed FWD from treefall	Branch wood	Transects (km)				1610 (0, 6490)	100 (0, 1625)
Standing CWD	Stocks	Plots (ha)	100 m^2	112 ha	2009-2016	1210 (600, 1830)	560 (139, 1280)
	Inputs			80 ha	2009-2016	1610 (840, 2670)	956 (282, 2564)
	Outputs					1580 (860, 2580)	661 (149, 2009)
Standing FWD	Stocks	Plots (ha)	78.5 m^2	0.785 ha	2010	450 (80, 1560)	63 (2, 756)
Suspended CWD	Stocks	Plots (ha)	100 m^2	2 ha	2015	410 (200, 890)	64 (16, 308)
Suspended FWD						180 (120, 260)	12 (6, 26)

Table 3: The sample size, mass, and volume (±95% CI) of downed WD inputs separated into branchfall and treefall. Estimates for 2015 and 2016 were based on inputs of CWD into the dynamics plots, with mass calculated using penetrometer measurements, whereas 2017 estimates were based on the volume of WD stocks characterized using long transects. These are the only datasets that separated branchfall and treefall inputs.

Year	Woody Debris Pool	Total Volume (m^3 ha^{-1})	Treefall Volume (m^3 ha^{-1})	WD Pieces per category (N)				Treefall WD (%)		Trunk Wood (%)	
				Branchfall	Treefall	Branch Wood	Trunk Wood	Volume	Mass	Volume	Mass
2015	>20cm inputs	7.8 (3.81, 12.9)	6.4 (3.5, 9.8)	14	43	5	35	82 (64, 95)	78 (54, 95)	95 (87, 99)	95 (89, 99)
2016	>20cm inputs	11.5 (4.4, 22.7)	10.9 (4.2, 21.6)	10	52	17	35	95 (85, 98)	94 (83, 98)	88 (65, 96)	84 (59, 96)
2015-2016	>20cm inputs	9.6 (5.1, 16.0)	8.6 (4.7, 14.2)	24	95	22	70	90 (78, 96)	87 (72, 96)	90 (80, 96)	88 (75, 95)
2017	2-10cm stocks	8.2 (6.0, 10.6)	1.7 (0.9, 2.5)	210	26	3	22	21 (12, 30)	N/A	4.0 (2, 5)	N/A
2017	>10cm stocks	58.3 (35.0, 92.5)	53.6 (31.3, 86.5)	191	343	80	263	92 (87, 95)	N/A	93 (88, 97)	N/A
2017	>2cm stocks	66.49 (43.4, 103.0)	55.3 (34.0, 89.8)	401	369	83	285	83 (74, 89)	N/A	93 (87, 96)	N/A

Table 4. Estimates of downed and standing CWD residence time and decomposition constant (±CI) using a steady state model. These estimates either use measured values of CWD inputs (raw inputs) or iteratively corrected inputs to account for decomposition that occurred before inputs were measured (iteratively corrected inputs). The iterative corrections are the best estimates of residence time and decomposition.

CWD pool	Estimate type	Residence time (years)		Decomposition constant (k)	
		Mass	Volume	Mass	Volume
Downed CWD	Iteratively corrected inputs divided by stocks	3.44 (2.56, 4.68)	3.58 (2.62, 5.02)	0.29 (0.21, 0.39)	0.28 (0.2, 0.38)
	Raw inputs divided by stocks	3.96 (2.93, 5.40)	4.10 (3.00, 5.57)	0.25 (0.19, 0.34)	0.24 (0.18, 0.33)
Standing CWD	Iteratively corrected inputs divided by stocks	1.84 (1.21, 2.89)	2.01 (1.36, 3.03)	0.54 (0.35, 0.83)	0.5 (0.33, 0.74)
	Raw inputs divided by stocks	2.38 (1.57, 3.85)	2.55 (1.63, 3.93)	0.42 (0.26, 0.64)	0.39 (0.25, 0.61)

FIGURE LEGENDS

Figure 1. The pools and fluxes of woody debris as it cycles from living woody tissues to carbon dioxide and/or soil organic matter. Filled black arrows indicate fluxes in and out of dead WD pools, whereas hollow arrows represent fluxes among pools of dead woody debris. Arrows and boxes are not scaled to represent the magnitude of fluxes and pools.

Figure 2. The pools and fluxes of woody debris mass estimated in this study. Boxes are scaled to represent the relative mass of stocks in each pool. The aggregate totals of the CWD inputs and outputs are depicted as filled arrows. The arrows are proportional to the estimated fluxes at the point where they enter and exit the CWD stocks; the rest of the arrows are merely scaled to the size of the relevant stock because these sub-fluxes were not separately quantified. Estimated downed and standing CWD mass are based on penetrometer estimates from the 40x40m plots, whereas the other estimates use average density and volume from the 2010 and 2014 long transects (downed FWD) or subplots within the 40x40m plots (standing FWD and all suspended WD).

Figure 3. Estimated downed and standing CWD stocks (A) and inputs (B) as mass (Mg ha^{-1}) with 95% confidence intervals based on data from the 40x40m dynamics plots in individual years (filled symbols) and estimated stocks from the long transects in 2010 and 2014 (open symbols). The shaded regions represent the mean (±95% CI) of downed and standing CWD as calculated across all years from the 40x40m plots. See Figure S3 in Appendix I for parallel estimates of WD volume.

Figure 4. The mean percent of volume (mean ±95% CI) in downed WD >10cm diameter that was elevated above the forest floor for each decomposition stage (higher numbers indicate more advanced decomposition), based on data from the 2015 short transects. The solid line with the dark grey bar represents the overall mean and 95% confidence interval for WD from these short transects, whereas the solid line with the light grey bar represents the overall mean and confidence interval for WD from the 2017 long transects.

Figure 1

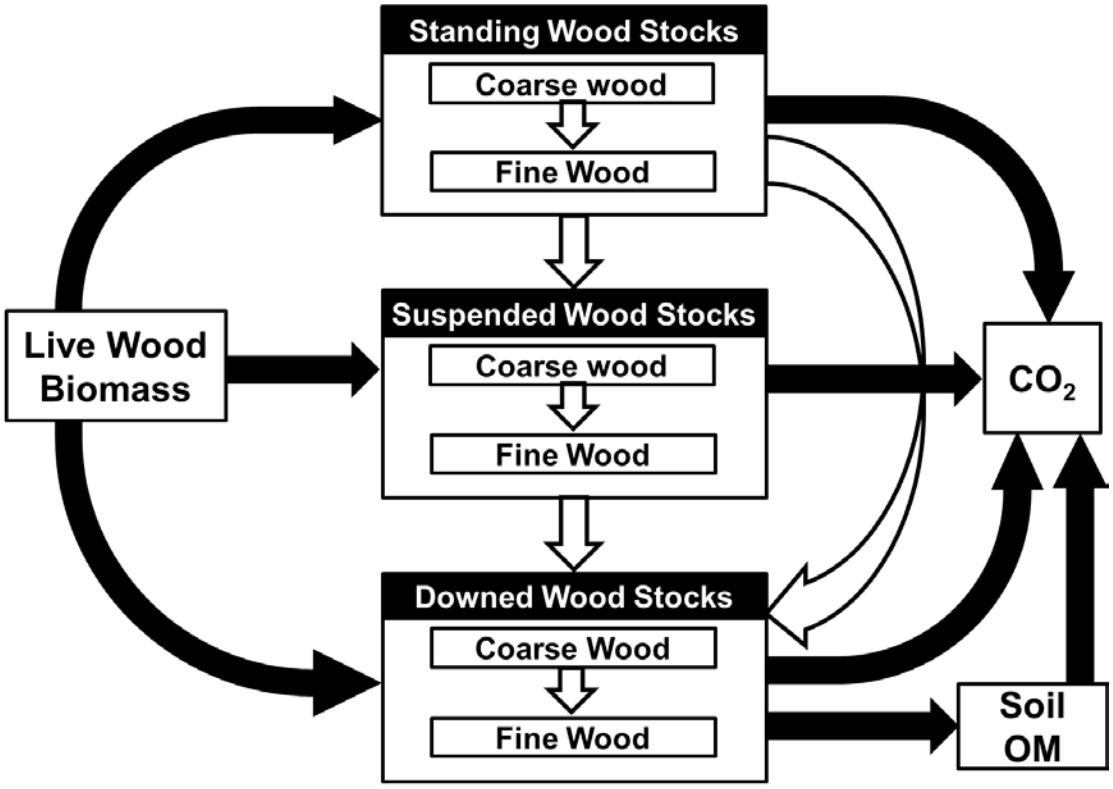
Standing Wood Stocks
Coarse wood
Fine Wood
Suspended Wood Stocks
Coarse wood
Fine Wood
Downed Wood Stocks
Coarse Wood
Fine Wood
Live Wood Biomass
CO_2
Soil OM

Figure 2

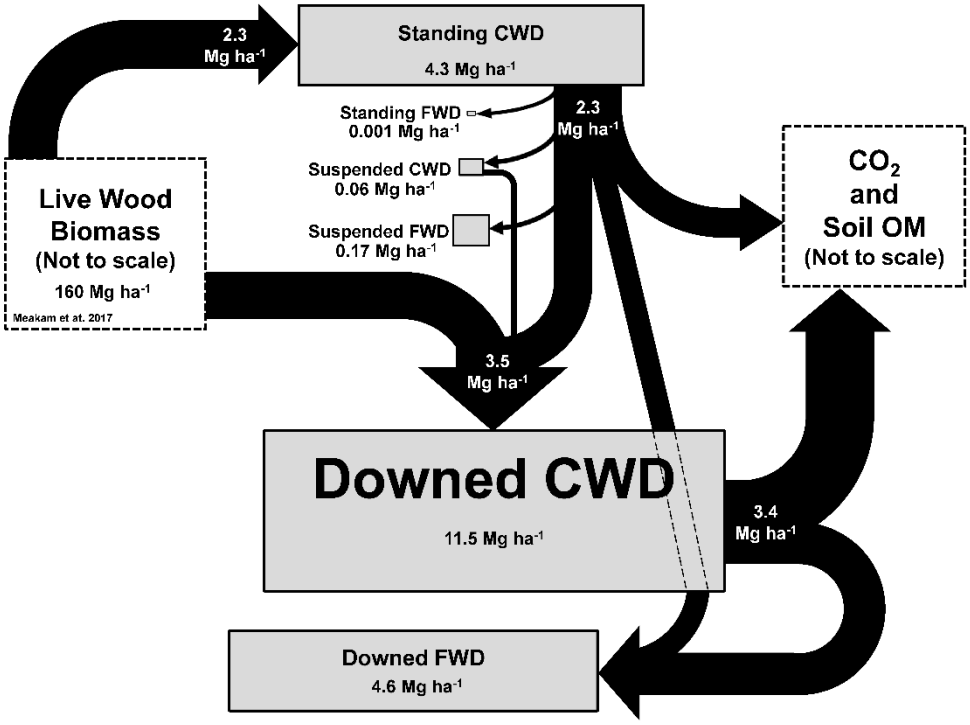
2.3
Mg ha-1
Standing CWD
4.3 Mg ha-1
Standing FWD
0.001 Mg ha-1
2.3
Mg ha-1
Suspended CWD
0.06 Mg ha-1
Suspended FWD
0.17 Mg ha-1
Live Wood
Biomass
(Not to scale)
160 Mg ha-1
Meakam et at. 2017
CO2
and
Soil OM
(Not to scale)
3.5
Mg ha-1
Downed CWD
11.5 Mg ha-1
3.4
Mg ha-1
Downed FWD
4.6 Mg ha-1

Figure 3

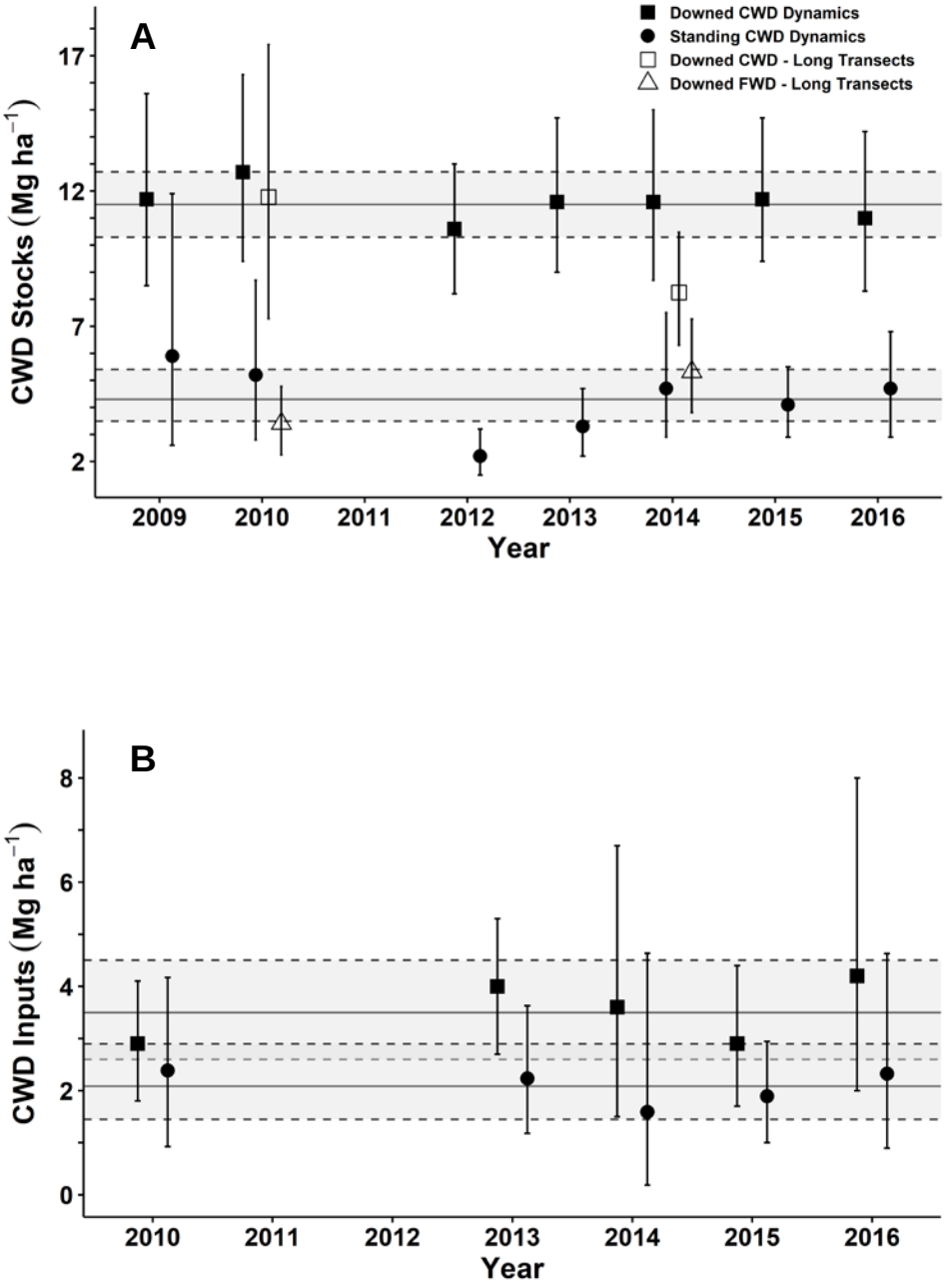
A
Downed CWD Dynamics
Standing CWD Dynamics
Downed CWD - Long Transects
Downed FWD - Long Transects
CWD Stocks (Mg ha^{-1})
17
12
7
2
2009
2010
2011
2012
2013
2014
2015
2016
Year
B
CWD Inputs (Mg ha^{-1})
8
6
4
2
0
2010
2011
2012
2013
2014
2015
2016
Year

Figure 4

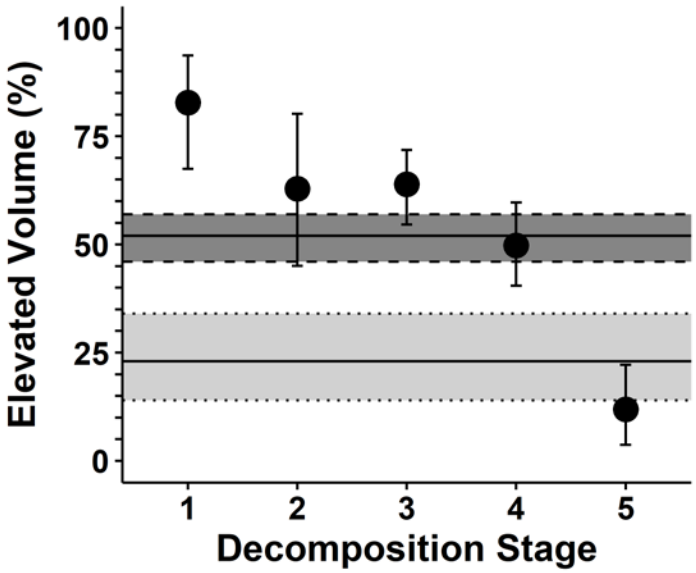

CHAPTER III

DECOMPOSITION OF COARSE WOODY DEBRIS IN A LONG-TERM LITTER MANIPULATION EXPERIMENT: A FOCUS ON NUTRIENT AVAILABILITY

SUMMARY

The majority of aboveground carbon in tropical forests is stored in wood, which is returned to the atmosphere during decomposition of coarse woody debris. However, the factors controlling wood decomposition have not been experimentally manipulated over time scales comparable to the length of this process. We hypothesized that wood decomposition is limited by nutrient availability and tested this hypothesis in a long-term litter addition and removal experiment in a lowland tropical forest in Panama. Specifically, we quantified decomposition using a 15 year chronosequence of decaying boles, and measured respiration rates and nutrient limitation of wood decomposer communities. The long-term probability that a dead tree completely decomposed was decreased in plots where litter was removed, but did not differ between litter addition and control treatments. Similarly, respiration rates of wood decomposer communities were greater in control treatments relative to litter removal plots; litter addition treatments did not differ from either of the other treatments. Respiration rates increased in response to nutrient addition (nitrogen, phosphorus, and potassium) in the litter removal and addition treatments, but not in the controls. Established decreases in concentrations of soil nutrients in litter removal plots and increased respiration rates in

response to nutrient addition suggest that reduced rates of wood decomposition after litter removal were caused by decreased nutrient availability. The effects of litter manipulations differed directionally from a previous short-term decomposition study in the same plots, and reduced rates of bole decomposition in litter removal plots did not emerge until after more than 6 years of decomposition. These differences suggest that litter-mediated effects on nutrient dynamics have complex interactions with decomposition over time.

INTRODUCTION

Tropical forests influence global carbon dynamics more than any other terrestrial biome; they contain 25% of terrestrial biomass and account for ca. 40% of the terrestrial carbon sink (Pan et al. 2011, Feldpausch et al. 2012). The majority of aboveground carbon in tropical forests is sequestered in wood (Rice et al. 2004) and the process of decomposition eventually releases most of this carbon as CO_2. Indeed, actively decomposing dead woody debris accounts for as much as 20% of aboveground carbon and 15% of CO_2 emissions in tropical forests (Chambers et al. 2004, Rice et al. 2004, Palace et al. 2008). To understand and accurately predict changes in tropical forest carbon cycling, it is therefore necessary to determine what factors control the decomposition of trees and large branches (cumulatively referred to as coarse woody debris [CWD] or individually as “boles”).

Experiments investigating factors that control decomposition are generally restricted to leaf litter and fine woody debris. Substrate characteristics and microclimate are important to litter and fine woody decomposition rates (reviewed by Berg and Laskowski 2005, Fasth et al. 2011), and one or more nutrients typically limit litter decomposition rates in non-desert ecosystems (Hobbie and Vitousek 2000, Austin and

Vivanco 2006, Kaspari et al. 2008). For small woody substrates (< 20 cm^3), controlled experiments indicate that decomposer species composition, community assembly history, nitrogen (N) availability, and phosphorus (P) availability all influence decomposition rates (Boddy 2001, Fukami et al. 2010, Bebber et al. 2011). For small branches in a lowland tropical forest (5 cm diameter), decomposition rates increased with P and P+N addition for some tree species but not for others, indicating that substrate characteristics influence the effects of fertilization (Chen et al. 2015). Although these studies form a useful foundation for understanding wood decomposition, it remains unknown if results from short-term decomposition studies using small woody substrates are predictive of CWD decomposition.

Uncertainty regarding wood decomposition exists in part because fine woody debris is chemically different from CWD and decomposition of entire boles occurs over long time scales (Kimmey 1955, Harmon et al. 1986). Decomposition rates of larger boles are often slower than for smaller boles, but it remains unclear how this phenomenon is influenced by chemical composition and geometry (surface area-to-volume ratio; Oberle et al. 2017, reviewed in Harmon et al. 1986). Small woody debris is mostly composed of relatively labile sapwood, whereas a large portion of mature tree mass is recalcitrant heartwood that often contains complex compounds and lower nutrient content (Grubb and Edwards 1984, Sellin 1994, Meerts 2002, Taylor et al. 2002). These types of compositional differences can have complex effects on decomposition (Carreiro et al. 2000) that are not well understood for woody substrates (Chen et al. 2015). Despite these differences, the vast majority of experimental investigations of wood decomposition focus on fine woody debris, yet most dead wood carbon is stored in coarse woody debris.

Circumstantial evidence and natural experiments provide some information about long-term wood decomposition. Wood decomposition often differs among tree species and it is faster for smaller, less dense, and low lignin woody debris in tropical forests (Chambers et al. 2000, van Geffen et al. 2010). Wood has higher carbon-to-macronutrient ratios than decomposer organisms, resulting in an initial stage of nutrient translocation into wood during decomposition (Boddy 2001, Mooshammer et al. 2014). The bulk translocation of soil nutrients for wood decomposition is so substantial that CWD removal and multi-nutrient fertilization had similar positive effects on net primary productivity in a secondary tropical forest (Zimmerman et al. 1995). However, it is not known for how long nutrient translocation occurs and how the process of nutrient import influences decomposition rates. In a relevant study, the effects of fertilization were inconsistent through time (Chen et al. 2015), suggesting that nutrient limitation is only important during some stages of decomposition. Without long-term experiments spanning the duration of CWD decomposition (Cornelissen et al. 2012), it is impossible to determine how nutrient availability influences dead wood decomposition.

Long-term litter manipulations are useful for investigating the roles of soil nutrients during decomposition. Litter functions as a complete, stoichiometrically balanced fertilizer that releases nutrients as it decomposes over months (Sayer et al. 2012), and thus litter addition provides insight into the influence of bulk nutrient addition on rates of decomposition. Two features of this approach are (1) that it does not change nutrient ratios in the same way as fertilization with select elements (Sayer and Banin 2016) and (2) that it approximates future forest conditions because increased litter inputs are expected in response to increased CO_2 concentrations (Liu et al. 2009). By contrast, litter removal can provide information about the roles of soil nutrient pools during decomposition. To our knowledge, no studies to date have considered how litter inputs influence long-term wood decomposition.

We investigated long-term CWD decomposition in a litter manipulation experiment in lowland tropical forest in Panama. In this experiment, litter addition plots are relatively nutrient-rich (elevated soil nitrate and P), whereas litter removal plots are nutrient-poor (reduced soil inorganic N, soil P, litter N, and litter potassium [K]; Sayer et al. 2012, Sheldrake et al. 2017a). We hypothesized that long-term rates of wood decomposition increase with greater litter input as a result of enhanced nutrient availability (N, P, and K), whereas decomposition rates decrease with very low litter input due to nutrient limitation. We tested three predictions related to this hypothesis: 1) CWD decomposition rates are higher in litter addition treatments and lower in litter removal treatments compared to controls; 2) similarly, wood decomposer activity (respiration rates) during late-stage decomposition is greater in litter addition plots and reduced in litter removal plots; 3) respiration rates of decomposer communities exhibit a greater increase in response to nutrient addition in litter removal plots than in litter addition or control plots. We used tree survey data to establish the species and year of death for decaying boles within the plots, which allowed us to test our predictions using a 15-year chronosequence of CWD.

METHODS

Study site

The study site was lowland tropical forest located on the Gigante Peninsula within the Barro Colorado Nature Monument in central Panama. Forest structure and tree composition are typical of mature lowland tropical forest in Mesoamerica (Wright et al. 2011) with an average annual temperature of 27˚C, mean annual rainfall of 2600 mm, and a short dry season (January-April, < 100mm monthly rainfall; (Leigh 1999). The soils are Oxisols with moderate to low concentrations of exchangeable cations and resin-extractable phosphorus (Yavitt et al. 2011, Wright et al. 2011).

Litter Manipulation Plots

The Gigante Litter Manipulation Project (GLiMP) comprises 15 plots (45 x 45 m) in five replicate blocks of three treatments. The litter in the five "litter removal" plots has been raked and moved to the five "litter addition" plots once a month since January 2003, five unmanipulated plots were maintained as controls (estimated litterfall = 991 g m^{-2} y^{-1}, Sayer and Tanner 2010a). The experimental design is described in detail elsewhere (Sayer et al. 2006). All trees with > 10 cm diameter at breast height (DBH) in the plots were measured, tagged, identified, and mapped with *c*. 0.5 m accuracy in 2000, this process has been repeated annually, with the exception of 2006 and 2008, through to the conclusion of this study (August 2016). Soil nutrient concentrations were last measured in these plots in 2010 and 2012 (Sayer et al. 2012, Sheldrake et al. 2017a).

Bole survey

In 2016, we used a chronosequence approach to compare CWD decomposition among litter treatments (van Geffen et al. 2010). The tree census data from the litter manipulation plots indicated the year in which a given tree died, the size of the tree at death, the species of the tree, and its location in the plot. Boles were not moved away from their original location by human activity because access to the study site is restricted. Using census information, we were able to locate remaining boles and determine if others had completely decomposed.

We returned to the original location of each dead tree and categorized these trees into two groups. The first group (n = 115) included downed and standing dead trees that we were able to unambiguously identify. Specifically, unambiguous identification relied on detecting a remnant bole with sufficient elliptical-cylindrical structure that we could determine its orientation and position relative to the original location of the tree. The second group comprised trees that had completely decomposed (n =99). Boles were only

recorded with this fate if no intact sections of wood existed near their original location. We did not consider small wood fragments (typically <500 cm^3) as evidence of a remaining bole for two reasons: 1) it is nearly impossible to determine the original source of individual fragments and 2) the presence or absence of litter biases detection rates for small fragments. Consequently, small woody fragments of "completely decomposed" boles may persist in these plots, but any omissions were consistent among litter treatments. To account for species-specific differences in initial wood density, we used the published values for each species or its closest known relative (global wood density database, Chave et al. 2009).

We excluded dead trees from our analyses if they were unidentifiable or lacked important covariates (diameter, species, or location; n = 104), and we did not consider dead palms (n = 82). We omitted dead trees that lacked tree species identifications (n = 67) or accurate locations (n = 7). Trees that fell outside of the plots were not affected by the litter manipulation treatments and were thus removed (n = 4). We also removed trees from analyses if the tree location was obscured by a treefall (n = 7), or multiple boles were clustered and/or in an orientation that precluded a confident assignment to single point of origin (n = 19). Trees omitted from our analyses were smaller and denser than those retained, but their cross-sectional masses did not differ (Appendix II: Table S1). Regardless, all criteria were applied equally to all plots, and the characteristics of excluded trees did not differ among litter treatments (Appendix II).

Wood Respiration

We used respiration measurements to estimate short-term decomposer community activity. We selected 28 boles in each of the three litter treatments so that bole ages (i.e., time since tree death) were relatively evenly distributed across the course of the study. To ensure accurate measurements, we only chose boles with sufficient

structure (diameter, length, and shape) to support respirometry collars. We attached 10 cm tall respirometry collars (7 cm diameter PVC sections) to each bole using silicon sealant and all collars were located at least 0.3 m from a bole end.

Beginning one week after collar attachment, we began measuring respiration rates using a Viasala respirometer (GMP343 CO_2 probe, Vaisala Inc.). We attached the respirometer to each collar for 5 minutes and recorded CO_2 (ppm) every 15 seconds. We removed the initial portion of each recording (ca. 15-45 seconds) because of inconsistency and we approximated respiration rates as the slope of the linear CO_2 accumulation curve during the remaining portion of the recording period (Bréchet et al. 2017). To control for temporal variability and estimate baseline respiration rates of wood decomposer communities, we measured respiration of each bole three times over a two-week period.

All respiration measurements were taken during the wet season (June-July 2016). Rainfall (June = 326.5 mm; July = 486.8 mm) far exceeded potential evapotranspiration (June = 48.5 mm; July = 45.4 mm) during these months, and this typical pattern causes soil moisture (and presumably wood moisture) to be consistent among years (Steve Paton, STRI Environmental Monitoring Program, pers. com.). These measurements primarily capture microbial effects on decomposition and they are representative of the conditions underlying the majority of carbon mineralization. Specifically, decomposition occurs much more rapidly during the wet season than the dry season in this forest (Wieder and Wright 1995), and the wet season is twice as long as the dry season. However, the effects of infrequent fragmentation events and transient invertebrates are not captured by this method given its small spatial and temporal scale.

We estimated the current density of these boles using a dynamic penetrometer, as described by Larjavaara and Muller-Landau (2010). Briefly, we inserted the

penetrometer vertically into each bole ca. 5 cm from the respirometry collar and measured the distance of penetration. We estimated density using the relationship between penetration and wood density previously established for CWD in this forest (Larjavaara and Muller-Landau 2010). To create a proxy for decomposition state, we then calculated bole density (%) as the percent of original density remaining (hereafter *bole density remaining*; original density estimated using the global wood density database, Chave et al. 2009). Although the variability of penetrometer measurements can increase with decomposition stage (Oberle et al. 2014), they are more accurate on a case-by-case basis than other non-destructive techniques that consider both void space and heterogeneity in wood density (Larjavaara and Muller-Landau 2010).

Sensitivity to nutrient addition

To quantify nutrient limitation of wood respiration among litter treatments, we installed a second respirometry collar on a subset of the boles (litter addition: $n = 9$: litter control: $n = 6$, litter removal: $n = 5$). The added collars were at least 1 m apart from the original collars to reduce the likelihood of short-term nutrient translocation. We used all boles that met two criteria: 1) the trees had died > 3 years previously, and 2) they were either long enough to support two collars or separated into two large fragments. We chose boles that were > 3 years old (hereafter *old boles*) to focus on late-stage decomposition (i.e., longer than typical decomposition studies).

After concluding our baseline wood respiration measurements, we performed a one-time fertilization of each bole to test for sensitivity to nutrient addition. Specifically, one collar per bole received 50 mL of nutrient solution (hereafter *NPK addition*) and the other collar received 50 mL of distilled water (*H_2O addition*). The nutrient solution contained total amounts of N, P, and K commonly used in other fertilization experiments (described by Kaspari et al. 2008). Specifically, we fertilized the collars with the

equivalent of 125 kg N ha^{-1} (as NH_4Cl), 60 kg P ha^{-1} (as KH_2PO_4), and 75 kg K ha^{-1} (as KH_2PO_4). Respiration rates were measured 3, 11, and 18 days after treatment application.

Differences in chemical composition and the historic interactions with biotic or abiotic factors (e.g., insects, pathogens, and soil contact) are important to bole decomposition, yet they were unknown in this study. By pairing NPK and water treatments, our intent was to control for chemical composition and bole history. We assessed the magnitude of the respiration response to NPK and water addition by calculating the percentage change in respiration rates from average pre-treatment respiration of each collar.

Core collection and elemental analysis

We also compared the elemental composition of each fertilized bole prior to NPK and H_2O addition. We collected a small core (2 cm diameter, 2 cm depth) from the top of each bole and 5 cm from each respirometry collar. Wood cores were oven-dried (60˚C) and ground with a Wiley-Mill before chemical analysis. Total carbon and nitrogen were determined by elemental analysis (Thermo Flash EA1112, CE, Elantech, Lakewood, NJ, USA), while concentrations of mineral elements (P, K, Na, Zn, Ca, Mn, Mg, Al, B, Cu, Fe) were determined by nitric acid digestion at 180°C under pressure in PTFE vessels, with detection by inductively-coupled plasma optical-emission spectrometry (ICP-OES) on an Optima 7300 DV (Perkin Elmer, Inc, Shelton, CT). Analytical quality was confirmed in both procedures using the NIST peach leaves standard. All elemental analyses were performed in the Soils Laboratory at the Smithsonian Tropical Research Institute.

Statistical methods

Analyses were performed in the R statistical environment (R Core Team 2016) using the lme4 and lmertest packages for logistic regression and linear mixed effects models (Bates et al. 2014, Kuznetsova et al. 2016) and the vegan package for multivariate analyses *(*Oksanen et al. 2007*)*. The significance of each term in the models was determined by comparing nested models with likelihood ratio tests. We sequentially dropped terms according to AICs and likelihood ratio p-values until a minimum adequate model was identified (Pinheiro and Bates 2000, Bolker et al. 2009). Finally, we examined residuals to confirm appropriate model fit.

We compared the likelihood of complete decomposition of boles among litter manipulation treatments using the initial bole survey data. We used a generalized linear mixed effect model (*glmer* function; logistic regression) with a binary response variable: either the bole was present in 2016 or had completely decomposed. We approximated bole "size" at the time of death as the product of basal area and density (*cross-sectional mass*) because basal area and initial density were correlated and would violate the assumption of independence (R = -0.36, t = 5.57, df = 212, $p < 0.001$). We included litter treatment, bole age, and cross-sectional mass as fixed effects and plot as a random effect. The random effect 'plot' did not affect the fit of the model, likely because the tested phenomenon occurs at a smaller scale than a plot, and therefore we removed this term to identify the minimum adequate model. The grouping effect 'plot' was removed from all other linear models after being similarly tested. The interactions between cross-sectional mass and the other predictors were sequentially dropped because they did not affect the fit of the model. To further investigate the interaction between litter manipulations and bole age, we performed pairwise comparisons among litter treatments with the same three main effects as above and the interaction effect between bole age and litter treatment (*glm* function). We log-transformed cross-sectional mass

to improve the model fit. Finally, we used the Bonferroni correction to account for multiple comparisons using the same data.

Although tree species characteristics (e.g., chemical composition and wood density) influence decomposition, we could not directly account for tree species in our linear models because species were not evenly distributed across litter treatments (71 of 74 species were present in ≤1 replicate set of plots). Alternatively, we considered the species composition of dead trees among litter treatments using perMANOVA (Bray-Curtis distance) and pseudo-F values. The perMANOVA included litter treatment and bole status (completely decomposed or remaining in 2016) as fixed effects and plot as a random effect. We also performed blocked indicator species analysis (PC-ORD v6.08) for bole status to identify tree species with particularly labile or recalcitrant wood and to statistically control for the effects of litter treatment (Dufrene and Legendre 1997). Apart from these multivariate tests, we accounted for species effects using species-specific density in the logistic regression and elemental composition in models for the NPK and H_2O manipulation experiment.

We used a linear mixed effects model (*lmer* function) to compare respiration rates among litter treatments. For boles that supported two respiration collars, we used the means of measurements that occurred on the same day. As respiration rates are influenced by wood decay status and decomposition rates differed among treatments (see results), we used bole density remaining (defined above) instead of bole age as a proxy for decomposition status. The initial model therefore included litter manipulation treatment and bole density remaining as fixed effects and the unique bole identifier nested within plot as random effects. We tested for differences among litter treatments using a post-hoc Tukey HSD test.

We used this same model to compare the elemental concentrations of boles used in the NPK limitation experiment. We also considered interspecific differences in chemical composition by exploring differences in elemental composition among fertilized boles with a Principal Components Analysis using standardized variables (Table 6). We fit each input variable as a vector to the ordination (*envfit* function) to visually display which elements best explained the separation of boles along the first two ordination axes.

Finally, we compared the change from baseline respiration rates among litter treatments after NPK and H_2O addition using a repeated measures mixed-effect model. Litter manipulation and NPK/H_2O treatment were included as fixed effects, and both plot and unique bole identifier were random effects. For repeated measures covariance, bole identifier was the subject and the days post-treatment was the repeated measure. We included the scores from the first two PCA axes as covariates to account for differences in elemental composition. The bole identifier term standardized our nutrient addition comparisons within a single bole and thereby accounted for the effects of bole history and chemical composition when comparing NPK and H_2O treatments (analogous to the structure of a paired t-test). To further explore the interaction effect between litter manipulations and nutrient addition, we made pairwise comparisons between nutrient additions within each litter addition treatment.

RESULTS

Bole decomposition

The likelihood that boles decomposed completely was affected by the initial size of the bole, bole age, and the litter treatment. In all cases, the likelihood of decomposition increased with lesser initial cross sectional mass ($\chi^2_1 > 28.46$, $p < 0.001$, $\alpha = 0.0167$) and greater bole age ($\chi^2_1 \geq 28.87$, $p < 0.001$, $\alpha = 0.0167$, Figure 5). However,

the likelihood of a bole completely decomposing during the 15-year study was not consistent among the three litter manipulation treatments (treatment x bole age interaction: $\chi^2_2 = 6.67$, $p = 0.036$, Figure 5). Specifically, the pattern of bole decomposition with increased bole age differed between the control and litter removal treatments (pairwise treatment x bole age interaction: $\chi^2_1 = 5.86$, $p = 0.015$, $\alpha = 0.0167$). Decomposition was similar between control and litter removal plots in the short-term, but the long-term probability of complete decomposition in control plots was substantially higher than in removal plots (Figure 5). The probability of complete decomposition was marginally significantly greater in the litter addition treatment than in the litter removal treatment (pairwise comparison: $\chi^2_1 = 5.42$, $p = 0.02$, $\alpha = 0.0167$), whereas bole decomposition was similar in the litter addition and control treatments (pairwise comparison: $\chi^2_1 = 0.016$, $p = 0.899$, $\alpha = 0.0167$).

Tree species effects

Neither tree species nor species-related characteristics influenced differences in the probability of decomposition among litter treatments. Both predictors in the best-fit model, bole age ($\chi^2_2 = 1.94$, $p = 0.38$) and initial cross-sectional mass ($\chi^2_2 = 4.07$, $p = 0.13$), did not differ among litter treatments. Moreover, tree species composition was similar among litter treatments (pseudo-$F_{2,23} = 0.54$, $p = 0.99$, Appendix II: Figure S1). By contrast, the composition of tree species that had completely decomposed during the 15-year study differed from the tree species that remained in 2016 (pseudo-$F_{1,23} = 2.24$, $p = 0.001$). Indicator species analysis revealed that *Tetragastris panamensis* (IV = 38.5, $p = 0.021$), *Lonchocarpus heptaphyllus* (IV = 30.8, $p = 0.048$), and *Zanthoxylum acuminatum* (IV = 30.8, $p = 0.058$) had a large proportion of boles remaining and thus were identified as species with potentially recalcitrant wood. Only *Cordia bicolor* (IV =

42.9, p = 0.017) was indicative of completely decomposed boles and therefore was identified as a species with particularly labile wood.

Wood respiration and NPK addition

Respiration rates from decomposing wood differed among litter treatments (χ^2_2 = 8.63, p = 0.013, Figure 6). Specifically, wood respiration rates in control plots were approximately 60% greater than those in litter removal plots (Tukey HSD: z = 2.83, p = 0.013). Wood respiration rates in litter addition plots were intermediate and did not differ significantly from either control or litter removal plots (Tukey HSD: z < 2.06, p > 0.10). Respiration rates were unaffected by bole density remaining (χ^2_1 = 0.39, p = 0.53, α = 0.0167).

Changes in respiration rates in response to NPK and H_2O additions differed among litter treatments (Figure 7, litter treatment x NPK/H_2O addition interaction: χ^2_2 = 10.61, p = 0.005, α = 0.0167). NPK addition increased wood respiration rates more than H_2O addition in the litter removal (χ^2_1 = 7.13, p = 0.008, α = 0.0167) and litter addition plots (χ^2_1 = 12.85, p < 0.001, α = 0.0167). By contrast, the NPK addition did not change wood respiration rates more than H_2O in the control plots (χ^2_1 = 1.06, p = 0.304, α = 0.0167). Regardless of treatment, scores from PCA axes 1 and 2, representing bole chemical properties, were not related to changes in respiration (χ^2_1 < 0.671, p > 0.413). Respiration rates of NPK and H_2O treatments were consistent between 3 and 18 days post-treatment (X^2_1 < 1.75, p > 0.417) and bole density remaining did not differ among treatments (X^2_2 = 2.75, p > 0.254).

Wood chemistry

The first two PCA axes from the ordination of bole chemical properties explained nearly 50% of the variation in the elemental composition of old boles (Figure 8). Boles

from litter addition and removal treatments separated along PCA axis 2, but there was no clear separation between either litter treatment and the controls. PCA axis 2 loadings (loading > 0.3) indicated that concentrations of Ca, K, Mg and Na were higher in litter addition boles, whereas B, C, N, and Zn were all greater in the litter removal boles (Table 6). PCA axis 1 (31% of variation) explained nearly twice as much variation in elemental composition as PCA axis 2 (17% of variation), but axis 1 was not clearly related to differences among litter treatments.

Despite apparent differences in ordination space, concentrations of individual elements in old boles were generally similar regardless of treatment (Table 5). Neither N concentrations nor ratios of C:N and C:P differed among treatments ($\chi^2_2 > 4.58$, $p > 0.1$). Na concentrations were lower in litter removal plots relative to litter addition plots ($\chi^2_2 = 8.23$, $p = 0.016$, Tukey: $t = 2.78$, $p = 0.015$), but Na concentration in the litter manipulations did not differ from controls (Tukey: $t < 1.53$, $p > 0.27$). Similarly, there was a trend towards lower K in the litter removal plots relative to the other treatments ($\chi^2_2 = 5.15$, $p = 0.08$) and K concentrations were weakly related to bole density remaining ($\chi^2_2 = 2.83$, $p = 0.09$). C and Cu concentrations exhibited interaction effects between bole density remaining and litter treatments ($\chi^2_2 > 8.19$, $p < 0.017$). However, these interaction effects were largely due to a single high-leverage outlier, and thus it is unlikely that they indicate a biologically relevant response. Concentrations of all other elements (P, Zn, Ca, Mn, Mg, Al, B, Fe) were similar among treatments ($\chi^2 < 4.06$, $p > 0.13$). Calcium and K concentrations were correlated with bole density remaining ($\chi^2_1 > 5.7$, $p < 0.02$), but bole density remaining was unrelated to nutrient concentrations for Al, B, Fe, Mg, Mn, N, P, and Zn ($\chi^2_1 < 2.07$, $p > 0.15$).

DISCUSSION

The controls of CWD decomposition, particularly exogenous factors such as nutrient availability, remain poorly understood. Here we provide experimental evidence that litter is important to CWD decomposition and that the effects of litter manipulation on wood decomposition are mediated by nutrient availability. These differences in decomposition outcomes were only apparent after 6 years (Figure 5), and the directional differences in these outcomes among litter treatments were counter to a previous, co-located experiment using small substrates over a short time frame.

Greater availability of macronutrients is generally expected to increase decomposition rates, but relevant data for CWD are lacking (Harmon et al. 1986, Chen et al. 2015). A previous short-term study (70 days) in the GLiMP plots concluded that increased nutrient availability explained faster rates of birch stick decomposition in the litter addition treatments relative to removal and control treatments (Sayer, Tanner and Lacey 2006). By contrast, respiration rates (Figure 6) and long-term CWD decomposition (Figure 5) did not differ between the litter addition and control treatments in our study. In terms of nutrients, decomposer respiration rates in the litter addition plots were relatively nutrient limited (Figure 7) despite greater soil inorganic N and resin-P measured previously. It is likely that differences between our study and the earlier study from these same plots (Sayer et al. 2006) were caused by substrate effects (decomposition of birch sticks versus CWD) and a difference between the short and long-term effects of litter manipulations, as suggested by the interaction effect between litter treatment and bole age (Figure 5). The moderate increases in soil nutrients did not influence long-term decomposition, and the contrasting results demonstrate that short-term and small-scale experiments (such as Sayer et al. 2006) are not necessarily predictive of the long-term outcomes for CWD.

Results from the litter removal plots provide direct and indirect evidence that reduced soil nutrients decreased long-term rates of CWD decomposition. The importance of soil nutrients during CWD decomposition was clearly established by previous work (Swift 1977, Zimmerman et al. 1995), and experiments at our study site demonstrated that P and K limit decomposition of more labile substrates (Kaspari et al. 2008). Without litter inputs, long-term decomposition rates decreased, soil P concentrations were reduced (as were soil Ca, Mg, and inorganic N; Sheldrake et al. 2017a), and there was a trend towards decreased K concentrations in old boles in the litter removal plots. Moreover, experimental NPK addition provided direct evidence that the activity of wood decomposers in the litter removal plots is limited by N, P, and/or K availability (Figure 7). Finally, there was a greater proportion of standing dead trees (*snags*) in the litter removal plots than in controls or litter addition plots (Appendix II: Table S2), suggesting that decreased decomposition rates increased snag residence time. This potentially explains the interaction between litter treatment and bole age – snags decompose more slowly than downed boles (Harmon et al. 1986, Song et al. 2017) and the accumulation of snags should have a positive feedback effect that further reduces long-term CWD decomposition rates. Cumulatively, these results suggest that reduced nutrient availability decreased wood decomposition rates, and thus soil nutrient availability is important to long-term CWD decomposition.

Apart from N, P, and K, it is likely that other nutrients influence wood decomposition. In the same forest used for our study, fertilization with a combination of other nutrients (B, Ca, Cu, Fe, Mg, Mn, Mo, S, and Zn) increased leaf litter decomposition more than N, P, and/or K (Kaspari et al. 2008). The soil concentrations of two of these nutrients, Mg and Ca, were lower in the litter removal plots, but the relative concentrations of Mn, Al, and Zn were unchanged (Sayer et al. 2012, Sheldrake et al. 2017a) and the others were not quantified. The PCA indicated that the elemental

composition of boles differed between litter manipulations (Figure 8), but high variation in the concentrations of individual nutrients likely obscured biologically relevant differences among litter treatments (mean coefficient of variation ± SD: 108 ± 74).

Only sodium (Na) concentrations in boles differed among litter treatments (addition > removal, Table 5). This is potentially important because Na influences decomposition (Kaspari et al. 2009) and catalyzes the use of N and P by soil invertebrates (Kaspari et al. 2017) and potentially other saproxylic eukaryotes. A detailed investigation of how Na influences CWD decomposition was beyond the scope of this study, but our results suggest it is worthy of future exploration.

It is also likely that changes in microbial community structure decreased CWD decomposition rates in the litter removal plots. Although total soil microbial biomass did not differ among litter treatments (Sayer et al. 2012), communities of arbuscular mycorrhizal fungi were significantly altered in the litter removals (Sheldrake et al. 2017a) and similar substrate addition experiments changed bacterial communities as well (Nottingham et al. 2009). Reduced nutrient availability in the litter removal plots potentially limited fungal growth (Swift 1977, Kaye and Hart 1997, Sheldrake et al. 2017a) and it is possible that the lack of litter substrate for decomposition decreased the biomass of fungal saprotrophs. Without sufficient nutrients or substrate, the resulting fungal community is potentially optimized for other strategies (e.g., scavenging for soil nutrients and symbiosis with plants, Zimmerman et al. 1995, Sheldrake et al. 2017a; Sheldrake et al. 2017b) leading to reduced wood decomposition.

Tree species effects likely caused substantial variability within the patterns observed in our study. Although bole species composition was similar among litter treatments (Appendix II: Figure S1), most species had low replication and thus the statistical power of this comparison was limited. We identified three relatively

recalcitrant tree species and one relatively labile species. The separation of these species suggests that shade-tolerant species (e.g., *Tetragastris panamensis* and *Lonchocarpus heptaphyllus*) are likely to have recalcitrant wood, whereas certain pioneer species have particularly labile wood (*Cordia bicolor*; Ruger et al. 2009). However, these results were potentially influenced by unbalanced sample sizes. Wood density and concentrations of nutrients, lignin, and other compounds differ among species and profoundly affect decomposition (reviewed by Harmon et al. 1986). Consequently, we used proxy variables (wood density and chemical composition) to consider the role of tree species. Given these considerations, our results demonstrate that the influence of litter manipulation was strong enough to emerge despite unstructured variation in tree species composition between treatment blocks.

Temporal differences in bole selection, year-to-year decomposition dynamics, and environmental effects potentially influenced the patterns observed in our study. Boles omitted from this study tended to be smaller and denser than boles that were retained (Appendix II: Table S1), and respiration measurements required structurally stable boles that are likely more recalcitrant than average. However, both of these differences were consistent among litter treatments and unlikely to affect the observed differences in decomposition. Given that our study was performed across a chronosequence, we only captured outcomes of long-term decomposition, which we related to single time-point measurements of respiration and relative differences in nutrient limitation. Thus possible year-to-year differences in decomposition within and among litter treatments were not considered. Moisture and temperature are important controls of decomposition, but previous measurements indicated that neither soil moisture content nor temperature differed among litter treatments (Sayer and Tanner 2010b). Given the unusually large sample size (n = 214) and multiple lines of evidence, it is unlikely that these caveats affected our finding of nutrient limitation of decomposition

in the litter removal plots. However, these sources of error could have obscured other biologically significant responses, such as our unsupported prediction that increased nutrient availability in the litter addition plots would increase decomposition and respiration rates.

In general, studies of wood decomposition aim to understand how carbon and other nutrients return to the atmosphere and biosphere. Short-term studies of small substrates provide a great foundation for understanding how endogenous (e.g., size, chemical composition, density) and exogenous (e.g., nutrient availability, climate, organismal effects, and their complex interactions) factors control wood decomposition (reviewed by Harmon et al. 1986, Cornwall et al. 2009). However, CWD comprises the majority of all wood mass and, to date, studies of factors that control long-term decomposition of entire boles are limited to the effects of substrate characteristics (species, size, density, and chemistry; Lang and Knight 1979, Brias et al. 2006, van Geffen et al. 2010) and climate (Chambers et al. 2000, Přívětivý et al. 2016). Conspicuously missing from the literature are experimental manipulations of exogenous factors, such as nutrient availability, that influence CWD decomposition.

Using litter manipulations, we provide evidence that soil nutrients are partially responsible for maintaining long-term rates of CWD decomposition, but moderate increases in soil nutrient availability do not meaningfully affect decomposition or wood respiration. Moreover, our results suggest that short-term studies potentially miss biologically important effects. To improve our understanding of decomposition and carbon cycling, further experimental manipulations of CWD decomposition are necessary, particularly investigations into the roles of exogenous nutrient availability, decomposer organisms, and their interactions (Fukami et al. 2010). We suggest that

long-term CWD experiments be paired with more traditional manipulations of small substrates to test the connection between short-term and long-term decomposition.

TABLES

Table 5. Elemental concentrations (±SE) of old boles distributed among the three litter manipulation treatments prior to NPK addition. Superscript letters denote differences among treatments. Sample sizes (N) indicate the number of total samples, but two separate samples were taken from each individual bole.

Elements	Control (N = 12)	Litter Addition (N = 18)	Litter Removal (N = 10)
Al (mg/g)	6.01 (4.28)	1.19 (0.49)	4.71 (2.46)
B (mg/g)	0.01 (<0.01)	<0.01 (<0.01)	0.01 (<0.01)
C%	42.10 (1.39)	43.16 (0.58)	46.42 (1.26)
Ca (mg/g)	6.50 (0.94)	13.01 (2.52)	6.56 (1.38)
Cu (mg/g)	0.01 (<0.01)	0.01 (<0.01)	0.02 (0.01)
Fe (mg/g)	4.97 (3.46)	1.01 (0.41)	4.20 (2.22)
K (mg/g)	0.67 (0.12)	0.63 (0.09)	0.39 (0.06)
Mg (mg/g)	0.28 (0.09)	0.39 (0.11)	0.31 (0.08)
N%	0.74 (0.10)	0.69 (0.07)	1.04 (0.13)
Na (mg/g)	0.08^{ab} (0.02)	0.12^{a} (0.01)	0.05^{b} (0.01)
P (mg/g)	0.07 (0.02)	0.07 (0.02)	0.07 (0.02)

Table 6. The PCA loadings for axes 1 and 2 reported along with the results of vector fitting for each variable (R-squared). These values are from older boles used in the NPK limitation experiment before they were treated with aqueous NPK.

Variable	PC1 loadings	PC2 loadings	R^2
Al	0.95	-0.04	0.81
B	0.61	-0.35	0.44
C	-0.58	-0.47	0.50
C:N	-0.39	0.59	0.44
Ca	0.33	0.53	0.35
Cu	0.32	0.00	0.09
Fe	0.95	-0.06	0.81
K	0.42	0.54	0.42
Mg	0.56	0.49	0.50
Mn	0.96	0.00	0.81
N	0.23	-0.75	0.54
Na	0.02	0.77	0.53
P	0.58	0.14	0.31
Zn	0.71	-0.48	0.64
Bole density remaining	0.26	-0.02	0.06

FIGURE LEGENDS

Figure 5. The log odds of complete decomposition (with 95% confidence interval) for boles in different litter manipulation treatments considering both their age and initial cross-sectional mass (litter removal: triangles and dashed line; litter control: squares and solid line; litter addition: circles and dotted line) across a 15 year chronosequence of tree death in lowland tropical forest in Panama. Greater log odds correspond with greater likelihood of complete decomposition, whereas lesser log odds indicates reduced likelihood of decomposition.

Figure 6. Average wood respiration rates (CO_2 efflux ± 95% confidence interval) of decomposing boles in litter addition, litter removal and control treatments (n= 28 for each litter treatment).

Figure 7. Change in wood respiration (%) for older boles (> 3 years old) in response to both NPK and water addition. Changes in respiration presented here are averages from three different measurement periods over 18 days. The treatments were divided among litter addition (circles and dotted line), litter removal (triangles and dashed line), and litter control treatments (squares and solid line).

Figure 8. PCA ordination of the elemental concentrations of boles from the NPK limitation experiment. Each point represents the average elemental concentrations of a bole and boles are grouped by litter manipulation treatment. Vectors indicate the direction and magnitude of correlations ($R^2 > 0.3$) among elemental concentrations of each bole (Table 6). Note that Mn, Fe, and Al overlap in the positive direction along the X axis. Ellipses are the 95% confidence interval wherein the centroid for boles of each litter treatment is located (addition = dashed, removal = dotted, control = solid).

Figure 5

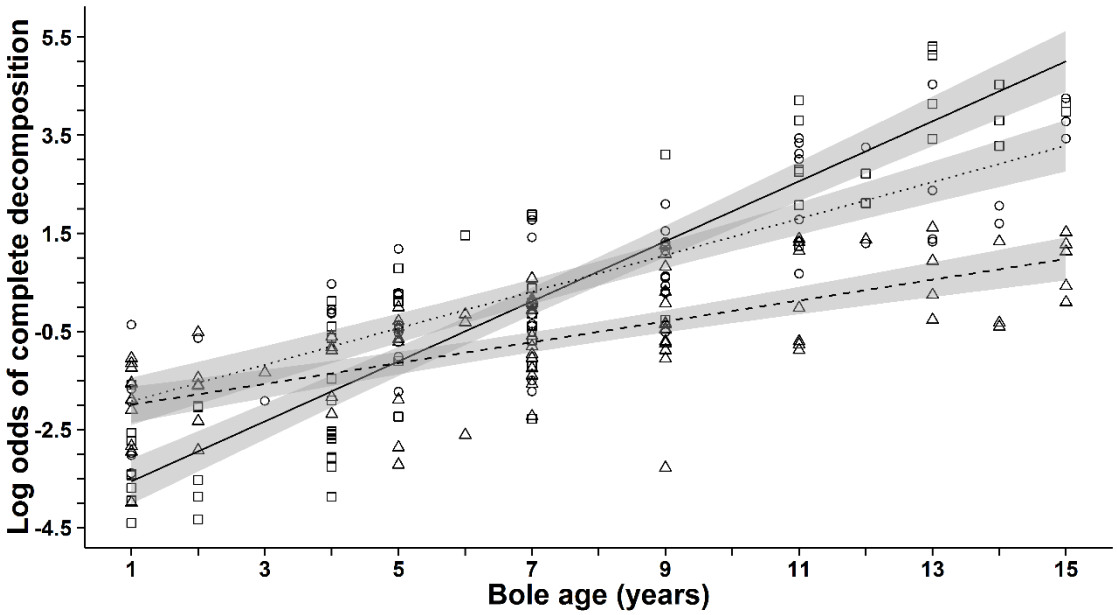
Log odds of complete decomposition
5.5
3.5
1.5
-0.5
-2.5
-4.5
1
3
5
7
9
11
13
15
Bole age (years)

Figure 6

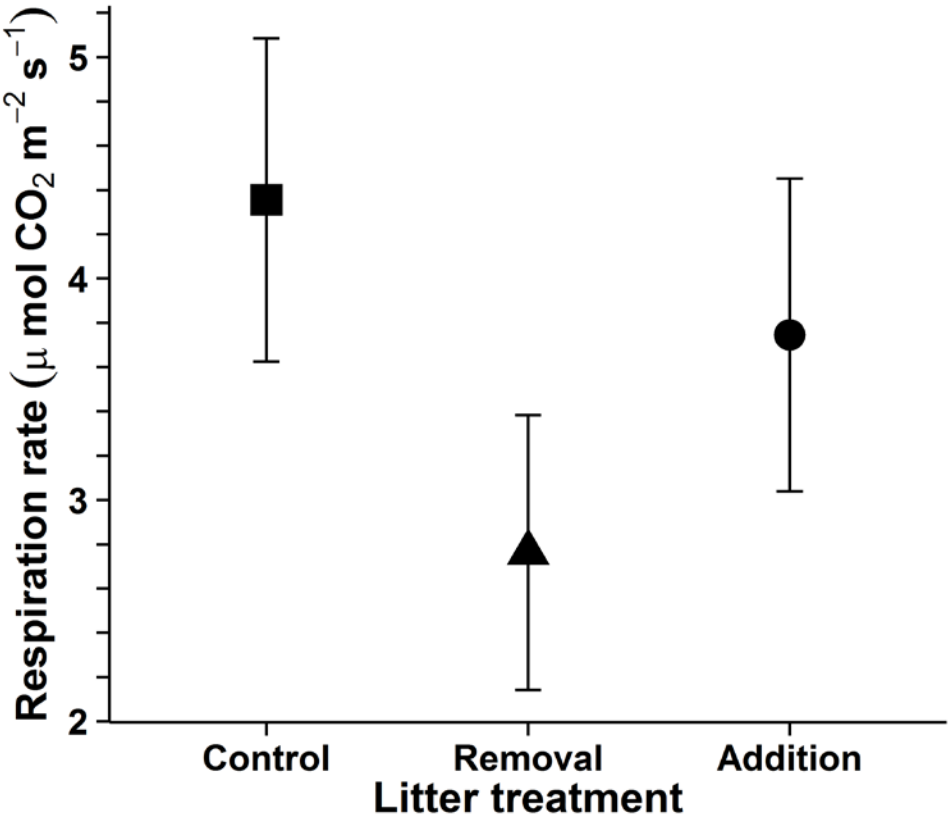
Respiration rate (μ mol CO2 m−2 s−1)
5
4
3
2
Control
Removal
Addition
Litter treatment

Figure 7

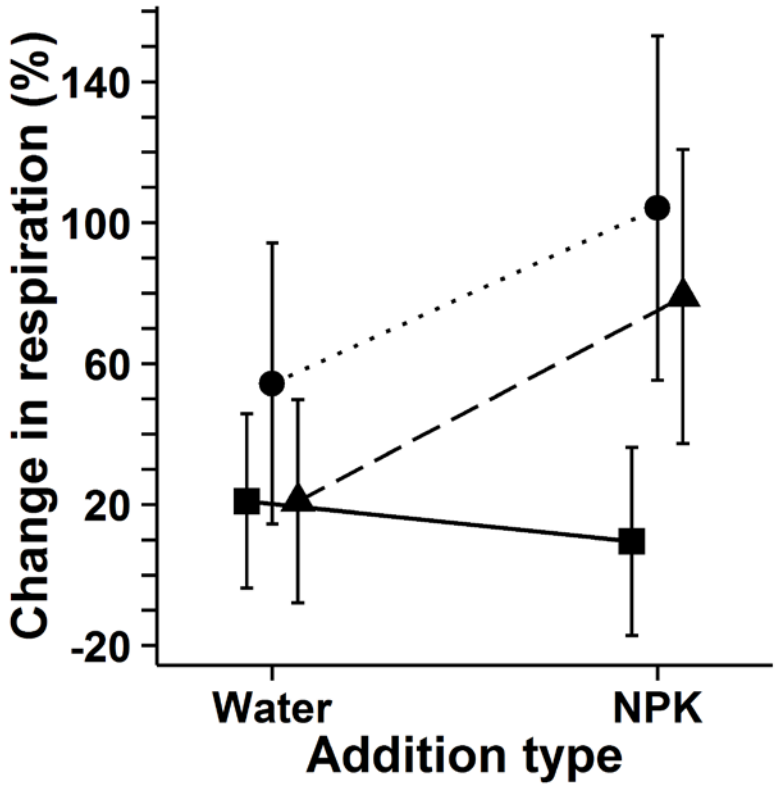
Change in respiration (%)
140
100
60
20
-20
Water
NPK
Addition type

Figure 8

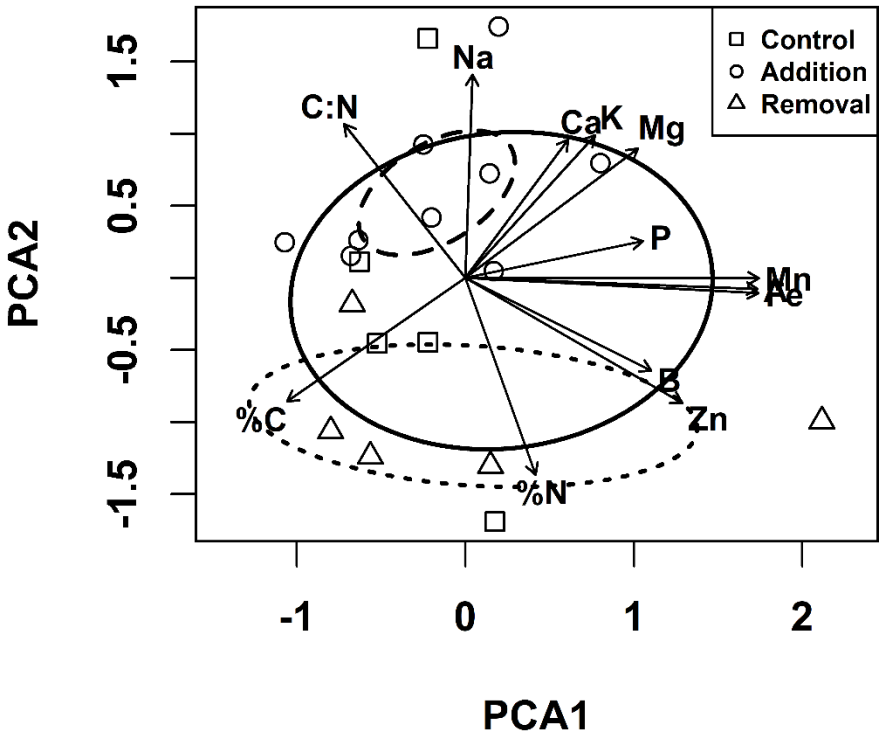
Control
Addition
Removal
Na
C:N
Ca
K
Mg
P
Mn
Fe
B
Zn
%C
%N
PCA1
PCA2
-1
0
1
2
-1.5
-0.5
0.5
1.5

CHAPTER IV

DECOMPOSITION FROM THE GROUND TO THE CANOPY OF A TROPICAL FOREST: A VIEW OF MICROBIAL COMPOSITION AND FUNCTION

SUMMARY

Carbon cycling models typically focus on regional abiotic conditions and local biotic effects as key drivers of variation in wood decomposition rates. However, at least half of all dead wood decomposes *in situ* above the forest floor, and the local processes regulating decomposition of suspended wood remain unclear. Here I used standardized, sterile wood sticks to quantify vertical patterns of microbial (fungal and prokaryotic) community structure, wood decomposition rates, and microclimatic conditions in a tropical forest. The successional trajectories of saproxylic fungal and bacterial communities were strongly correlated, and differed compositionally and functionally along a vertical forest gradient. Patterns of phylogenetic dispersion suggest that environmental filtering regulates microbial community assembly in the forest canopy, whereas competitive interactions are more important on the forest floor. A mechanistic model showed that decomposition rates vary predictably based on microclimate variability and fungal assemblage composition. However, because abiotic conditions

also regulate community assembly, microclimate is the primary factor controlling local rates of decomposition in this forest. Collectively, these results indicate that environmental factors regulate decomposition across all spatial scales, challenging the ground-based assumption that biotic processes are more important locally. Understanding the relative contributions of environmental and biotic factors to decomposition across forest height will inform carbon cycling models.

INTRODUCTION

Carbon cycling models rely on the accurate quantification of decomposition rates across multiple spatial scales (Adair et al. 2008, Bradford et al. 2014). Dead wood is particularly important to these models as it constitutes 73 ± 6 Pg C globally and contributes 10-20% of CO_2 emissions from tropical forests – the largest global terrestrial carbon sink (Brown 1997, Pan et al. 2011, Palace et al. 2012). It is widely accepted that abiotic factors control decomposition globally, whereas biotic effects (wood traits and decomposer organisms) regulate decomposition at regional and local scales (Parton et al. 2007, Adair et al. 2008, Cornwell et al. 2009, Bradford et al. 2014, Zanne et al. 2015). However, evidence for these patterns comes almost entirely from measurements of ground-level decomposition. This approach is somewhat flawed because, at any given time, at least half all dead wood is decomposing above the forest floor (either as elevated, suspended, or standing dead wood – hereafter collectively referred to as *suspended dead wood*; Ovington and Madgwick 1959, Christensen 1977, Gora and Muller-Landau in prep). Without information regarding the decomposition of suspended dead wood, the local factors that regulate wood decomposition are essentially unknown.

One of the most important local regulators of decomposition rates, microbial community structure (richness, diversity, and composition), should differ predictably

from the ground to the canopy of tropical forests. This vertical gradient is characterized by dramatic differences in abiotic factors, and microbial taxa depend on specific habitat conditions for successful colonization (i.e., environmental/habitat filtering; Kivlin et al. 2014, Freedman and Zak 2015). Specifically, environmental conditions shift from a wet and dark environment on the forest floor to an arid environment with extreme exposure to sunlight, a natural disinfectant, in the canopy (Juniper 1991, Beattie and Lindow 1995, Parker 1995). Propagule pressure (e.g., fungal spore density) also decreases with canopy height due to differences in dispersal distance and abilities (i.e., dispersal limitation; Gilbert and Reynolds 2005, Nemergut et al. 2013, Albright and Martiny 2017). Because habitat filtering likely increases with height and typically exhibits a trade-off with competitive interactions (Tilman 1988, Webb et al. 2002), competition should be relatively more important to community assembly on the forest floor than at higher vertical positions.

Variation in microbial community assembly has important effects on decomposition rates (Fukami et al. 2010, Fukami 2015). In most cases, the assemblage structure of saproxylic (i.e., dead wood inhabiting) fungi is the principal determinant of wood decomposition rates (Boddy et al. 1989, van der Wal et al. 2015). Co-occurring prokaryotes also influence decomposition both directly and via interactions with fungi (reviewed by Johnston et al. 2016). Although vertical patterns of saproxylic microbial composition are poorly described, both decomposition rates and microbial diversity tend to decrease above the forest floor. Small branches decompose slower when suspended in the understory than on the forest floor (Fasth et al. 2011), and even "downed" logs that are partially elevated decompose ca. 40% slower than those with more soil contact (Přívětivý et al. 2016). Morphospecies surveys suggest that the diversity of saprotrophic fungi decreases with increasing height (Stone et al. 1996, Unterseher and Tal 2006; reviewed by Lodge and Cantrell 1995). The diversity of phyllosphere bacteria also tends

to decline with height within forests (Andrews et al. 1980, Griffin and Carson 2015), but research on bacterial communities in forests is still a young field (Lambais et al. 2006, Kembel et al. 2014); to my knowledge there is no information regarding the vertical distribution of saproxylic prokaryotes. Moreover, variation in relationships between any combination of decomposition, microbial communities, and abiotic conditions along vertical gradients within forests remain unexplored. Here, I provide the first quantitative assessment of such variation.

I hypothesized that variation in rates of wood decomposition along vertical gradients within tropical forests is associated with microbial community structure. To test this hypothesis, I quantified differences in microclimate, decomposition rates, and microbial community structure (i.e., richness, diversity, composition) at multiple points between the ground and the emergent layer of a tropical forest. I evaluated three specific predictions. First, I expected that decomposition rates along this vertical gradient are strongly correlated with fungal community composition, but only weakly associated with microclimate and bacterial composition. Second, I predicted that bacterial composition shifts from primarily decomposers on the forest floor to primarily photosynthetic and nitrogen fixing taxa in higher levels of the forest. Finally, I expected phylogenetic dispersion to reflect a vertical shift in the dominant community assembly process from competitive interactions on the forest floor to environmental filtering on suspended dead wood. I tested this hypothesis over two years using a decomposition experiment in a lowland tropical forest.

METHODS

Study site

All field work was performed in the seasonally moist lowland tropical forest on Barro Colorado Island (BCI) in central Panama (09.210°N, 79.745°W). Mean annual

temperature is 26˚C and mean annual rainfall is ca. 2600 mm, concentrated during a long wet season (mid-May to December). Additional details about the site are provided elsewhere (Croat 1978, Leigh 1999).

Experimental substrates

I focused my measurements on 10 emergent trees that are seasonally deciduous (9 *Pseudobombax septenatum* and 1 *Cavanillesia platanifolia*, Appendix III: Tables S1-2). Sampling was conducted along vertical transects on each tree in a randomized complete block design. Specifically, I recorded data at five vertical positions: forest floor (or leaf litter), understory, subcanopy, canopy, and emergent, following historical uses of this terminology (Parker 1995). I based the location of each position on the relative height of surrounding vegetation and used the single-rope climbing method to conduct sampling at same locations over 2 years (Perry 1978). In the dry season of 2015, I measured decomposition, moisture mass, and microclimate (see below) in only 5 trees, but all 10 trees were used for remaining data collection (Appendix III: Table S1).

Using a traditional litter bag technique (Bocock and Gilbert 1957), I quantified decomposition as mass loss from standardized cellulose (9 cm diameter, Whatman quantitative filter paper) and wood popsicle stick substrates (11.5 x 1.0 x 0.15 cm, *Betula sp.*). Before placement in the field, substrates were sterilized with ethanol, oven dried, and weighed to the nearest 1.0 mg on an electronic balance. They were then separated within mesh litter bags (0.5 cm diameter mesh) and placed within the leaf litter or attached to tree trunks using insulated wire and nails at each relative vertical position. To compare seasonal patterns of decomposition, the litter bags remained at each tree for only the wet season (May-November 2015, June-November 2016) or dry season (December-May 2015, December-June 2016).

Within 5 hours of collection, samples were cleaned to remove attached soil before being weighed to the nearest 1.0 mg to record wet mass. I then dried samples at 60˚C to a constant weight, which I recorded as dry mass. Decomposition was estimated as the percent of initial mass lost. Moisture content (%) equaled the difference between final wet mass and final dry mass, divided by final wet mass. Nearly all samples decomposed naturally; however, some samples were omitted from analyses because they were badly disturbed or displaced to unreachable locations (e.g., by monkeys or treefalls; Appendix III: Table S1).

Microclimate

I measured microclimate during a 24-hmy cycle at each location using an environmental data logger (HOBO H08-004-0 with TMCx-HD thermometer, Onset Computer Corporation). The data loggers measured temperature (˚C) and light intensity (lumens) at 10 minute intervals. During each 24-hmy cycle, data were simultaneously recorded at all 5 relative vertical positions in a single tree.

Respiration measurements

I measured respiration from wood sticks (hereafter *wood respiration*) to estimate microbial activity and abundance. At the end of the 2016 wet season, wood sticks were placed in a cylindrical PVC respirometry chamber (20cm length, 7cm diameter) with an attached respirometer (GMP343 CO_2 probe, Vaisala Inc.). I then recorded CO_2 (ppm) every 5 seconds over a 5 minute period and calculated the CO_2 flux per gram of the remaining wood substrate. The initial portion of each recording (ca. 15-45 seconds) was ignored to allow stabilization. Respiration rates were approximated as the slope of the linear portion of the resulting CO_2 accumulation curve (Bréchet et al. 2017). To avoid the confounding effect of photosynthesis, wood sticks were allowed to acclimate to the darkened respirometry chamber for 5 minutes before CO_2 concentrations were recorded.

Microbial community sampling

I collected and stabilized microbial DNA from wood sticks at the conclusion of the wet season in 2015. I stabilized DNA in the field to minimize community turnover during transport from field sites to the lab. Wood sticks were retrieved via climbing and then placed on a stainless steel sampling platform. The platform was sterilized with ethanol, remnant DNA was oxidized with hydrogen peroxide, and the surface was dried with sterile gauze. I then used a 2 mm bit and a battery powered drill (DCD780C2 20V, DeWalt) to grind the wood into a fine powder. DNA from this wood powder was immediately stabilized using Xpedition Soil/Fecal DNA MiniPrep extraction kits (Zymo Research, Inc) and the microbial cells were pulverized via bead beating (1 minute). All samples were then returned to the lab and frozen at -40˚C until extraction was performed according to manufacturer's protocols.

Community structure was assessed separately for prokaryotes (archaea and bacteria) and fungi using DNA barcoding. With the DNA stabilized above, I amplified the V2 region of the bacterial/archaeal 16S ribosomal gene (primers: S-D-Arch-0519-a-S-15 and S-D-Bact-0785-b-A-18; Klindworth et al. 2013) and the fungal ITS1 region (primers: ITSF-1 and ITS2; McGuire et al. 2013). The S-D-Arch-0519-a-S-15 and ITS-F1 primers were modified to include a 16 bp M13 sequence (GTAAAACGACGGCCAG) at the 5' end to allow for the attachment of a unique 12 bp barcode in a subsequent PCR reaction. Barcoded amplicons were cleaned and product was standardized using SequalPrep Normalization plates (ThermoFisher, Inc; Harris et al. 2010). Amplicons were sequenced using a MiSeq instrument with 500 V2 chemistry for paired end reads (2 x 250bp).

Bioinformatics

Illumina sequencing reads were analyzed and demultiplexed using QIIME (Caporaso et al. 2010). Sequencing reads that contained errors in the barcoded region, ambiguities, homopolymers (greater than six nucleotides in length), or an average quality score < 25 were discarded. Primer sequences were trimmed, and chimeric sequences were eliminated using USEARCH (version 6.1) and the "gold" reference database for bacterial and archaea (Edgar 2010), and the UNITE reference data base for fungi (Kõljalg et al. 2013). All sequences were clustered into de novo operational taxonomic units (OTUs) at 97% similarity. Bacterial and archaeal taxonomic classification was assigned via the SILVA reference database (release 119, Quast et al. 2012) using the pyNAST alignment algorithm. Fungal taxonomic classification was assigned using the UNITE reference database (version 7.1, Kõljalg et al. 2013).

Singletons and sequences that could not be assigned Phyla-level taxonomy were omitted (Leff 2016). To account for differences in sampling depth, I rarefied samples to 2635 sequences and 764 sequences for bacterial and fungal taxa, respectively. When possible, I assigned putative functional guilds to fungal OTUs using FunGuild (Nguyen et al. 2016).

Statistical analyses

Most analyses were performed in the R statistical environment (R Core Team 2017). For mixed effect models, I performed nested model reduction based on AIC values and P-values from likelihood ratio tests. However, if all random effects were removed because they did not contribute to the model, I compared model fit using F-statistics instead. In all cases, I examined residuals to confirm appropriate model fits. I used the Bonferroni correction to correct for multiplicity and I report alpha when different from 0.05.

I compared total decomposition as recorded at the end of the dry and wet seasons of 2015 and 2016. I included season (wet or dry), relative vertical position, and their interaction as fixed effects. I also included year (2015 or 2016) and the unique tree identifier (hereafter *tree ID*) as random grouping effects. Year did not contribute meaningfully to the fit of any model, but tree ID was often statistically important. For wood sticks, there was an interaction between relative vertical position and season, indicating that differences among vertical positions were not consistent between seasons. Consequently, I analyzed wood decomposition separately for the wet season and the dry season. I compared OTU richness, diversity indices (Shannon-Weiner for fungal functional groups and beta diversity), and the relative abundance of taxonomic orders of microbial taxa (only those with >1.5% relative abundance) using mixed effect models of similar construction; relative vertical position was a fixed effect and tree ID was a random effect.

I compared overall community structure and microclimate using Primer (Ver. 7.0.13) and R (package *vegan*). All analyses used vertical position as a fixed effect and tree ID as a random effect (9999 permutations). The environmental parameters input to the PCA were maximum light intensity, average light intensity, maximum temperature, minimum temperature, average temperature, and wood moisture content from 2015. Environmental data were re-scaled (0-1) and I used Euclidean distance for environmental comparisons. Microbial community data were square root transformed before calculating Bray-Curtis dissimilarity. I used the community distance matrices to generate ordinations (non-metric multidimensional scaling or NMS) for both bacteria (2 NMS axes) and fungi (3 NMS axes). I fit vectors to these ordinations to visualize associations between the ordinations and either input variables (environmental and bacterial) or putative functions (fungi). I then performed PERMANOVA of the environmental and community distance matrices to compare these factors among

relative vertical positions and individual trees (Anderson et al. 2008). For the microbial communities, I also compared beta diversity among relative vertical positions using PERMDISP tests (Anderson et al. 2008). PERMDISP tests calculate within vertical position dissimilarity in community composition and then compares the magnitude of dissimilarity among relative vertical positions (9999 permutations). Finally, I determined if bacterial and fungal communities co-vary by examining the correlation between the community dissimilarity matrices using a permutation-based Mantel test (Legendre and Legendre 1998).

I also tested a mechanistic model of wood decomposition using axes from the environmental and microbial ordinations. Wet season wood mass loss from 2015 was the response variable and tree ID was again the random effect. The fixed effect predictors were the first three axes of the environmental PCA from the wet season of 2015, all three fungal NMS axes, and both bacterial NMS axes. After selecting the best model using AIC criteria, I then performed dominance analysis to determine the relative contributions of significant terms (package *relaimpo*; Grömping 2006). To determine if biota and environment can predict decomposition better than the physical location of the substrates, the fit of the final model was compared to an alternative that used only relative vertical position as a fixed effect.

Analysis of bacterial phylogenetic dispersion

I compared phylogenetic dispersion among bacterial communities to evaluate the relative importance of competitive and environmental filters (package *picante*;Horner-Devine and Bohannan 2006). Functional similarity is associated with environmental filtering (Weiher and Keddy 1995), and functional similarity among taxa is negatively correlated with phylogenetic distance (Webb et al. 2002, Emerson and Gillespie 2008, Philippot et al. 2010). Phylogenetic distances for this analysis were extracted from a

phylogenetic tree generated using the clustalw method in QIIME (Price et al. 2009). I calculated the mean pairwise distance (MPD) among all individuals because MPD is sensitive to tree-wide patterns of phylogenetic diversity (Webb et al. 2002). Positive values of MPD suggest phylogenetic evenness and greater competitive filtering, whereas negative values indicate phylogenetic clustering and relatively greater environmental filtering. I compared phylogenetic dispersion among vertical positions using the same mixed-effect linear model as described for indices of microbial diversity.

RESULTS

Vertical patterns of community composition and function

Fungal and bacterial communities exhibited directional turnover with increasing height in the forest (Figures 9-10; Appendix III: Tables S3-4). With the exception of canopy-level fungi (which were similar to fungi at both the subcanopy and emergent positions), microbial community composition differed among all vertical positions. The magnitude of dissimilarity increased with distance between vertical positions (See SI for statistical results). These differences persisted despite spatial autocorrelation wherein bacterial and fungal communities within each individual tree were more similar than expected at random. Overall patterns of community similarity were strongly correlated between bacteria and fungi (Mantel test: $R = 0.71$, $p < 0.001$), indicating that these communities are ecologically linked and respond similarly to the same external factors.

Differences in microbial community structure along the vertical gradient were largely due to turnover; i.e., differences in taxa identity, rather than diversity or richness, were primarily responsible for the observed vertical patterns. Bacterial OTU richness decreased with increasing height and fungal beta diversity was greater on the forest floor than in the subcanpy or above (Table 7). However, there were no other differences in OTU richness, beta diversity, or Shannon-Weiner diversity for the composition or

function of bacteria and fungi (Table 7). By contrast, the most abundant orders of bacteria and fungi changed categorically with forest height (Tables 8-9). The dominant taxa at each vertical position were also associated with different putative and inferred functions (Appendix III: Table S5).

Three broad and functionally-based microbial subcommunites were identifiable: the first occurs on the forest floor, the second is distributed across the understory and subcanopy, and the third exists in the canopy and emergent positions. For fungi, the forest floor community was dominated by Agaricales and soil/litter saprotrophs, whereas an entirely distinct community of wood saprotrophs (Pleosporales and Polyporales) defined fungal communities in the understory and subcanopy (Table 8). Fungal community composition was similar between the canopy and emergent positions where endophytes and pathogens were the prominent functional groups. As for bacteria, phylogenetic evenness indicated that litter-level communities were uniquely structured around competitive interactions rather than just environmental filtering (Figure 11). The greater importance of competitive interactions was also supported by the abundance of antagonistic competitors, such as bacterial pathogens (Xanthomonadales) and predators (i.e., Myxococcales; Figure 10). Similar to fungi, the understory and subcanopy bacterial communities were dominated by decomposers that were relatively uncommon on the ground (Table 9). The canopy and emergent communities were also dominated by these bacterial decomposers, but the other prominent orders were primarily photosynthetic (Chlorophyta) and nitrogen fixing (Nostocales) bacteria. Overall, these patterns suggest that small woody debris functions as a substrate for competitive and saprotrophic interactions in the litter, mild saprotrophic activities in middle layers of the forest, and as physical support for photosynthetic and nitrogen fixating taxa in the upper canopy.

I was unable to quantitatively assess Archaea because they were exceedingly rare. In total, I isolated only 41 archaeal sequences distributed among Nitrososphaerales (25 sequences) and the candidate orders WCHD3-30 (2 sequences) and YLA114 (14 sequences). Archaea were concentrated on wood sticks in the leaf litter (80% of sequences) and, to a lesser degree, the understory (10%). Only 4 sequences were isolated from higher vertical positions, and zero archaeal sequences were found at the emergent level of the forest.

Phylogenetic evenness and dispersion

The phylogenetic dispersion of bacteria indicated differences in the strength of environmental and competitive filtering (Figure 11). The phylogenetic evenness of bacterial communities in the leaf litter was not different from random, but evenness in the litter was significantly greater than all other vertical positions (dAIC = 19.2, X^2_4 = 27.2, $p < 0.001$; $z > 4.1$, $p < 0.001$). By contrast, phylogenetic structure was similar among communities above the forest floor ($z = 0.88$, $p = 0.91$) and they exhibited phylogenetic clustering typically associated with strong environmental filtering.

Microclimate

Wet season microclimate exhibited a pattern of vertical gradation similar to microbial community composition (Figure 12; Appendix III: Table S5). The canopy positions separated along PCA axis 1 (54% of variation), indicating that these differences were caused by greater moisture content at lower levels of the forest and elevated levels of maximum and average light and maximum temperature at higher levels of the forest (Figure 12). By contrast, PCA axes 2 (24% of variation) and 3 (13% of variation) generally explained differences within vertical positions and were associated with minimum and average temperature. Differences in microclimate exhibited distinct seasonal patterns as well (season x vertical position interaction: pseudo-$F_{4,56} = 5.32$, $p <$

0.001). By contrast with the wet season, dry season differences in microclimate were driven by contact with the forest floor (pseudo-$F_{4,16}$ = 7.44, p = 0.003; Figure S1). Forest floor microclimate during the dry season differed from all higher levels (pseudo-t > 3.2, p < 0.011), but microclimate was similar among all levels above the forest floor (pseudo-t < 2.50, p > 0.076).

Decomposition

Fungal composition and environmental variability were strongly associated with patterns of wood decomposition during the wet season of 2015 ($F_{4,43}$ = 13.64, p < 0.001, α = 0.025; Table 10). Two axes from each of the fungal and environmental ordinations were predictive of mass loss, and the combined effects of these axes were similar for fungi and environment. Specifically, dominance analysis demonstrated that fungal composition and environmental variation explained 29% and 27% of the variation in decomposition, respectively (Table 10). The combined effects of fungi and microclimate predicted decomposition rate (R^2 = 0.56) better than relative vertical position alone ($F_{4,43}$ = 9.61, p < 0.001, α = 0.025, R^2 = 0.47).

Mass loss from wood tended to be greater during the wet season, but did not differ seasonally in the upper reaches of the canopy, causing an interaction effect between vertical position and season (dAIC = 11.7, X^2_1 = 19.7, p < 0.001; Figure 13). During the wet season, wood decomposed fastest on the forest floor (dAIC =33.5, X^2_4 = 41.5, p < 0.001; z > 4.4, p < 0.001, α = 0.025), but there were no other differences among vertical positions (z < 2.1, p > 0.229). During the dry season ($F_{4,57}$ = 7.1, p < 0.001, α = 0.025), mass loss on the forest floor was greater than in the understory, subcanopy, and canopy (t > 3.9, p < 0.003), and wood decomposed similarly at all levels above the forest floor (t < 1.3, p > 0.71). However, the dry season diverged from the wet season in that mass loss was similar for the litter and emergent levels (t = 1.6, p = 0.49).

Cellulose decomposition differed among vertical positions and between seasons (Figure 13). Cellulose decomposed more rapidly in the wet season than the dry season (dAIC = 18.3, $X^2_1 = 20.3$, $p < 0.001$), and decomposition decreased with height regardless of season (dAIC = 275.1, $X^2_4 = 285.1$, $p < 0.001$). Mass loss from cellulose was similar between the understory and subcanopy ($z = 0.3$, $p = 0.99$) and between the canopy and emergent positions ($z = 0.2$, $p = 0.99$), but these groups differed from each other ($z > 3.1$, $p < 0.018$) and litter-level decomposition was greater than all other vertical positions ($z > 21.8$, $p < 0.001$).

Wood Respiration

Wood respiration, a proxy for microbial biomass and activity, differed among vertical positions at the end of the wet season in 2017 (dAIC = 12.1, $X^2_3 = 18.1$, $p < 0.001$; Figure 14). Wood respiration in the leaf litter was greater than in the understory ($z = 2.84$, $p = 0.023$), subcanopy ($z = 3.81$, $p < 0.001$), and canopy ($z = 4.44$, $p < 0.001$). However, wood respiration was similar among all levels above the forest floor ($z < 1.66$, $p > 0.35$). I lacked sufficient emergent-level samples, and therefore did not include this position in analyses of respiration.

DISCUSSION

The majority of dead wood is decomposing above the forest floor (Ovington and Madgwick 1959, Christensen 1977, Gora and Muller-Landau in prep), yet little is known about processes underlying the decomposition of suspended dead wood. Here I provide evidence that fungi and microclimate collectively control rates of wood decomposition across a vertical forest gradient. I also demonstrate that saproxylic bacterial and fungal community compositions are strongly correlated, and that environmental filters appear to be relatively more important to community assembly aboveground than on the forest floor. Finally, saproxylic microbial community composition and function differentiates

across a vertical gradient, representing a previously unquantified dimension of microbial diversity.

Contrary to my predictions and the current understanding of local decomposition processes (Adair et al. 2008, Bradford et al. 2014), I provide correlative evidence that that microclimate is the primary factor determining local rates of wood decomposition. In addition to the variance explained in the mechanistic model, the phylogenetic clustering aboveground indicates that environmental filtering likely shapes microbial community assembly at most vertical positions. Consequently, the direct and indirect (via community assembly) contributions of microclimate to decomposition are greater than the independent effects of bacteria or fungi. Given evidence that local processes regulate decomposition regionally (Bradford et al. 2014), this suggests that environmental factors control of wood decomposition at local, regional, and global scales.

Although decomposition rates were not associated with bacterial community composition, I cannot conclude that bacterial decomposers were inactive. Bacteria likely were not associated with decomposition rates because they perform decomposition relatively slowly (Greaves 1971, Johnston et al. 2016) and microbial activity decreased with height (Figure 14). Fungal decomposers were abundant where decomposition was fastest (forest floor and understory), but they were rare in the subcanopy and above. By contrast, bacterial decomposers in orders Sphingomonadales and Actinomycetales were the dominant taxa at all positions above the forest floor (Table 8). Of particular importance was the bacterial genus *Sphingomonas*. *Sphingomonas* consists of unusual oligotrophs capable of decomposing recalcitrant aromatic compounds, such as lignin (Masai et al. 1999) and industrial waste products (e.g., *S. wittichii*, Yabuuchi et al. 2001). In addition to *Sphingomonas*, other Actinomycetales and Sphingomonadales are capable

of complete lignin degradation (Bugg et al. 2011, Chen et al. 2012). The contrasting shifts in the abundance of bacterial and fungal decomposers suggests that saprotrophic and ligninolytic bacteria fill a niche in aboveground microbial decomposition.

Differences in the processes underlying community assembly likely contributed to the vertical turnover in community structure observed in my study. Bacterial phylogenetic dispersion indicated that the forest floor community is largely structured by competitive interactions, whereas aboveground communities are strongly regulated by environmental filtering (Webb et al. 2002, Horner-Devine and Bohannan 2006). These phylogenetic patterns could also arise as a result of other processes (e.g., priority effects; Kraft et al. 2015), but the conspicuous vertical changes in abiotic conditions within tropical forests suggest that environmental filtering is the cause. Given the strong correlation between bacterial and fungal community composition ($R = 0.74$), it is likely that fungal community assembly follows the same general patterns. Regardless, vertical turnover in the primary functions of microbial organisms suggests the presence of vertically distinct niches, most of which were previously unexplored.

Seasonal patterns of decomposition and microclimate highlight a potential role for photodegradation in wet tropical forests. There was only one exception to the pattern of faster decomposition on the forest floor than all higher vertical positions – dry season decomposition rates were similar between the emergent and forest floor positions. Decomposition rates in the desert-like conditions (Parker 1995) of the emergent stratum were aseasonal, and respiration results suggest that microbial activity was negligible in the canopy. Consequently, it is likely that abiotic factors regulating emergent-level decomposition in the dry season caused mass loss at similar rates to biotic processes on the forest floor. Photodegredation likely caused this abiotic decomposition – light intensity increases with canopy height (Figures 12, S1) and is greater in the dry season

when leaves are abscised and clouds are less common. The importance of photodegredation for leaf litter is known in arid ecosystems (Austin and Vivanco 2006), but this is the first indication of this phenomenon for wood substrates in tropical forests.

Caveats and conclusions

Conducting this study with standardized and sterilized wood substrates facilitated comparisons of community assembly among vertical positions but, despite its advantages, this approach has some limitations. By using sterile substrates, I did not capture the priority effects of endophytic and epiphytic microbial communities that colonize wood prior to decomposition. These microbial taxa often begin decomposing wood in the canopy and exhibit priority effects on subsequent colonizers (Boddy 2001, Osono 2006, Cline et al. 2018). Standardization of substrates allowed us to exclude many confounding variables that are important in nature, including differences in wood traits (Zanne et al. 2015) and the effects of bark. Bark changes wood microclimate, and many invertebrate taxa, particularly beetles, will only colonize wood with intact bark (Dossa et al. 2016). Lastly, I used small substrates to enable sampling of the complete saproxylic microbiome. However, larger wood substrates decompose differently and support different taxa (e.g., termites) than smaller substrates (Harmon et al. 1986, Ulyshen 2016). Consequently, further work is needed to understand how interactions with invertebrates and phyllosphere microbes shape aboveground microbial community assembly and decomposition rates among diverse wood substrates (e.g., Leopold et al. 2017)).

Despite these considerations, this study is an important first step in understanding the mechanisms regulating rates of aboveground decomposition. Filling this knowledge gap is particularly important given the expectation that changing disturbance regimes (e.g., drought, lightning; Phillips et al. 2009, Greenwood et al. 2017)

will create more standing dead trees and shift the physical distribution of woody debris to higher vertical positions. Moreover, I provide evidence that microclimate is the primary factor regulating rates of decomposition locally and thus climatic effects on local microclimate (e.g., via precipitation) will potentially change future rates of wood decomposition. Understanding the importance of these and related factors will help us understand local processes underlying wood decomposition and their links to carbon cycling.

TABLES

Table 7. Measures of diversity for fungal and bacterial taxa. All values are averages (±SE). Beta diversity is the average distance from the centroid in ordination space. Richness is OTU richness after rarefication and Shannon represents the Shannon diversity index (H).

Vertical position	N	Bacteria		Fungi		Fungal Functional Groups	
		Richness	Beta	Richness	Beta	Beta	Shannon
Forest floor	10	1287[a] (53)	0.51 (0.01)	118 (4)	0.59[a] (0.01)	0.20 (0.02)	1.55 (0.13)
Understory	10	994[bc] (16)	0.48 (0.01)	142 (3)	0.56[ab] (0.02)	0.14 (0.02)	1.78 (0.07)
Subcanopy	10	1047[b] (45)	0.48 (0.01)	127 (2)	0.54[b] (0.01)	0.15 (0.02)	1.65 (0.04)
Canopy	9	852[cd] (46)	0.49 (0.01)	117 (3)	0.53[b] (0.01)	0.17 (0.03)	1.82 (0.06)
Emergent	10	824[d] (55)	0.52 (0.01)	110 (1)	0.54[b] (0.02)	0.17 (0.02)	1.61 (0.06)

Table 8. Mean percentages of total sequences (±SE) within a vertical position for the eleven most abundant phyla and orders of fungi, along with statistical results of comparisons. Superscript letters denote similar abundances and bold text indicates orders that represent more than 5% of total sequences within that vertical position.

Taxanomic level	Phylum/Order	Litter	Understory	Subcanopy	Canopy	Emergent	dAIC	X^2	p-value
Phyla	Ascomycota	45.1 (2.3)^{a}	72.4 (1.4)^{b}	64.2 (2.1)^{ab}	59.2 (1.3)^{ab}	53.6 (2.1)^{ab}	3.9	11.9	0.018
	Basidiomycota	38.8 (2.9)^{a}	8.8 (1)^{b}	27.2 (2.3)^{ab}	20.9 (1.2)^{ab}	34.4 (2.4)^{a}	5.1	13.1	0.011
Orders	Agaricales	**33.8 (3.1)^{a}**	0.8 (0.0)^{b}	0.8 (0.0)^{b}	0.5 (0.0)^{b}	0.9 (0.1)^{b}	32.4	40.4	<0.001
	Capnodiales	**10.1 (0.8)**	**11.6 (0.8)**	**17.2 (1.5)**	**16.9 (1.6)**	**8.8 (0.6)**	2.98	5.0	0.285
	Pleosporales	0.4 (0.0)^{a}	**12.6 (1.3)^{b}**	**11.0 (0.8)^{b}**	**6.7 (0.6)^{ab}**	**5.5 (0.6)^{ab}**	7.36	15.4	0.004
	Polyporales	0.6 (0.1)^{a}	1.3 (0.2)^{ab}	**11.2 (1.8)^{b}**	0.9 (0.2)^{ab}	2.3 (0.5)^{ab}	2.59	10.6	0.032
	Chaetothyriales	2.3 (0.4)	4.6 (0.4)	4.6 (0.3)	**7.1 (0.8)**	7.0 (0.7)	1.7	6.3	0.176
	Tremellales	0.0 (0.0)^{a}	0.4 (0.0)^{a}	2.2 (0.1)^{a}	**6.3 (0.6)^{b}**	3.1 (0.3)^{ab}	16.9	24.9	<0.001
	Orbiliales	0.6 (0.1)^{a}	0.3 (0.0)^{ab}	1.7 (0.2)^{a}	**8.1 (1.0)^{ac}**	**15.7 (1.2)^{c}**	25.8	33.8	<0.001
	Russulales	0.1 (0.0)	0.0 (0.0)	4.9 (1.0)	4.1 (0.9)	**5.1 (0.8)**	-	-	-
	Xylariales	2.3 (0.3)	3.2 (0.3)	3.0 (0.3)	2.4 (0.2)	1.8 (0.2)	6.3	1.7	0.783
	Helotiales	0.5 (0.1)	0.1 (0.0)	4.0 (0.8)	1.6 (0.5)	2.2 (0.3)	1.7	6.3	0.177
	Hypocreales	2.7 (0.3)	3.1 (0.4)*	1.9 (0.2)	0.8 (0.1)	0.5 (0.1)*	2.2	10.2	0.037

Table 9. Mean percentages of total sequences (±SE) within a vertical position for the fifteen most abundant orders of bacteria, along with statistical results of comparisons. Superscript letters denote similar abundances and bold text indicates taxa that represent more than 5% of total sequences within that vertical position.

Order	Litter	Understory	Subcanopy	Canopy	Emergent	dAIC	X^2	p-value
Rhizobiales	**9.9 (0.9)^{a}**	**15.1 (1.5)^{b}**	**13.3 (0.4)^{b}**	**13.6 (1.0)^{b}**	**15 (0.5)^{b}**	13.9	21.9	<0.001
Sphingomonadales	2.3 (0.3)^{a}	**10.4 (1.1)^{b}**	**13.9 (1.9)^{bc}**	**22.0 (2.3)^{c}**	**14 (3.2)^{b}**	47.0	55.0	<0.001
Actinomycetales	3.3 (0.7)^{a}	**10.1 (1.5)^{b}**	**8.8 (0.7)^{b}**	**10.2 (1.9)^{b}**	**7.9 (1.2)^{b}**	12.4	20.4	<0.001
Acidobacteriales	0.6 (0.2)^{a}	0.8 (0.2)^{ab}	2.0 (0.5)^{bc}	4.8 (1.7)^{cd}	**11.4 (2.4)^{d}**	36.4	44.4	<0.001
Chlorophyta	0 (0)^{a}	0.1 (0.0)^{a}	0.1 (0.0)^{a}	0.4 (0.1)^{a}	**8.5 (3.3)^{b}**	31.7	39.7	<0.001
Burkholderiales	3.4 (0.4)	4.6 (0.5)	6.4 (1.0)	**8.8 (2.1)**	**5.0 (1.4)**	1.1	9.1	0.06
Caulobacterales	1.1 (0.2)^{a}	2.0 (0.2)^{b}	2.0 (0.3)^{b}	1.8 (0.2)^{b}	3.9 (0.8)^{c}	29.5	37.5	<0.001
Nostocales	0 (0)^{a}	0.2 (0.1)^{ab}	1.3 (0.7)^{ab}	4.6 (3.7)^{ab}	3.4 (1.1)^{b}	4.0	12.0	0.017
Rhodospirillales	**5.5 (0.6)^{a}**	4.7 (0.9)^{ab}	3.9 (0.7)^{ab}	3.0 (0.4)^{b}	**5.6 (1.0)^{ab}**	2.3	10.3	0.036
Chthoniobacterales	**5.6 (1.3)^{x}**	**5.3 (0.5)^{x}**	**5.6 (0.8)^{x}**	3.1 (0.7)^{x}	3.1 (0.9)^{x}	5.4	13.4	0.01
Gemmatales	**8.1 (0.8)^{a}**	**6.1 (0.7)^{ab}**	4.9 (0.5)^{bc}	2.5 (0.4)^{d}	3.0 (0.3)^{cd}	34.6	42.6	<0.001
Solirubrobacterales	1.3 (0.4)^{a}	3.5 (0.5)^{bc}	4.7 (0.5)^{c}	2.2 (0.5)^{ab}	2.9 (0.5)^{bc}	16.0	24.0	<0.001
Myxococcales	**7.9 (1.4)^{a}**	2.6 (0.3)^{b}	2.3 (0.3)^{b}	1.5 (0.4)^{bc}	1.1 (0.3)^{c}	36.6	44.6	<0.001
Saprospirales	2.1 (0.3)^{a}	3.5 (0.4)^{a}	2.6 (0.3)^{a}	1.4 (0.5)^{b}	0.7 (0.2)^{b}	27.9	35.9	<0.001
Xanthomonadales	**5.8 (0.7)^{a}**	**5.6 (0.6)^{a}**	3.9 (0.4)^{a}	2.1 (0.8)^{b}	0.6 (0.3)^{b}	46.0	53.0	<0.001

Table 10. The best predictors of decomposition as determined using AIC model reduction (the change in AIC or dAIC) and comparing the change in residual sum of squares with the removal of each term (dRSS). The variation explained by each variable was determined using Dominance analysis and summed to estimate the relative contributions of fungi and environment.

Variable type	Variable	Estimate	Std. Err.	dRSS	dAIC	Variation explained (%)	Cumulative variation (%)
Intercept	-	0.82	0.02	-	-	-	
Fungal composition	NMS axis 1	0.12	0.06	0.07	2.7	23.6	28.7
	NMS axis 3	0.14	0.07	0.07	2.3	5.1	
Environmental Variation	PCA axis 1	0.08	0.05	0.04	0.53	15.2	27.2
	PCA axis 3	-0.09	0.04	0.08	3.48	12.0	

FIGURE LEGENDS

Figure 9. Ordination of fungal community structure along the vertical forest gradient. Circles represent 95% confidence intervals for the location of the centroid from each group. Vectors indicate significant associations between functional groups and points in the ordination. The length of each vector is proportional to the strength of the correlation.

Figure 10. Ordination of bacterial community composition along the vertical forest gradient. Vertical positions are color coded and ellipses are the 95% confidence interval wherein the centroid for communities from each vertical position is located. Vectors are visual representations of significant associations between the major bacterial taxa and points in the ordination. The length of each vector is proportional to the strength of the correlation.

Figure 11. Phylogenetic structure of bacterial communities along the vertical forest gradient. The points represent the mean z value (±95% CI) for each vertical position as calculated using the mean pairwise distance measure of phylogenetic dispersion. Points that are significantly below zero are phylogenetically clustered, indicating that community assembly is driven by environmental filters, whereas values above zero are phylogenetically evenly distributed, suggesting that competitive interactions are more important to community assembly.

Figure 12. Principle components analysis of wet season microclimate with sampling locations color coded by relative vertical position. Ellipses depict the location of the centroid for each vertical position with 95% confidence and the vectors indicate the strength of the correlations between each environmental variable and the axes.

Figure 13. Total mass loss from wood sticks (circles) and cellulose (squares) at the end of the wet (hollow points) and dry (filled points) seasons. Points represent average mass loss (95% CI) across both 2015 and 2016.

Figure 14. Respiration per unit mass from wood sticks collected at the end of the wet season in 2016. The emergent level was excluded due to low sample size.

Figure 9

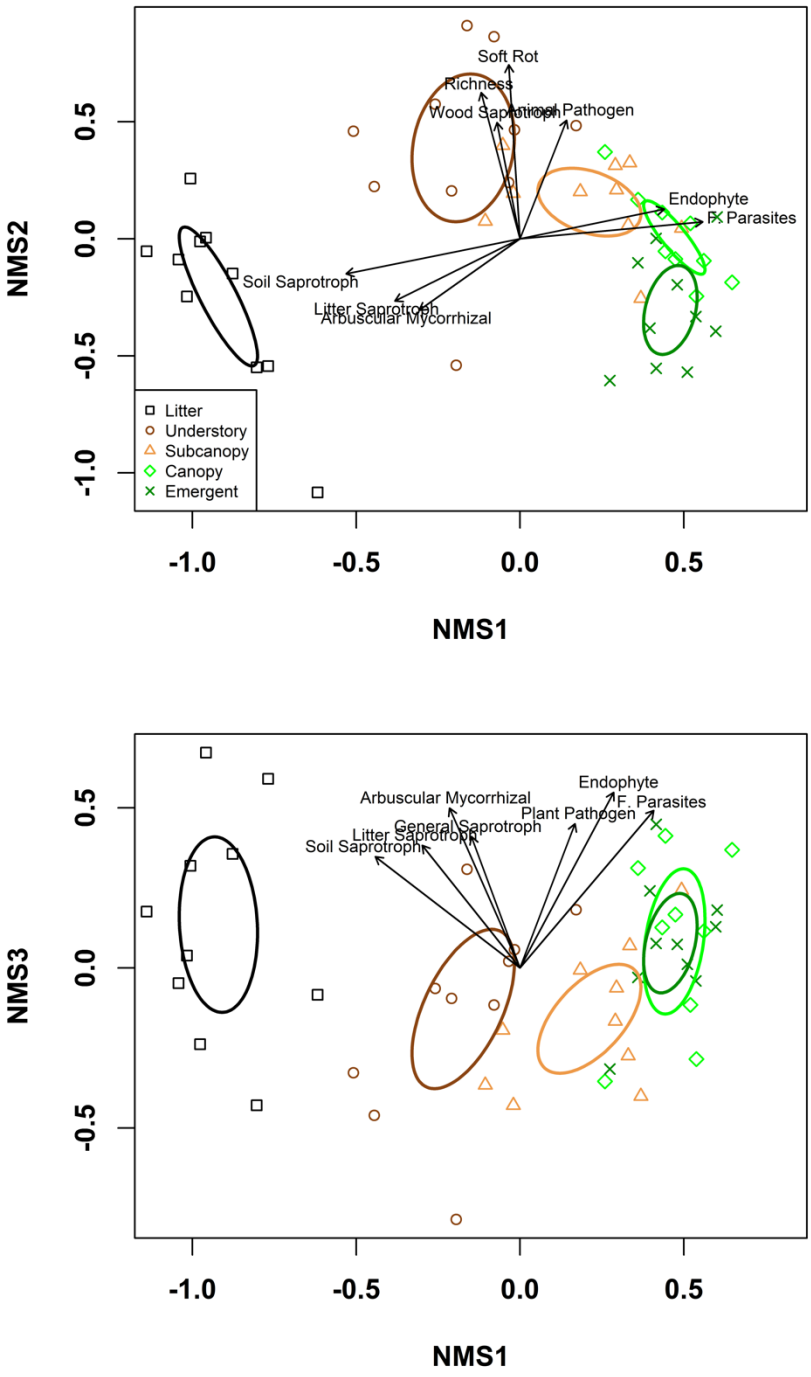
Soft Rot
Richness
Wood Saprotroph
Plant Pathogen
Endophyte
F. Parasites
Soil Saprotroph
Litter Saprotroph
Arbuscular Mycorrhizal
Litter
Understory
Subcanopy
Canopy
Emergent
NMS2
NMS1
0.5
0.0
-0.5
-1.0
Arbuscular Mycorrhizal
Endophyte
F. Parasites
Plant Pathogen
General Saprotroph
Litter Saprotroph
Soil Saprotroph
NMS3
NMS1

Figure 10

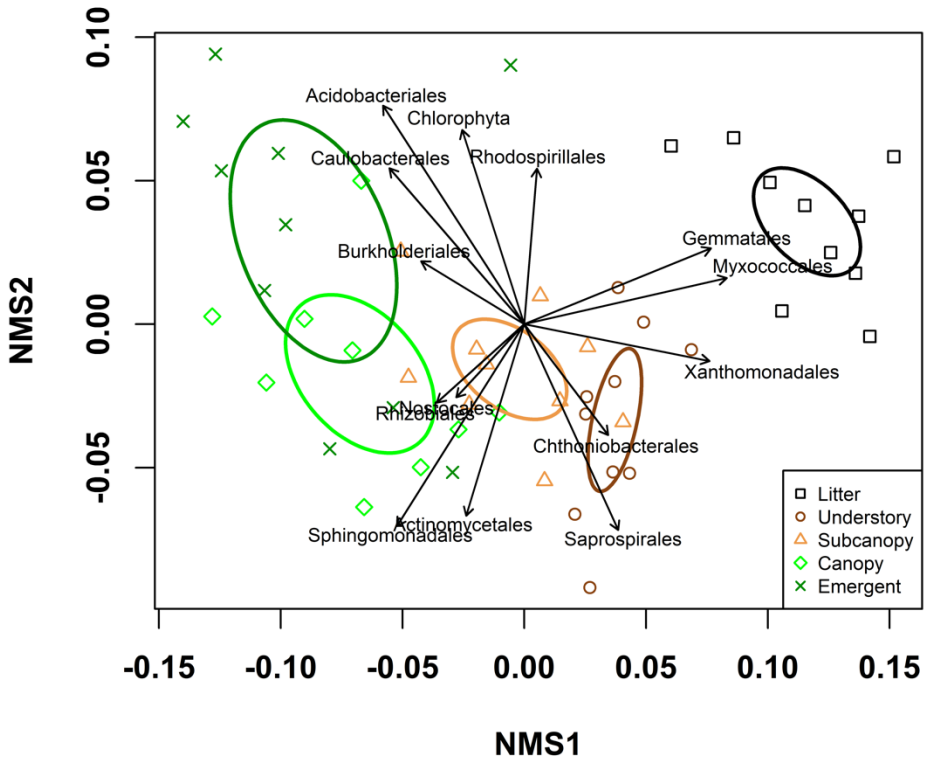
NMS2
0.10
0.05
0.00
-0.05
NMS1
-0.15
-0.10
-0.05
0.00
0.05
0.10
0.15
Acidobacteriales
Chlorophyta
Caulobacterales
Rhodospirillales
Burkholderiales
Gemmatales
Myxococcales
Xanthomonadales
Rhizobiales
Chthoniobacterales
Actinomycetales
Sphingomonadales
Saprospirales
Litter
Understory
Subcanopy
Canopy
Emergent

Figure 11

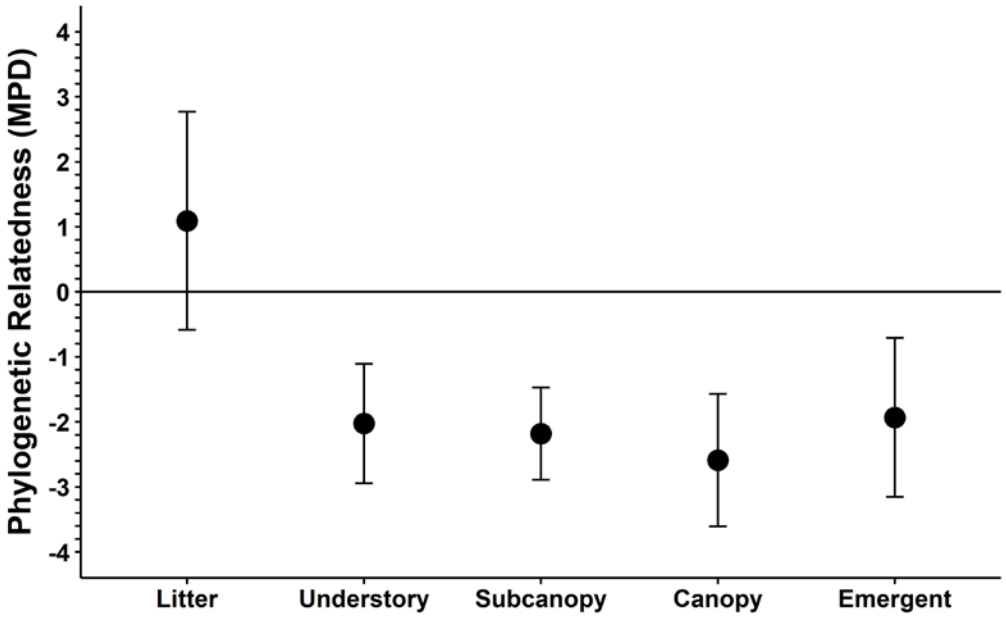
Phylogenetic Relatedness (MPD)
4
3
2
1
0
-1
-2
-3
-4
Litter
Understory
Subcanopy
Canopy
Emergent

Figure 12

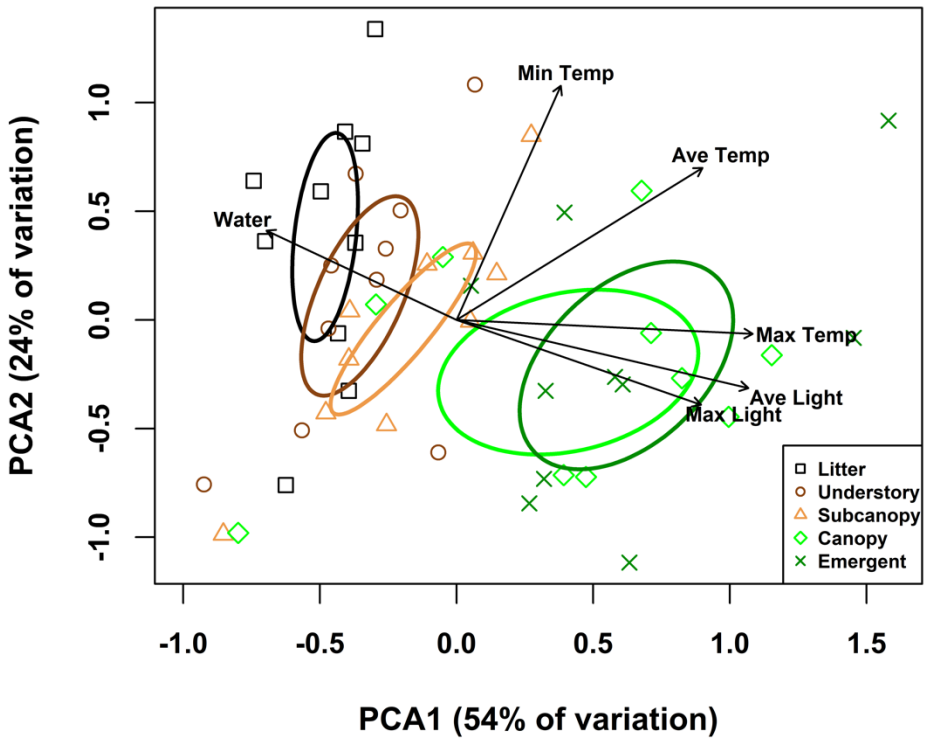
Min Temp
Ave Temp
Water
Max Temp
Ave Light
Max Light
Litter
Understory
Subcanopy
Canopy
Emergent
PCA2 (24% of variation)
PCA1 (54% of variation)
-1.0
-0.5
0.0
0.5
1.0
1.5

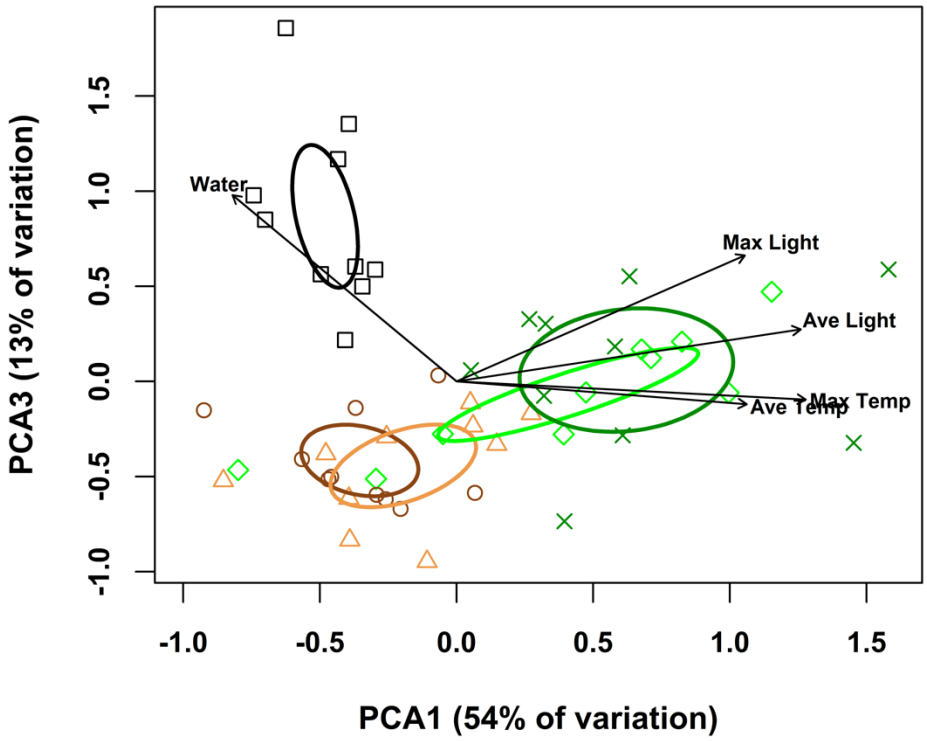
Water
Max Light
Ave Light
Max Temp
Ave Temp
PCA3 (13% of variation)
PCA1 (54% of variation)
-1.0
-0.5
0.0
0.5
1.0
1.5

Figure 13

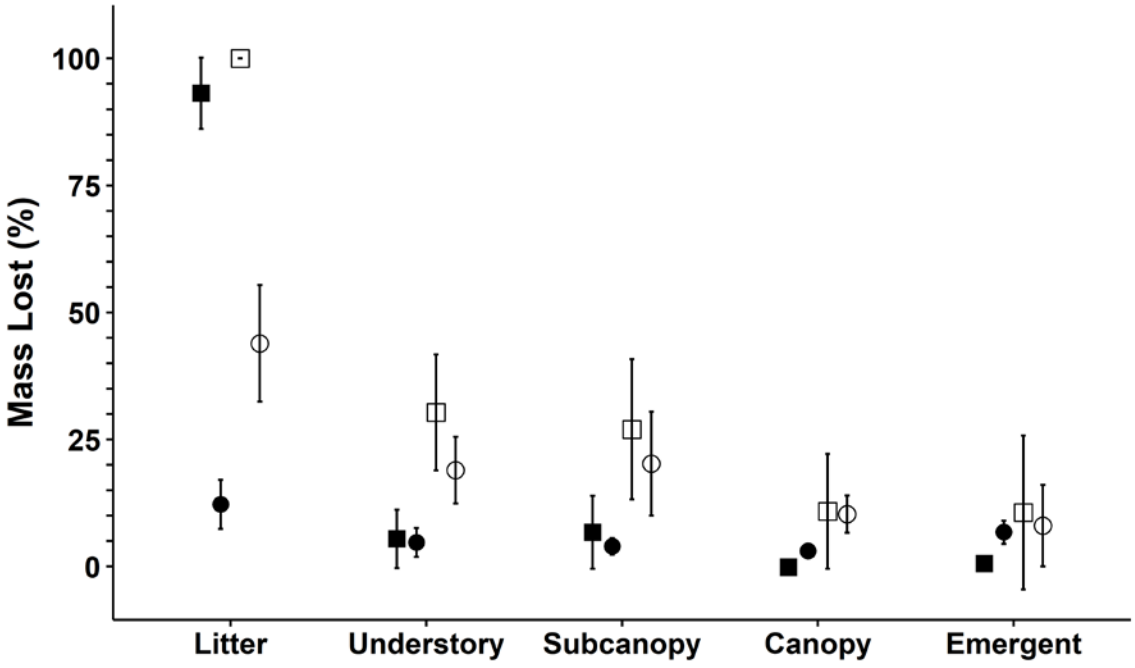
Mass Lost (%)
100
75
50
25
0
Litter
Understory
Subcanopy
Canopy
Emergent

Figure 14

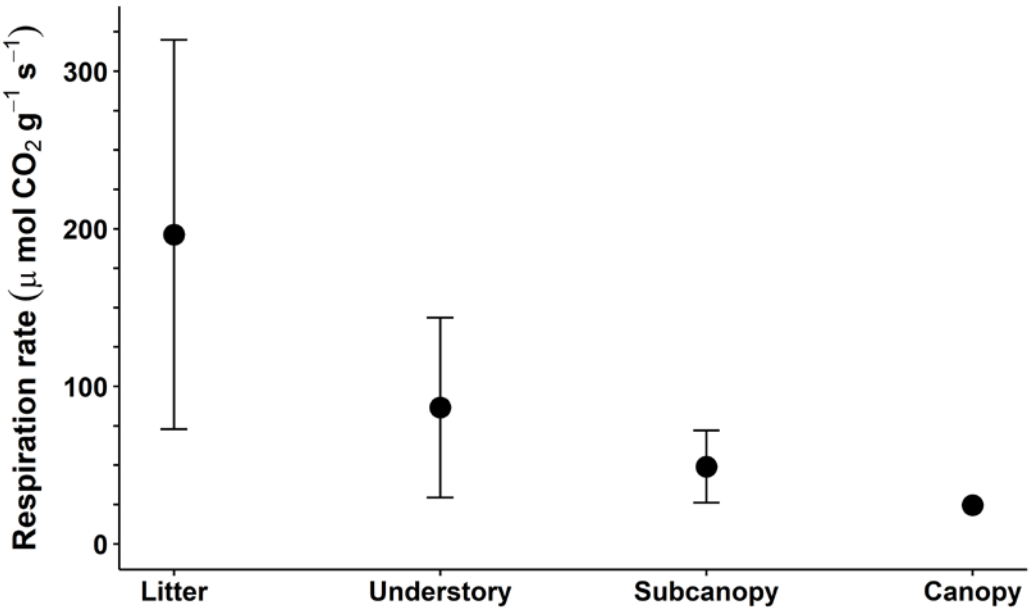
Respiration rate (μ mol CO_2 g^{-1} s^{-1})
300
200
100
0
Litter
Understory
Subcanopy
Canopy

CHAPTER V

EFFECTS OF LIGHTNING ON TREES: A PREDICTIVE MODEL BASED ON *IN SITU* ELECTRICAL RESISTIVITY

SUMMARY

The effects of lightning on trees range from catastrophic death to the absence of observable damage. Such differences may be predictable among tree species, and more generally among plant life history strategies and growth forms. We used field-collected electrical resistivity data in temperate and tropical forests to model how the distribution of power from a lightning discharge varies with tree size and identity, and with the presence of lianas. Estimated heating density (heat generated per volume of tree tissue) and maximum power (maximum rate of heating) from a standardized lightning discharge differed 300% among tree species. Tree size and morphology also were important; the heating density of a hypothetical 10 m tall *Alseis blackiana* was 49 times greater than for a 30 m tall conspecific, and 127 times greater than for a 30 m tall *Dipteryx panamensis*. Lianas may protect trees from lightning by conducting electric current; estimated heating and maximum power were reduced by 60% (± 7.1%) for trees with one liana and by 87% (± 4.0%) for trees with three lianas. This study provides the

first quantitative mechanism describing how differences among trees can influence lightning-tree interactions, and how lianas can serve as natural lightning rods for trees.

INTRODUCTION

Lightning strikes thousands of trees each day (Taylor 1974), and ca. 500 million hectares of forest exist in regions with high lightning frequency (i.e., > 30 flashes km-2 yr-1; Christian et al. 2003, Albrecht et al. 2016). The dramatic effects of lighting on trees have interested scientists for more than a century (Anonymous 1898, Stone 1914, Komarek 1964, Taylor 1977), but the spatial and temporal stochasticity of lightning remain major obstacles in the comprehensive understanding of its ecological significance (Knight 1987, Yanoviak et al. 2015, Mäkelä et al 2016). Clearly lightning often kills trees directly or indirectly (e.g., via fire or subsequent fungal and beetle infestations; Sharples 1933, Hodges and Pickard 1971). However, tree mortality rates remain unknown for most forests (Franklin et al. 1987, Shugart 1987, Stephenson et al. 2011), and the different mechanisms of individual tree death rarely are quantified. This is particularly problematic for trees in the relatively large "standing dead" category (Carey et al. 1994), many of which are due to lightning. Resolving these ambiguities is increasingly important as lightning frequency is expected to increase in a warmer world (Williams 2005, Romps et al. 2014). Here, we explore how variation in a key trait - electrical resistivity - can explain the varied effects of lightning on trees (hereafter, "lightning-tree interactions").

Whereas lightning is a frequent cause of tree mortality in some regions (Yanoviak et al. 2015, Covert 1924, Reynolds 1940, Brünig 1964), many trees struck by lightning suffer no apparent ill effects (Stone 1914, Taylor 1977, Orville 1968). The most parsimonious hypotheses to explain this variation focus on differences in lightning

intensity and physiological or anatomical differences among struck trees. In particular, the size, location, and species identity of trees are presumed to be key factors (Yanoviak et al. 2015, Taylor 1964, Baker 1973). The potential role of tree species-level traits remains especially ambiguous, with historical references to "starchy" oak vs. "oily" beech trees differing in their attractiveness or response to lightning (Covert 1924). Despite these and many other suggested patterns, the majority of evidence concerning the probability that any given tree will be damaged by lightning remains anecdotal and post hoc, mainly for logistical reasons (Mäkelä et al. 2009, Yanoviak et al. 2015, Yanoviak et al. 2017).

Lightning damages trees mainly through heat energy--both the extreme quantity of heat and the high rate at which it is applied to tree tissues (hereafter referred to as heating and maximum power, respectively; Uman 2008, Courty 2016). These two properties are proportional to the total current and peak current, respectively, of a lightning discharge. High peak current (typically 15-30 kA) causes high maximum power that is hypothesized to generate steam explosions in the vascular cambium. Such localized explosions create the stereotypical lightning scars on tree trunks, and sometimes catastrophically shatter entire trees (Taylor 1964, Mäkelä 2009, Plummer 1912, Stone and Chapman 1912). Similarly, a prolonged lightning discharge (i.e., "continuing current" or CC lightning, typically 200 A for 115 ms; Bitzer 2016) causes sustained heating that presumably kills trees and ignites forest fires (Kitagawa 1962, Anderson 1964, Fuquay 1972). What humans commonly perceive as a single lightning flash is actually a very complex phenomenon having three main properties: 1) the number of return strokes (visible pulses of electric current), 2) the duration of the current in each return stroke, and 3) the peak current of each return stroke (Uman 2001). These properties are highly variable among flashes, potentially contributing to stochastic variation in lightning-tree interactions.

Variation in electrical resistivity among trees is also expected to affect the amount of heating and maximum power experienced during a lightning discharge (Stone 1912, Komarek 1964). The amount of heating and maximum power are directly proportional to the electrical resistance (R) of the struck tree (Uman 2008), which varies among tree species and their general morphology (the three-dimensional shape of a tree, see *Equation 1* below). Specifically, electrical resistivity differs consistently among species and increases with tree diameter in all cases (Gora and Yanoviak 2015). Such differences may explain why lightning-caused tree deaths appear to be twice as common for relatively resistant conifers as they are for more conductive hardwoods (Reynolds 1940, Baker 1973, Taylor 1977). Differences in tree size also are potentially relevant in this context; biomass increases exponentially with diameter for healthy trees, thus larger trees may survive lightning by distributing a similar amount of heat across more biomass.

Although many plant traits vary predictably with latitude (e.g., freeze tolerance, deciduousness), structural differences in vascular tissue between growth forms (trees and climbing plants) generally are consistent between temperate and tropical regions (Christensen-Dalsgaard 2007, Angyalossy et al. 2015). Specifically, climbing plants typically hold more water per unit of stem volume than do trees in both temperate and tropical regions. Relative water content (and other factors, like ion content) partly determines the electrical resistance of plant tissues (Stone 1914, Stamm 1927, Bieker and Rust 2010) and likely explains the lower resistivity of vines vs. trees in the temperate zone (Gora and Yanoviak 2015). However, similar comparative data do not exist for tropical plants.

Other factors extrinsic to lightning flash characteristics and tree traits also likely influence the extent of damage that occurs during a lightning discharge. Although hard evidence is lacking, lightning damage to trees may be influenced by soil type (Plummer

1912, Taylor 1974, Yanoviak et al. 2015), elevation (Muzika et al. 2015), or swampy conditions (Anderson 1964). Recent observations indicate that another factor - the presence of lianas (woody vines) - influences the effect of lightning on trees (Yanoviak 2013). Specifically, the tendency for liana stems to be more conductive than tree branches of similar diameter (Yanoviak 2013, Gora and Yanoviak 2015) suggest that lianas function as natural lightning rods. This effect should be particularly important in tropical forests, where lightning frequency is high and ca. 40% of the forest canopy is carpeted by liana foliage (Putz 1984, Christian et al. 2003, Schnitzer et al. 2012).

The principal objective of this study was to determine how variation in electrical resistivity within and among trees and lianas could influence lightning-tree interactions. The electrical properties of tropical plants are unknown, so we quantified the electrical resistivity of some common woody plants in central Panama. We hypothesized that lianas would have lower resistivity than trees, as observed in temperate regions (Gora and Yanoviak 2015). Because resistivity is linked to moisture content, we further hypothesized that differences in electrical resistivity between and within growth forms (lianas vs. trees) would correspond to differences in their relative water content. We explored how resistivity as a plant trait should affect the heating and maximum power experienced by trees during three common types of lightning discharges. Specifically, we predicted that heating and maximum power decrease with increasing tree size (increased height and diameter), and differ among tree species due to differences in their general morphology and electrical resistivity. Finally, we estimated the potential for lianas to reduce heating and power within host trees by diverting electric current. Our overall goal was to model the directional effects of tree characteristics on heating and maximum power as a basis for predicting the varied ecological effects of lightning.

METHODS

Field work for this project was conducted in the Barro Colorado Natural Monument (BCNM) in Panama (9.15° N, 79.85° W). The BCNM is a seasonally moist lowland tropical forest administered by the Smithsonian Tropical Research Institute. Additional information about this forest is available elsewhere (Leigh et al. 1996).

Electrical resistivity measurements

We selected six common species of trees and seven common species of lianas to measure differences in resistivity between growth forms, and among species within growth forms (Table 11). We measured only tree and liana stems 1-10 cm in diameter for the growth form comparison because liana stems larger than this size range are uncommon for most species (Schnitzer et al. 2012). To reduce confounding phylogenetic effects, we chose species that minimized phylogenetic similarity within the growth forms and maximized similarity between trees and lianas. Specifically, three pairs of lianas and trees were in the same taxonomic families, whereas all species within each growth form were in different families (Table 11). We also performed a separate comparison of larger stems (10-77 cm) for a subgroup of three tree species (*Alseis blackiana*, N = 19; *Dipteryx panamensis*, N = 12; and *Jacaranda copaia*, N = 20).

The field methods for this project followed those of Gora and Yanoviak (2015). Briefly, we measured the electrical resistance of stems or branches of lianas and trees (saplings or larger trees, hereafter all are referred to as *stems*) using a megaohmmeter (DR-6605; Ruby Electronics, Saratoga, California, USA) secured to two electrodes (aluminum nails). The electrodes were separated by 30 cm and inserted on the same longitudinal axis of a liana or tree stem. We measured diameter of the stem at the midpoint between the two electrodes and recorded air temperature. We then calculated electrical resistivity using *Equation 1*,

[1] $p = R * A * L^{-1}$

where R is resistance (ohms, Ω), p is resistivity (Ωm), A is cross-sectional area (m^2), and L is length (m) of the measured section. To avoid potentially confounding environmental effects, all measurements were taken during dry conditions and at consistent temperatures during peak lightning season (i.e., wet season; June-October). To verify that minor variation in electrode depth was not an important source of error, we measured resistance with electrodes inserted 1.5 cm, 2.5 cm, and 3.5 cm into the vascular tissues of two or more of the individuals for each of the 11 tree species used in the model (> 30 individuals in total). Resistance was consistent regardless of probe depth over this range.

We used one focal species from each growth form (the liana *Arrabidaea patellifera*, N = 15; and the tree *Alseis blackiana*, N = 15) to quantify how resistivity changes with stem moisture content. We measured electrical resistance as described above, except that the electrodes were separated by 20 cm. After recording resistance, we removed the 20 cm section of stem using a handsaw and sealed it in a pre-weighed plastic bag. We then weighed each fresh stem section, dried it to constant mass in an oven at 60°C, and recorded its dry weight. Dry mass was subtracted from wet mass to calculate moisture mass and percent moisture content.

Heating and maximum power modeling

The amount of heating and maximum power generated in tree tissues during a lightning strike fundamentally are determined by stem resistance. Using 533 *in situ* measurements of resistivity, we modeled how heating and maximum power during a lightning strike differ within and among tropical and temperate tree species given different initial conditions (i.e., different lightning flash characteristics). The model included three types of lightning discharges, 11 species of trees, one temperate liana, and one tropical liana. We assumed no irregularities in tree morphology and no variation within each of the three types of lightning. We also assumed that the resistivity of plant

tissues does not change during a lightning discharge, that heat is evenly distributed among tree tissues and not dissipated away from the tree during a discharge (which typically occurs in < 1 ms), and that lightning current does not flashover to nearby objects. Finally, electric current flows longitudinally through tree vascular tissues regardless of the source (e.g., lightning or an ohmmeter; Taylor 1974, Taylor 1977, Carter and Blanchard 1978, Smith and Blanchard 1984). Thus, we assumed that an ohmmeter measures patterns of resistance relatively similar to those experienced by lightning current. These assumptions were consistent for all model iterations. If some of these assumptions are violated then the magnitude of heating or maximum power will change, but the directional effects (e.g., whether lianas decrease heating) of tree characteristics are unlikely to be affected.

We used *Equation 2* to compare the resistive heating (referred to as "heating") of different tree species in response to each type of lightning discharge. In this equation, heating is equal to the action integral multiplied by the resistance of a tree:

[2] $H = \text{Integral}[I^2(t)\, R\, dt]$

where H is total resistive heating of a tree (joules, J), I is current (amperes, A), t is the duration of the current in the lightning return stroke (seconds), and R is the resistance (Ω) of the selected tree (Uman 2008). The action integral ($I^2 * t$) is specific to each type of lightning, and resistance differs among tree species, sizes (as trunk volume), and tree morphologies (as change in diameter with height). Thus, this formula can be used to calculate the heating of any free-standing tree given the values for these two terms. Because the thermal properties of tree tissues are poorly quantified, we did not estimate increases in temperature as a result of heating. Similarly, we calculated maximum power by multiplying the squared peak current by the resistance of the tree. Time was excluded from this calculation because peak current is an instantaneous value. Hereafter, the heat values calculated using *Equation 2* are referred to as *heating* (J) and calculated

maximum power is referred to as *maximum power* (J s^{-1}). To facilitate the comparison of heating for different sizes of trees, we normalized heating by tree volume to determine the *heating density* (J cm^{-3}).

We combined *Equation 2* and Ohm's Law to quantify the potential for lianas to function as natural lightning rods. Lianas were conspicuously damaged by electric current in >90% of the lightning strikes on BCI (Yanoviak et al. 2017) in a separate study, demonstrating that electric current flows through both trees and their resident lianas during a strike. Consequently, we assume that the electrical potential (voltage) across all main stems in a liana-tree complex is the same during a lightning discharge. However, the proportion of lightning current flowing through each stem in the complex will differ according to its resistance (obtained from field measurements). Given this relationship, we modeled the distribution of electric current between liana and tree stems during a lightning discharge as the ratio of tree resistance to liana resistance. We then used the methods described above to calculate heating and maximum power in the tree-liana complex. To estimate the protective effects of multiple lianas in a single tree, we substituted liana resistance in the above ratio with the combined resistance of all lianas as if connected in a parallel circuit.

Resistance calculations

Using the same 533 resistance measurements mentioned above, we constructed hypothetical trees and lianas similar to a model tree used in a previous lightning-focused study (Defandorf 1955). We approximated tree and liana shape as a conical stack of 1 cm tall cylinders incrementally decreasing in diameter from the base to the top. This approach simulated the relatively linear path that electric current follows from the end of any given canopy branch to the base of the tree (Taylor 1974). The top (minimum) diameter was fixed at 1 cm in all cases, and the incremental increase was calculated as (maximum diameter - minimum diameter) / height in centimeters. We determined the

resistivity of each cylinder in the stack based on species-specific logarithmic functions of resistivity vs. diameter calculated from field data (Table 12; also see Gora and Yanoviak 2015). Consequently, we estimated the heating and maximum power experienced by an average tree of each species. The resistivity of each cylinder was multiplied by height (i.e., 1 cm) and divided by its cross-sectional area to determine resistance. This conversion makes no assumption about the composition of tissues within each cylinder, but rather assumes that electric current from the *in situ* resistance measurements follow a similar path in the model tree. We calculated total resistance and total volume as the summed resistance (as if in a series circuit) and volume, respectively, of all cylinders in a given tree or liana. We used total tree volume to estimate heating density (rather than estimating the volume and resistivity of specific tissues; al Hagrey 2006) because we assumed that heat is distributed evenly among tree tissues.

We compared heating and maximum power among 11 tree species – the three tropical tree species in this study and eight temperate species surveyed in a separate study (Table 12; Gora and Yanoviak 2015). We used 20 m as tree height for interspecific comparisons because mature canopy trees in temperate and tropical forests tend to be at least that tall (Mascaro et al. 2011). We calculated maximum diameter at ground level using height-to-diameter ratios of *Prioria copaia*, which is the only common emergent tropical tree in the BCNM for which such data exist (O'Brien et al. 1995).

We used region-specific liana data to estimate the effectiveness of lianas as natural lightning rods. Specifically, we created hypothetical tropical and temperate lianas using resistivity data from liana stems measured in Panama and Kentucky (Gora and Yanoviak 2015), respectively. We conservatively used 6 cm as the maximum liana diameter for the model. Many lianas with greater diameter reside in the canopy on BCI (Kurzel et al. 2006), thus the size of our model liana underestimates their potential protective effects. We also assumed that liana stems are 25% longer than their host tree

height due to their sinuous growth and scandent habit. We calculated the reduction in heating and maximum power for trees supporting either one or three lianas. We chose this range because it reflects actual liana abundances in trees of the BCNM (Putz 1984).

Intraspecific tree size comparisons focused on *D. panamensis* and *A. blackiana*. We chose *D. panamensis* because it is the closest relative of *P. copaia* in the suite of focal species used for this study, and because both species have similar general morphology. We chose *A. blackiana* because its morphology is distinct from *D. panamensis*. Height-to-diameter ratios were determined using the same methods for both species (O'Brien et al. 1995), and we used these parameters to calculate the heating and maximum power for seven sizes of each species (10, 15, 18, 20, 22, 25, and 30 m).

Lightning current profiles

It is impractical to model every possible type of lightning, so we focused on three common canonical lightning discharges (single stroke, multiple stroke, and continuing current) to capture a range of the potential energetic effects of lightning on trees. In each hypothetical discharge, the current at the strike point (i.e., the tree) was estimated using a binomial exponential model (Heidler 1985, Diendorfer and Uman 1990, Heidler and Cvetic 2002) in which each term is of the form:

$$i(t) = \frac{I_0}{\mu} * \frac{\left(\frac{t}{\tau_1}\right)^2}{\left(\frac{t}{\tau_1}\right)^2 + 1} * \exp\left(-\frac{t}{\tau_2}\right)$$

where I_0 is the current amplitude, μ is an amplitude correction factor, and τ_1, τ_2 are decay time constants.

We created three different types of hypothetical lightning discharges based on Diendorfer and Uman (1990). The simplest type, *Discharge 1*, was a single cloud-to-ground (CG) return stroke discharge with a peak current of 30 kA. This, and other parameters, are the same as the CURRENT-2 flash in Table 1 of Diendorfer and Uman

(1990). Because most CG lightning discharges contain more than one stroke, we created hypothetical *Discharge 2* with three return strokes. In this case, the first return stroke was the same as *Discharge 1*, but the second and third strokes followed the parameters of the CURRENT-1 flash in Table 1 of Diendorfer and Uman (1990). Finally, we modeled *Discharge 3* as a CC flash (Bitzer 2016, Kitagawa et al. 1962) that included a single stroke (the same as *Discharge 1*) of 50 μs duration immediately followed by a constant current of 200 A for 115 ms.

Statistical analyses

We used analysis of covariance (ANCOVA) to test for differences in resistivity among growth forms and species. Preliminary examination of the data revealed conspicuous heteroscedasticity. Specifically, variance in resistivity was much greater for stems <3 cm diameter than for larger stems. Consequently, we ran separate analyses for stems <3 cm and stems 3-10 cm. We tested for differences in resistivity between growth forms using species nested within growth form. When resistivity differed between growth forms, we tested for interspecific differences in resistivity within each growth form separately. Stem diameter was the covariate in all of these tests.

We ran a series of comparable analyses to test the hypothesis that differences in resistivity among stems are associated with variation in their relative moisture content. We used ANCOVA to determine how resistivity differed between species using stem diameter as the covariate. We repeated this analysis using moisture content as the covariate, and we used regression to determine how resistivity changed with moisture content independent of species. Finally, we compared the squared residual error of linear models with and without species as a fixed effect to determine whether the relationship between resistivity and moisture content was species-independent.

In all cases, we used stepwise model reduction to remove non-significant interaction terms and we present statistical results from these reduced models. We did

not include temperature in our analyses because it was relatively consistent (see results), and differences in temperature much larger than those observed here were unimportant in a similar study (Gora and Yanoviak 2015). We used the Bonferroni correction for multiplicity when necessary. Electrical resistivity data were log-transformed, and diameter was cube-root transformed to improve linear relationships among these variables. We used the Shapiro-Wilk test to assess normality and we examined residuals to confirm appropriate model fit.

Data were analyzed using the R statistical program (R Core Team 2017). We used the *lme4* package with the *LmerTest* modification to analyze mixed-effect models (Bates et al. 2014) and the base R package for basic linear models and t-tests. We tested for differences among individual species using post-hoc Tukey HSD test in the *multcomp* package (Hothorn et al. 2008).

RESULTS

The model supported the prediction that variation in resistivity among basic tree characteristics is likely to influence lightning-tree interactions. Specifically, the amount of heating and maximum power (i.e., the amount of tissue damage) expected to occur during a lightning discharge differed among tree species, sizes, and tree morphologies, and with the abundance of lianas (Figure 15). The model predicted that hypothetical trees experience heating from 3-80 GJ, heating density from 8-1685 kJ cm^{-3}, and maximum power of 197-3336 TW. For clarity, hereafter we focus on tree interactions with a single, non-CC return stroke (*Discharge 1*).

Predicted lightning-tree interactions differed among species and tended to be more severe for temperate trees. Interspecific differences in heating and maximum power were caused by variation in both the resistivity of stem tissues and overall morphology. When considering only resistivity, heating was lowest for the tropical trees *J. copaia* (18.9 GJ) and *D. panamensis* (19.0 GJ), whereas heating of *A. blackiana* (30.6

GJ) was ca. 60% greater than for either of these species (Table 12). Temperate trees typically had greater estimated heating than tropical trees. Specifically, heating of the tropical tree *A. blackiana* was lower than all temperate species except for *Acer rubrum* (25.4 GJ), and heating of the remaining seven temperate species was 81-189% greater than *J. copaia* (Table 12). After accounting for variation in trunk morphology as well (*A. blackiana* is narrower), heating density and maximum power of *A. blackiana* were 290% and 180% greater than for *D. panamensis*, respectively (Tables 12 and 13, Figure 16). Tree morphology was a species-specific property in this study, but differences in the shape of branches within the same species or even the same individual should similarly affect patterns of heating and maximum power.

Within a species, taller model trees experienced greater heating and maximum power, yet their heating density was substantially lower (Figure 16, Table 13). For *A. blackiana* trees, the maximum power expected for a 30 m tall individual (2384 TW) was 21% greater than for a 10 m individual (1966 TW). Taller trees also experience more total heating, but the heat is distributed over a larger volume of tree tissue, effectively reducing the impact of lightning. For example, heating density for a 10 m tall individual of *A. blackiana* (1684 kJ cm^{-3}) was ca. 49 times greater than for a 30 m tall individual (33 kJ cm^{-3}). These size-based differences compounded the interspecific resistivity-based differences described above. Specifically, the heating density of a 10 m tall *A. blackiana* tree was ca. 127 times greater than the heating density of a 30 m tall *D. panamensis* (Figure 16).

Inclusion of lianas in the model dramatically reduced the heating and maximum power experienced by their host trees, suggesting that lianas have the capacity to inadvertently protect trees from lethal lightning damage (Figure 17, Table 14). The presence of one liana reduced both heating and maximum power by more than half (Figure 17; mean ± SD: 60.4 ± 7.1% reduction). This protective effect increased when

more lianas were added; three lianas on a single tree reduced heating and maximum power by 87% (± 4.0%). The expected protective effect of lianas was higher in trees with greater electrical resistance (e.g., larger individuals or relatively resistant species) because the lianas diverted a larger fraction of the total lightning current. For example, as described above, a liana-free *A. blackiana* tree should be more heavily damaged by lightning than other liana-free tropical trees. However, adding three lianas to an *A. blackiana* would cause it to have the lowest heating and maximum power among all of the modeled species. Similarly, more conductive lianas, such as those with larger diameters, would divert more lightning current and thus provide greater protection for host trees.

Finally, variation in discharge types strongly affected the predicted heating experienced by the model trees. Relative to the single stroke event (*Discharge 1*), heating was 45% higher for the three stroke flash (*Discharge 2*), and ca. 31% higher for the continuing current flash (*Discharge 3*; Table 12). By contrast, maximum power was equal for all three types of lightning because each had the same peak current. Heating and maximum power are proportional to tree resistance, thus relative differences among species were the same for any type of lightning discharge.

Electrical resistivity of tropical plants

Electrical resistivity generally differed between lianas and trees; liana resistivity was on average ca. 50% lower than that of trees for stems 3-10 cm in diameter ($F_{1,103}$ = 7.01, p = 0.023, α = 0.025; Figure 18). By contrast, electrical resistivity did not differ between liana and tree stems < 3 cm diameter ($F_{1,94}$ = 0.937, p = 0.336). Temperature at the time of measurement was similar between growth forms (mean ± SD = 28.4 ± 1.8˚C; $F_{1,240}$ = 2.98, p = 0.08), and electrical resistivity increased with diameter in all cases (Figures 18 and 19).

As with temperate plants, electrical resistivity differed interspecifically within tropical trees and lianas for stems 3-10 cm in diameter (trees: $F_{5,40} = 115.16$, $p < 0.001$; lianas: $F_{6,48} = 22.03$, $p < 0.001$; $\alpha = 0.025$; Figure 19). Electrical resistivity also differed among tree species for stem diameters >10 cm ($F_{3,47} = 567.2$, $p < 0.001$; Figure 20). Regardless of stem size, *Alseis blackiana* had the highest resistivity by a substantial margin, whereas the resistivity of *D. panamensis* was either similar to (stems 3-10 cm) or slightly higher (stems > 10 cm) than that of *J. copaia*. We lacked sufficient data for similar post-hoc tests among liana species.

Differences in moisture content likely are driving the differences in resistivity described above. Electrical resistivity of *Arrabidaea patellifera* and *A. blackiana* increased with diameter ($F_{2,27} = 112.2$, $p < 0.001$, Figure 7a), but decreased with increasing moisture content ($F_{2,27} = 19.0$, $p < 0.001$, Figure 7b). *Alseis blackiana* consistently had higher resistivity than *A. patellifera* across a range of diameters ($F_{2,27} = 116.0$, $p < 0.001$), but their ranges of moisture content largely did not overlap (Figure 7). Variation in electrical resistivity was minimal above 55% moisture content, indicating that extremely wet stems exhibit a different relationship between resistivity and moisture content. Regardless, the strongest evidence that patterns of resistivity are driven by moisture content is that moisture was a species-independent predictor of resistivity. That is, when the species term was dropped from the linear model for moisture content vs. resistivity, the R^2 remained 0.55 (moisture with species: $F_{2,27} = 19.00$, $p < 0.001$; moisture without species: $F_{1,28} = 35.8$, $p < 0.001$, Figure 7b).

DISCUSSION

There is a long history of speculation regarding the differential effects of lightning among trees based on size, species, condition, and location (Anonymous 1898, Taylor 1974, Yanoviak et al. 2015, Anderson 1964). Here we present the first quantitative, mechanistic, predictive foundation for understanding how any healthy tree potentially

will be affected by lightning. Unlike all previous work on this topic, the modeled effects of lightning on trees in this study are based on empirical measurements of an emergent physical property (electrical resistivity), which varies consistently with tree species and morphology. Although every strike event is unique, and its consequences ultimately are influenced by many factors that are not easily quantified, this model provides a straightforward and ecologically relevant starting point. Most importantly, it shows how differences in basic characteristics of trees can cause substantial differences in the amount of damage they experience from a lightning strike, *ceteris paribus*. Note that the model does not account for factors affecting the probability that any tree will be struck. For example, the effects of tree height illustrated in Figure 15 could be less important in mature forests if large trees are more likely to intercept lightning strikes. However, the model does suggest that trees in regenerating secondary forests will have relatively higher rates of severe or lethal lightning-caused damage by virtue of their smaller average size.

The results of this study provide correlative support for the hypothesis that lianas function as passive lightning protection for trees (Yanoviak 2013). Lianas generally are considered to be structural parasites of trees (Stevens 1987), thus this potential protective role adds a new perspective on liana-tree interactions. Some tropical trees often are liana-free by the time they grow to canopy or emergent height (pers. obs.), and the results of this study suggest that lightning could contribute to that pattern by killing lianas in large, relatively conductive trees. Ultimately, uncovering such patterns will require experimental manipulation of lightning strike locations in a forest, or on accurate determination of lightning attachment locations across large areas of the forest canopy.

The tendency for lianas to have lower resistivity than trees likely reflects differences in moisture content between growth forms. Like Stamm (1927), we found that wood moisture content can supersede species identity as a determinant of electrical

resistivity. Although the important role of moisture in wood resistivity is well established (Carter and Blanchard, al Hagrey 2006, Gora and Yanoviak 2015), no other studies have compared moisture-resistivity patterns among growth forms or trees *in situ*.

The model developed in this study also indicates that small trees will suffer more damage from a lightning strike than nearby larger trees. This pattern is supported by our observations of more than a dozen recent strikes in the forest on BCI, but post hoc assessments of lightning damage in other forests provide mixed evidence for differential mortality among tree size classes (Anderson 1964, Magnusson et al. 1996). These latter studies were conducted months or years after the strike, thus counts of dead stems could be biased against smaller size classes due to their lower persistence (Magnusson et al. 1996). Regardless, accurate field data collected within a few weeks after a strike are required to adequately test the relevance of tree size and other characteristics to the distribution of damage.

The estimates generated in this study show that multi-stroke and CC flashes produce more heat than the hypothetical single-stroke flash (*Discharge 1*) used to generate the bulk of the heating and power estimates. In reality, ca. 80% of flashes have multiple (typically 3-5) return strokes, and ca. 40% are CC flashes (Bitzer 2016, Rakov and Uman 2003). Moreover, maximum peak current can be as much as 10 times greater than our model lightning discharges (300 kA instead of 30 kA), CC flashes can last up to 1 second (the modeled CC flash was 115 ms), and some discharges include >25 strokes (Uman 2001). Consequently, extrapolating the model to large spatial or temporal scales likely would underestimate the damage.

Finally, the results of this study are potentially relevant to understanding future forest dynamics. Specifically, the model indicates that the likelihood of lightning-caused death will be higher for tree species with high resistivity, smaller overall size, and relatively narrow trunks and branches. The relevance of these patterns depends on the

probability that any given tree will be struck by lightning, and the relative importance of lightning as an agent of tree mortality at the population and community levels, which remains undetermined for most forests. However, given the high frequency of lightning in the lowland wet tropics, we suspect that its contribution to canopy tree mortality in particular is underestimated. Regardless, resolving this problem is important because lightning frequency is expected to increase over the coming decades (Williams 2005, Romps et al. 2014).

The results of this study raise at least four potentially fruitful avenues for future research. First, the simple conical shapes of the model trees and lianas ignored the diverse and often species-specific three-dimensional architecture of their natural counterparts. However, the model could be modified in future studies to more realistically account for differences in crown shape and complexity. Second, the model predictions and assumptions could be tested with high voltage experimental discharges in the laboratory (Wakasa et al. 2012). For example, electric current, and thus heating and maximum power, could be isolated within smaller subsections of tree tissues and this non-uniform distribution of damage could either enable trees to survive lightning or increase the likelihood of localized explosive damage (i.e., lighting scars). Such studies would provide insight into the damaging effects of extreme heating and power on living plant tissues under a variety of conditions. Third, fully testing the model will require large amounts of data on the real-time distribution of CG lightning flashes, their characteristics, and their effects on trees, lianas, and other forest canopy elements. Such data are very difficult to obtain due to limitations in the spatial accuracy of lightning detection networks (Mäkelä et al. 2016), but advances in lightning sensing technology (Bitzer et al. 2013) suggest that this logistical hurdle soon will be overcome (Yanoviak et al. 2017). Finally, an accurate estimate of lightning-caused death also fundamentally depends on the probability that any given tree will be struck by lightning. Incorporating

this risk-based information into the model would enhance its predictive power and broaden its applicability.

TABLES

Table 11. List of the focal plant species used in this study. Stems were divided into three groups based on diameter. Values are sample sizes (N) for each diameter class. All data were independent; i.e., different stems were used for each measurement.

	Species	Family	<3 cm	3-10 cm	>10 cm
Trees (N = 145)	*Dipteryx panamensis*	Fabaceae	8	7	12
	Jacaranda copaia	Bignoniaceae	8	8	20
	Terminalia amazonia	Combretaceae	7	8	-
	Luehea seemannii	Malvaceae	5	8	-
	Miconia argentea	Melastomataceae	8	8	-
	Alseis blackiana	Rubiacaea	6	8	19
Lianas (N = 103)	*Clitoria javitensis*	Fabaceae	7	8	-
	Arrabidaea patellifera	Bignoniaceae	6	9	-
	Combretum decandrum	Combretaceae	8	8	-
	Connarus panamensis	Connaraceae	7	7	-
	Davilla nitida	Dilleniaceae	6	9	-
	Hippocratea volubilis	Celastraceae	7	8	-
	Coccoloba parimensis	Polygonaceae	11	7	-

Table 12. Resistance, maximum power, and heating for 11 different tropical and temperate tree species, and three types of lightning flashes (D1, D2, D3 = Discharges 1, 2, and 3 as described in the text). Maximum power is the same for all three types of lightning. All model trees were 20 m tall with a minimum diameter of 1 cm at their top and a basal diameter of 27.3 cm. Resistivity for each tree was calculated using the resistivity-diameter function: $\ln(p) = mD + b$, where p and D are resistivity and the cube-root of diameter, respectively.

Region	Species	Resistivity-diameter function		Resistance (kΩ)	Maximum power (TW)	Heating (GJ)		
		Slope	Intercept			D1	D2	D3
Tropical	*Jacaranda copaia*	8.29	2.07	1275	1154	18.9	27.6	24.7
	Alseis blackiana	8.66	2.39	2062	1867	30.6	44.7	40.0
	Dipteryx panamensis	8.77	1.87	1284	1163	19.0	27.9	25.0
Temperate	*Acer rubrum*	8.46	2.29	1716	1554	25.4	37.2	33.3
	Acer saccharum	8.17	2.83	2615	2368	38.8	56.7	50.7
	Quercus rubra	8.42	2.63	2359	2136	35.0	51.2	45.8
	Betula alleghaniensis	8.23	2.75	2471	2238	36.6	53.6	48.0
	Pinus virginiana	9.09	2.51	2706	2450	40.1	58.7	52.5
	Pinus resinosa	7.91	3.28	3685	3336	54.6	80.0	71.5
	Pinus strobus	8.66	2.55	2406	2178	35.7	52.2	46.7
	Tsuga canadensis	8.89	2.41	2306	2088	34.2	50.0	44.8

Table 13. Total heating, both as an absolute value and per volume of tissue, and maximum power among different sizes of hypothetical *Dipteryx panamensis* and *Alseis blackiana* trees. The minimum diameter at the top of each tree was defined as 1.0 cm, and maximum diameter was determined using different height:diameter relationships for each species as explained in the text.

Species	Height (m)	Maximum diameter (cm)	Resistance (kΩ)	Volume (m^3)	Maximum Power (TW)	Total heating (GJ)	Heat Density (kJ cm^{-3})
Dipteryx panamensis	30	47.4	1525	1.80	1380	22.6	12.5
	25	37.0	1394	0.92	1262	20.7	22.5
	22	31.1	1326	0.58	1200	19.6	34.2
	20	27.3	1284	0.40	1163	19.0	47.0
	18	23.7	1244	0.28	1126	18.4	66.7
	15	18.5	1190	0.14	1077	17.6	124.3
	10	10.6	1114	0.03	1009	16.5	509.7
Alseis blackiana	30	38.3	2633	1.18	2384	39.0	33.0
	25	29.5	2477	0.59	2243	36.7	62.3
	22	24.6	2396	0.36	2169	35.5	97.8
	20	21.4	2352	0.25	2130	34.9	138.7
	18	18.5	2302	0.17	2085	34.1	200.4
	15	14.2	2251	0.09	2038	33.4	392.1
	10	8.0	2171	0.02	1966	32.2	1684.8

Table 14. The predicted decrease in heating and maximum power experienced by trees with 0, 1, or 3 lianas present (0L, 1L, and 3L). Values are based on a single stroke lightning flash (*Discharge 1* in the text). Lianas divert an equal proportion heat and power away from the tree stem, thus the percentages are only presented once.

Region	Species	Total heating (GJ)			Maximum power (TW)			Total heating or power diverted (%)	
		0L	1L	3L	0L	1L	3L	1L	3L
Tropical	*Jacaranda copaia*	18.9	9.27	3.63	1154	566	222	51	81
	Alseis blackiana	30.6	10.7	3.23	1867	653	197	65	89
	Dipteryx panamensis	19	9.3	3.62	1163	569	222	51	81
Temperate	*Acer rubrum*	25.4	12.6	4.79	1554	771	293	50	81
	Acer saccharum	38.8	14	4.34	2368	854	265	64	89
	Quercus rubra	35	13.7	4.48	2136	836	273	61	87
	Betula alleghaniensis	36.6	13.9	4.42	2238	850	270	62	88
	Pinus virginiana	40.1	14.1	4.29	2450	862	262	65	89
	Pinus resinosa	54.6	14.6	3.78	3336	892	231	73	93
	Pinus strobus	35.7	13.8	4.46	2178	842	272	61	88
	Tsuga canadensis	34.2	13.6	4.51	2088	830	275	60	87

FIGURE LEGENDS

Figure 15. The canopy profile of a hypothetical tropical forest composed of *Dipteryx panamensis* (triangular tree crowns) and *Alseis blackiana* (rectangular tree crowns). The gray shade of each model tree and the superimposed number indicate heating density (kJ cm^{-3}). Gray shades span a gradient from "hot" (dark gray) to "cool" (light gray), indicating high and low levels of heating during a lightning discharge, respectively. Lianas are represented as sinuous structures descending from two of the trees. Tree height and relative trunk diameter are drawn to scale. Heating density is affected by tree species, tree height, tree diameter, and the presence of lianas (see text for details).

Figure 16. Predicted changes in heating density (filled shapes) and maximum power (unfilled shapes) during a lightning discharge vs. the height of hypothetical *Dipteryx panamensis* (squares) and *Alseis blackiana* (circles) trees.

Figure 17. Predicted total heating (mean ± SE) of temperate (filled circles, n = 8 species) and tropical (unfilled circles, n = 3 species) trees vs. the number of lianas present in each. Predicted maximum power follows the same pattern.

Figure 18. Electrical resistivity vs. diameter for tree (open circles, dashed line) and liana (solid circles, solid line) stems 3-10 cm in diameter. Note that the x-axis is cube-root transformed.

Figure 19. Electrical resistivity vs. diameter for tree stems > 10 cm in diameter (*Alseis blackiana* = circles, dashed line; *Dipteryx panamensis* = squares, solid line; and *Jacaranda copaia* = triangles, dotted line). The x-axis is cube-root transformed.

Figure 20. Resistivity across a range of diameter (A) and moisture content (B) for the same individuals of *Alseis blackiana* (solid line and open circles) and *Arrabidaea patellifera* (dashed line and filled circles). The Panel A x-axis is cube-root transformed.

Figure 15

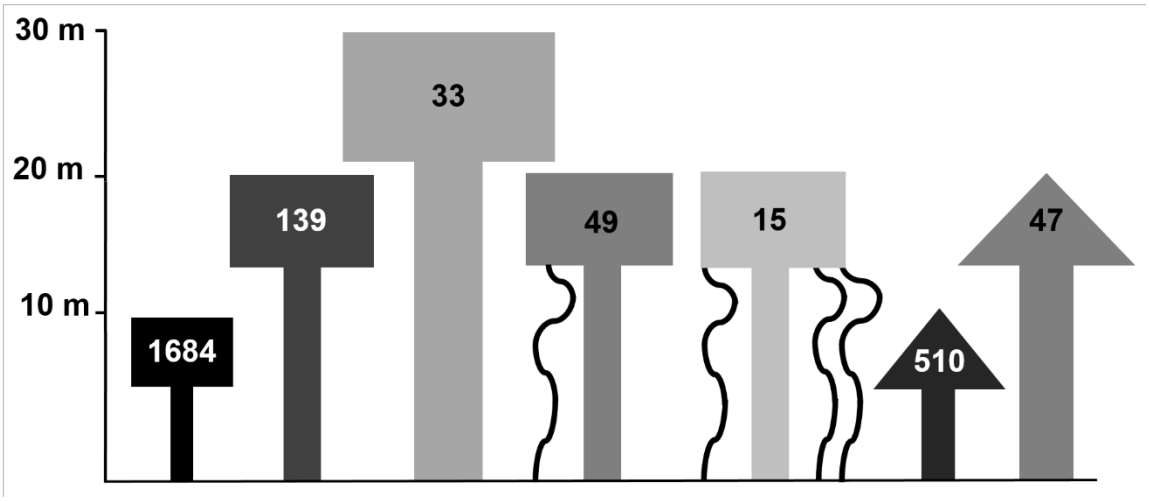

Figure 16

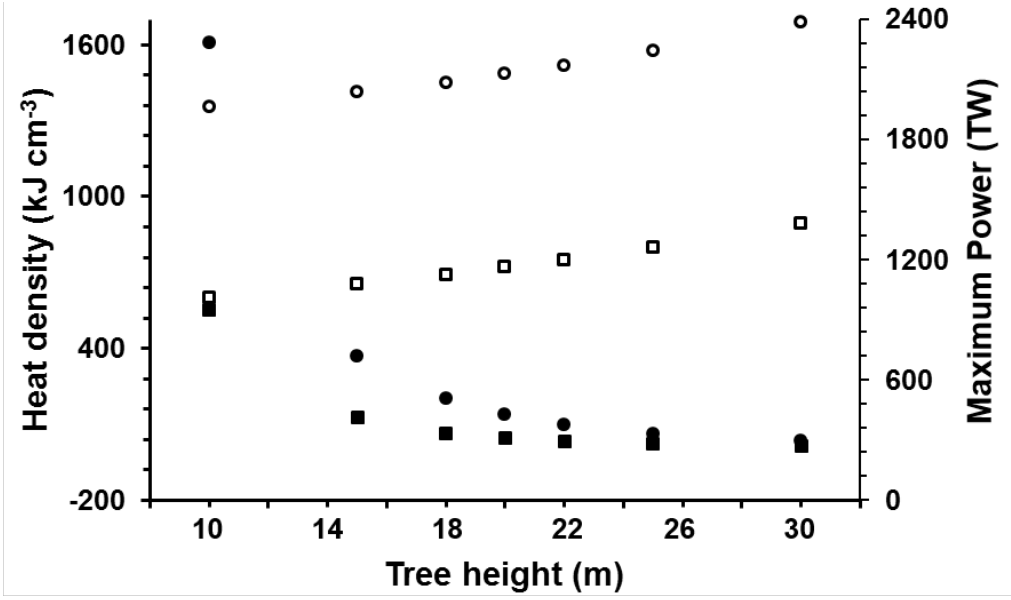
Heat density (kJ cm-3)
1600
1000
400
-200
2400
1800
1200
600
0
Maximum Power (TW)
10
14
18
22
26
30
Tree height (m)

Figure 17

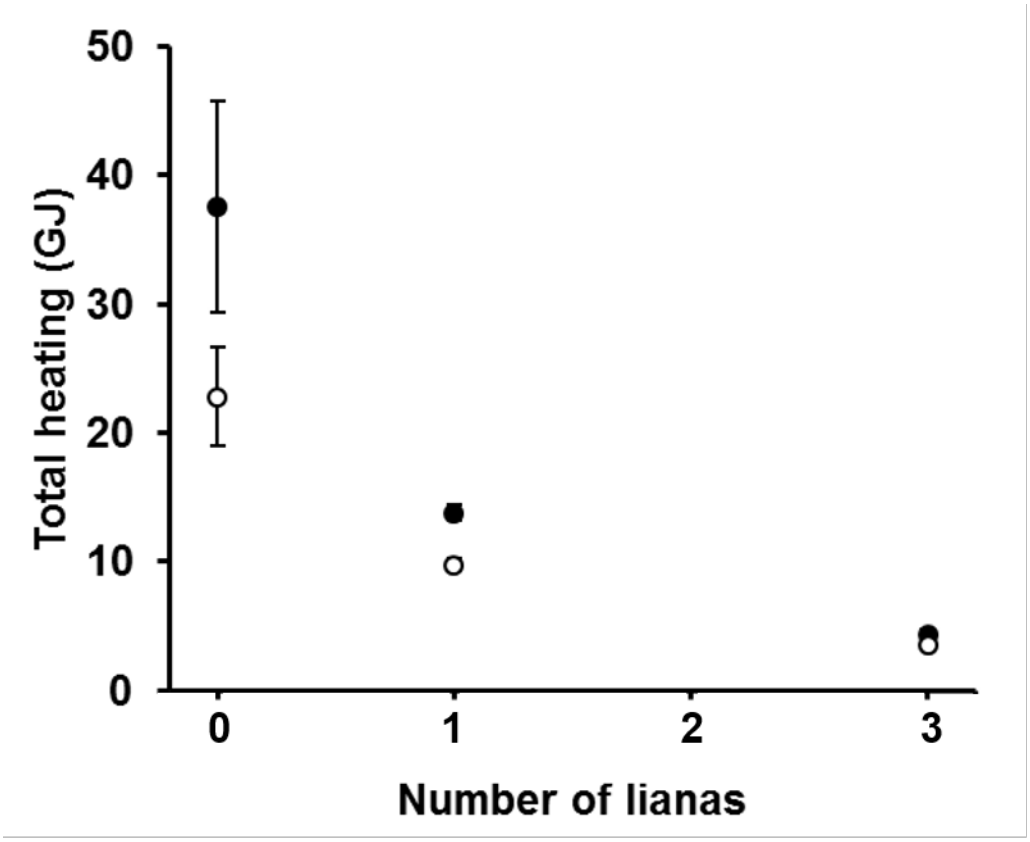

Figure 18

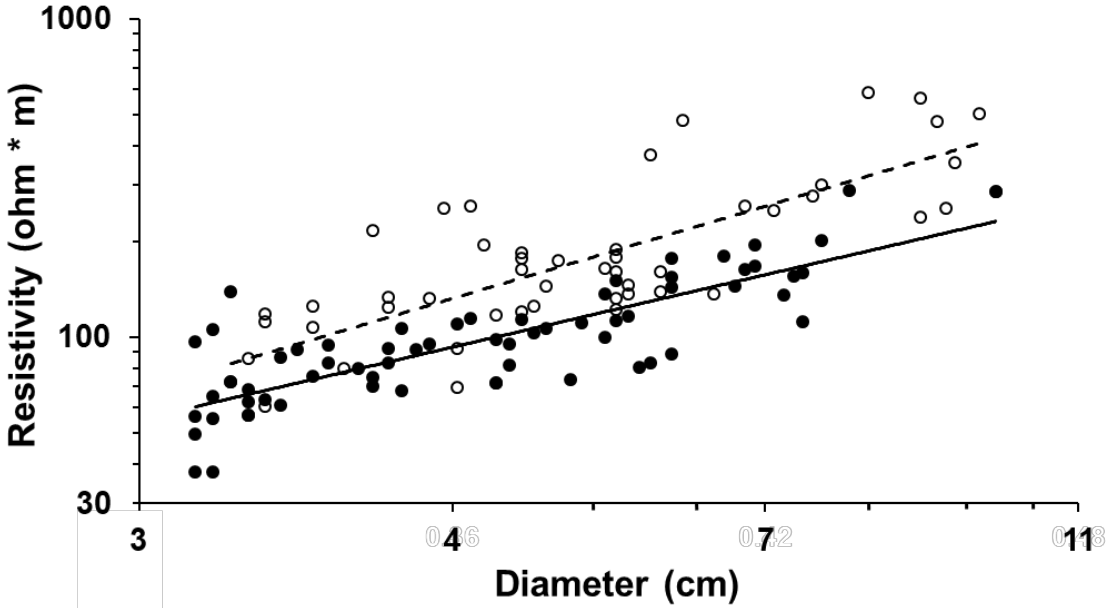

Figure 19

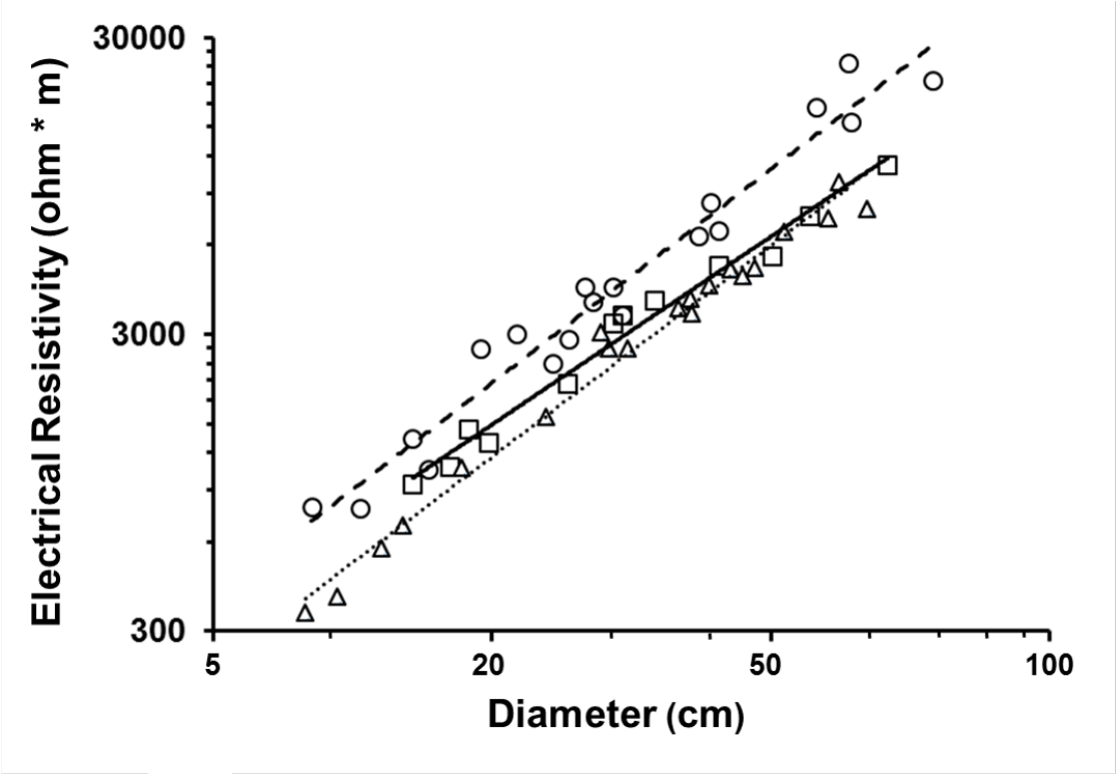
30000
3000
300
Electrical Resistivity (ohm * m)
5
20
50
100
Diameter (cm)

Figure 20

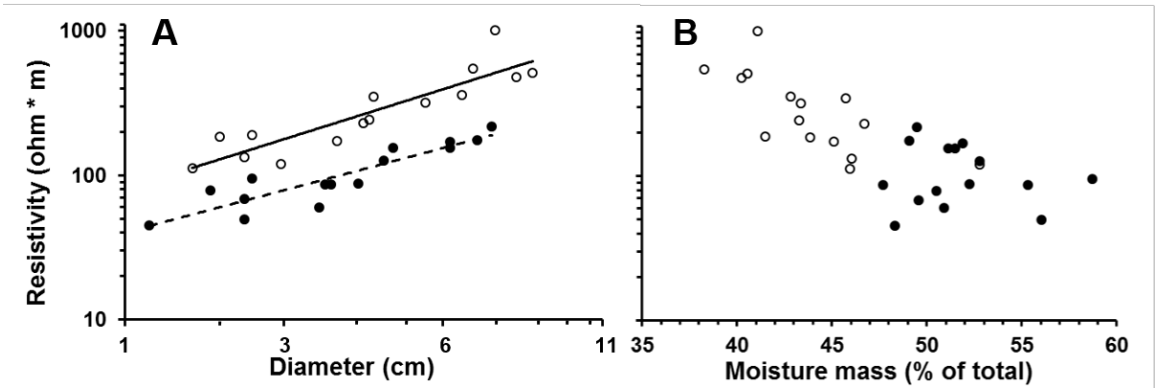
A
B
Resistivity (ohm * m)
1000
100
10
1
3
6
11
Diameter (cm)
35
40
45
50
55
60
Moisture mass (% of total)

CHAPTER VI

SUMMARY AND CONCLUSIONS

Dead wood is a major component of carbon cycling, but remains one of the least studied aspects of carbon inventories and models (Pan et al. 2011, Palace et al. 2012). Across multiple collaborations, I quantified how matter cycles through dead wood with a focus on factors that are important to wood production and decomposition. The results of these studies provide a framework for future investigations of woody debris and expand the scope of this field to consider vertical gradients within forests and the effects of nutrients over long-time frames.

I present multiple lines of evidence that elevated, standing, and suspended woody debris are important to decomposition and the role wood plays in carbon cycling. The vast majority of wood inputs and approximately half of downed woody debris stocks were not in contact with the soil at our study site. Moreover, I show that slowed decomposition in elevated portions of downed woody debris likely cause the longer residence times of downed woody debris that is partially elevated (Přívětivý et al. 2016). Given the proportion of downed woody debris that is elevated above the soil, it is likely that the majority of woody debris is decomposing above the forest floor globally (Palace et al. 2012). This is problematic because the contemporary understanding of decomposition is based exclusively on ground-level processes ((Thornton 1998, Liski et al. 2005, Weedon et al. 2009, van Geffen et al. 2010, Cornelissen et al. 2012, Bradford et al. 2014, Zanne et al. 2015, reviewed by Cornwell et al. 2009). To begin addressing this knowledge gap, I quantified the factors that regulate decomposition along a vertical forest gradient. Contrary to our expectations, biotic factors were most important to

decomposition on the forest floor, whereas abiotic factors were more strongly associated with decomposition in higher levels of the forest. Moreover, we provide evidence that saproxylic communities transition with increasing height within the forest from primarily fungal decomposers to bacterial decomposers and taxa with alternative functions (e.g., nitrogen fixation and photosynthesis). This information should form the foundation for future studies investigating aboveground decomposition and linking these processes to carbon cycling.

This dissertation also highlights the complex impacts of soil nutrient availability on wood decomposition over time. The vast majority of dead wood mass is stored in pieces of coarse woody debris that decompose over long time frames. However, studies of wood decomposition typically focus on small substrates over short time frames. Using a nutrient addition experiment (N, P, and K) nested within a long-term litter manipulation experiment, we demonstrated that small increases in soil nutrients did not affect long-term decomposition rates of entire trees, but decreased nutrient availability caused decreased decomposition with a lagged response (after 6 years). The residence time of snags also increased with decreased nutrient availability, suggesting that nutrients also influence how matter cycles among pools of woody debris. This is the first test of the effects of exogenous nutrient availability on long-term (> 3 year) decomposition and it indicates that longer studies are necessary to understand the long-term process of carbon cycling through dead wood.

The studies described here also quantified aspects of dead wood production and inputs with implications for carbon cycling. The dead wood inventory provided estimates that are important to calculations of forest productivity (branchfall; Clark et al. 2001, Malhi et al. 2011, Cleveland et al. 2015) and previously undescribed components of forest necromass (liana wood and elevated sections of downed woody debris). These

estimates will help parametrize carbon cycling models. I also used empirical data regarding the electrical characteristics of trees and lightning to begin understanding species-specific patterns of tree mortality and wood inputs. These results suggest that strong species effects influence lightning-caused tree mortality, as previously indicated by various anecdotes (Baker 1973, Taylor 1977). Further work is needed to apply our locally relevant findings to the scale of an entire forest. Improved models and empirical tests of their predictions will improve our understanding of forest dynamics, including effects on individuals, populations, communities, and ecosystem processes (reviewed by McDowell et al. 2018).

Collectively, the studies presented here make major contributions to our understanding of decomposition and carbon cycling. I provide a framework for forest inventories that will improve accuracy and precision while reducing biases. Future studies should build on this foundation by investigating long-term processes regulating the decomposition of large pieces of woody debris because these are most relevant to carbon cycling. Moreover, the dynamic process of decomposition as wood moves from standing, suspended, and elevated positions to the forest floor remains particularly poorly understood. The next step in this research is to link the effects of distinct processes above the forest floor to ground-level decomposer community structure and decomposition outcomes over long time frames. The findings presented here and the next steps outlined above will dramatically improve our understanding of carbon cycling in a changing world.

REFERENCES

Adair, E. C., W. J. Parton, S. J. Del Grosso, W. L. Silver, M. E. Harmon, S. A. Hall, I. C. Burke, and S. C. Hart. 2008. Simple three-pool model accurately describes patterns of long-term litter decomposition in diverse climates. Glob. Change Biol. 14: 2636-2660.

al Hagrey, S. A. 2006. Electrical resistivity imaging of tree trunks. Near Surf. Geophys. 4: 179-187.

Albrecht, R., S. Goodman, D. Buechler, R. Blakeslee, and H. Christian. 2016. Where are the lightning hotspots on Earth? Bull. Amer. Meteor. Soc. 97: 2051-2068.

Anderson, A. R. 1964. Observations on climatic damage in peat swamp forest in Sarawak. Commonw. For. Rev. 43: 145-158.

Angyalossy, V., M. R. Pace, and A. C. Lima. 2015. Liana anatomy: a broad perspective on structural evolution of the vascular system. In Ecology of Lianas (eds. SA Schnitzer, F Bongers, BJ Burnham, FE Putz), pp 253-287. Oxford, UK: John Wiley and Sons, Ltd.

Anonymous. 1898. Which trees attract lightning? Mon. Weather Rev. 26: 257-258.

Austin, A.T., and L. Vivanco. 2006. Plant litter decomposition in a semi-arid ecosystem controlled by photodegradation. Nature 442: 555-558.

Baker, W. W. 1973. Longevity of lightning-struck trees and notes on wildlife use. Proc. Tall Timbers Fire Ecol. Conf. 13: 497-504.

Bates, D., M. Maechler, B. Bolker, and S. Walker. 2014. lme4: Linear mixed-effects models using Eigen and S4. Ver. 1.0-6.

Bebber, D. P., S. C. Watkinson, L. Boddy, and P. R. Darrah. 2011. Simulated nitrogen deposition affects wood decomposition by cord-forming fungi. Oecologia 167: 1177-1184.

Berg, B., and R. Laskowski. 2005. Litter decomposition: a guide to carbon and nutrient turnover. Adv. Ecol. Res. 38: 1-17.

Bieker, D., and S. Rust. 2010. Electric resistivity tomography shows radial variation of electrolytes in *Quercus robur*. Can. J. For. Res. 40: 1189-1193.

Bitzer, P. M. 2016. Global distribution and properties of continuing current in lightning. J. Geophys. Res.-Atmos. 122: 1033-1041.

Bitzer, P. M., H. J. Christian, M. Stewart, J. C. Burchfield, S. Podgorny, D. Corredor, J. Hall, E. Kuznetsov, and V. Franklin. 2013. Characterization and applications of VLF/LF source locations from lightning using the Huntsville Alabama Marx Meter Array. J. Geophys. Res.-Atmos. 118: 3120-3138.

Boddy, L. 2001. Fungal community ecology and wood decomposition processes in angiosperms: From standing tree to complete decay of coarse woody debris. Ecol. Bull. 49: 43-56.

Boddy, L., E. M. Owens, and I. H. Chapela. 1989. Small scale variation in decay rate within logs one year after felling: Effect of fungal community structure and moisture content. FEMS Microbiol. Lett. 62: 173-183.

Boddy, L., J. Hynes, D. P. Bebber, and M. D. Fricker. 2009. Saprotrophic cord systems: Dispersal mechanisms in space and time. Mycoscience. 50: 9-19.

Bolker, B. M. et al. 2009. Generalized linear mixed models: a practical guide for ecology and evolution. Trends Ecol. Evol. 24: 127-135.

Bradford, M. A., R. J. Warren II, P. Baldrian, T. W. Crowther, D. S. Maynard, E. E. Oldfield, W. R. Wieder, S. A. Wood, and J. R. King. 2014. Climate fails to predict wood decomposition at regional scales. Nat. Clim. Change. 4: 625.

Brais, S., D. Paré, and C. Leirman. 2006. Tree bole mineralization rates of four species of the Canadian eastern boreal forest: implications for nutrient dynamics following stand-replacing disturbances. Can. J. Forest Res. 36: 2331-2340.

Bréchet, L. et al. 2017. Short- and long-term influence of litter quality and quantity on simulated heterotrophic soil respiration in a lowland tropical forest. Ecosystems: 1-15.

Brown, S. 1997. Estimating biomass and biomass change of tropical forests: A primer. Food and Agriculture Org., Rome, USA. 55 pp.

Brünig, E. F. 1964. A study of damage attributed to lightning in two areas of Shorea albida forest in Sarawak. Commonw. Forest Rev. 43: 134-144.

Carey, E. V., S. Brown, A. J. R. Gillespie, and A. E. Lugo. 1994. Tree mortality in mature lowland tropical moist and tropical lower montane moist forests of venezuela. Biotropica. 26: 255-265.

Carey, E. V., S. Brown, A. J. R. Gillespie, and A. E. Lugo. 1994. Tree mortality in mature lowland tropical moist and tropical lower montane moist forests of Venezuela. Biotropica 26: 255-265.

Carlson, B. S., S. E. Koerner, V. P. Medjibe, L. J. White, and J. R. Poulsen. 2017. Deadwood stocks increase with selective logging and large tree frequency in gabon. Glob. Change Biol. 23: 1648-1660.

Carreiro, M., R. Sinsabaugh, D. Repert, and D. Parkhurst. 2000. Microbial enzyme shifts explain litter decay responses to simulated nitrogen deposition. Ecol. 81: 2359-2365.

Carter, J. K., and R. O. Blanchard. 1978. Electrical resistance related to phloem width in red maple. Can. J. For Res. 8: 90-93.

Chambers, J. Q., N. Higuchi, J. P. Schimel, L. V. Ferreira, and J. M. Melack. 2000. Decomposition and carbon cycling of dead trees in tropical forests of the central amazon. Oecologia 122: 380-388.

Chambers, J.Q. et al. 2004. Respiration from a tropical forest ecosystem: partitioning of sources and low carbon use efficiency. Ecol. Appl. 14: 72-88.

Chave, J. et al. 2005. Tree allometry and improved estimation of carbon stocks and balance in tropical forests. Oecologia.145: 87-99.

Chave, J., D. Coomes, S. Jansen, S. L. Lewis, N. G. Swenson, and Z. E. Zanne. 2009. Towards a worldwide wood economics spectrum. Ecol. Lett. 12: 351-366.

Chave, J., R. Condit, S. Lao, J. P. Caspersen, R. B. Foster, and S. P. Hubbell. 2003. Spatial and temporal variation of biomass in a tropical forest: Results from a large census plot in panama. J. Ecol. 91: 240-252.

Chen, Y. et al. 2015. Nutrient limitation of woody debris decomposition in a tropical forest: contrasting effects of N and P addition. Funct. Ecol. 30: 295-304.

Christensen, O. 1977. Estimation of standing crop and turnover of dead wood in a danish oak forest. Oikos 28: 177-186.

Christensen-Dalsgaard, K. K., M. Fournier, A. R. Ennos, and A. S. Barfod. 2007. Changes in vessel anatomy in response to mechanical loading in six species of tropical trees. New Phytol. 176: 610-622.

Christian, H. J., R. J. Blakeslee, D. J. Boccippio, W. L. Boeck, D. E. Buechler, K. T. Driscoll, S. J. Goodman, J. M. Hall, W. J. Koshak, D. M. Mach, and M. F. Stewart. 2003. Global frequency and distribution of lightning as observed from space by the Optical Transient Detector. J. Geophys. Res-Atmos. 108: 4005.

Clark, D. A., S. Brown, D. W. Kicklighter, J. Q. Chambers, J. R. Thomlinson, and J. Ni. 2001. Measuring net primary production in forests: Concepts and field methods. Ecol. Appl. 11: 356-370.

Clark, D. B., D. A. Clark, S. Brown, S. F. Oberbauer, and E. Veldkamp. 2002. Stocks and flows of coarse woody debris across a tropical rain forest nutrient and topography gradient. Forest Ecol. Mgmt. 164: 237-248.

Clay, N. A., D. A. Donoso, and M. Kaspari. 2015. Urine as an important source of sodium increases decomposition in an inland but not coastal tropical forest. Oecologia 177: 571-579.

Cleveland, C. C., P. Taylor, K. D. Chadwick, K. Dahlin, C. E. Doughty, Y. Malhi, W. K. Smith, B. W. Sullivan, W. R. Wieder, and A. R. Townsend. 2015. A comparison of plot-based satellite and earth system model estimates of tropical forest net primary production. Global Biogeochem. Cy. 29: 626-644.

Cornelissen, J. H. C. et al. 2012. Controls on coarse wood decay in temperate tree species: Birth of the loglife experiment. AMBIO. 41: 231-245.

Cornwell, W. K., J. H. C. Cornelissen, S. D. Allison, J. Bauhus, P. Eggleton, C. M. Preston, F. Scarff, J. T. Weedon, C. Wirth, and A. E. Zanne. 2009. Plant traits and wood fates across the globe: Rotted, burned, or consumed? Glob. Change Biol. 15: 2431-2449.

Courty, M-A. 2016. Fuel origin and firing product preservation in archaeological occupation contexts. Quatern. Int. 431: 116-130.

Covert, R. N. 1924. Why an oak is often struck by lightning: a method of protecting trees against lightning. Mo. Weather Rev. 52: 492-493.

Cushman, K. C., H. C. Muller-Landau, R. S. Condit, and S. P. Hubbell. 2014. Improving estimates of biomass change in buttressed trees using tree taper models. Methods Ecol. Evol. 5: 573-582.

Defandorf, F. M. 1955. A tree from the viewpoint of lightning. J. Wash. Acad. Sci. 45: 333-339.

Delaney, M., S. Brown, A. E. Lugo, A. Torres-Lezama, and N. B. Quintero. 1998. The quantity and turnover of dead wood in permanent forest plots in six life zones of venezuela. Biotropica. 30: 2-11.

Diendorfer, G., and M. A. Uman. 1990. An improved return stroke model with specified channel-base current. J. Geophys. Res.-Atmos. 95: 13621-13644.

Doughty, C. E. et al. 2015. Drought impact on forest carbon dynamics and fluxes in amazonia. Nature. 519: 78.

Dufrene, M., and P. Legendre. 1997. Species assemblages and indicator species: the need for a flexible asymmetrical approach. Ecol. Monogr. 67: 345-366.

Falster, D. S., R. A. Duursma, J. L. Baltzer, C. Baraloto, M. Battaglia, J. J. Battles, B. Bond-Lamberty, M. van Breugel, J. Camac, and Y. Claveau. 2015. Baad: A biomass and allometry database for woody plants.

Fasth, B. G., M. E. Harmon, J. Sexton, and P. White. 2011. Decomposition of fine woody debris in a deciduous forest in north carolina. J. Torrey Bot. Soc. 138: 192-206.

Feldpausch, T.R. et al. 2012. Tree height integrated into pantropical forest biomass estimates. Biogeosciences 9: 3381-3403.

Franklin, J. F., H. H. Shugart, and M. E. Harmon. 1987. Tree death as an ecological process. Bioscience. 37: 550-556.

Fukami, T. et al. 2010. Assembly history dictates ecosystem functioning: evidence from wood decomposer communities. Ecol. Lett. 13: 675-684.

Fuquay, D. M., A. R. Taylor, R. G. Hawe, and C. W. Schmid Jr. 1972. Lightning discharges that caused forest fires. J. Geophys. Res. 77: 2156-2158.

Gora, E. M, and S. P. Yanoviak. 2015. Electrical properties of temperate forest trees: a review and quantitative comparison with vines. Can. J. For. Res. 45: 236-245.

Gora, E. M., L. L. Battaglia, H. B. Schumacher, and W. P. Carson. 2014. Patterns of coarse woody debris volume among 18 late-successional and mature forest stands in Pennsylvania. J. Torrey Bot. Soc. 141: 151-160.

Grubb, P.J., and P. J. Edwards. 1982. Studies of mineral cycling in a montane rain forest in new guinea: iii. the distribution of mineral elements in the above-ground material. J. Ecol. 70: 623-648.

Gurdak, D. J., L. E. Aragão, A. Rozas-Dávila, W. H. Huasco, K. G. Cabrera, C. E. Doughty, W. Farfan-Rios, J. E. Silva-Espejo, D. B. Metcalfe, and M. R. Silman. 2014. Assessing above-ground woody debris dynamics along a gradient of elevation in amazonian cloud forests in peru: Balancing above-ground inputs and respiration outputs. Plant Ecol. Divers. 7: 143-160.

Harmon, M. E., and J. Sexton. 1996. Guidelines for measurements of woody detritus in forest ecosystems. Page 73 *in* U. o. Washington, editor., Washington, USA.

Harmon, M. E., J. F. Franklin, F. J. Swanson, P. Sollins, S. V. Gregory, J. D. Lattin, N. H. Anderson, S. P. Cline, N. G. Aumen, J. R. Sedell, G. W. Lienkaemper, K. Cromack, Jr, and K. W. Cummins. 1986. Ecology of coarse woody debris in temperate ecosystems. Adv. Ecol. Res. 15: 133-302.

Heidler, F. 1985. Analytische blitzstromfunktion zur LEMP-berechnung. In Proc. of the 18th Intl. Conf. Lightning Protection, pp. 63-66., Munich, Germany.

Heidler, F., and J. Cvetic. 2002. A class of analytical functions to study the lightning effects associated with the current front. Eur. T. Electr. Power 12: 141-150.

Hobbie, S. E., and P. M. Vitousek. 2000. Nutrient limitation of decomposition in Hawaiian forests. Ecol. 81: 1867-1877.

Hodges, J. D, and L. S. Pickard. 1971. Lightning in the ecology of the southern pine beetle, *Dendroctonus frontalis* (Coleoptera: Scolytidae). Can. Entomol. 103: 44-51.

Hothorn, T., F. Bretz, and P. Westfall. 2008. Simultaneous inference in general parametric models. Biometrical J. 50: 346-363.

Hubbell, S. P., and R. B. Foster. 1983. Diversity of canopy trees in a neotropical forest and implications for conservation. *In* Tropical rain forest: Ecology and management. *Edited by* S. L. Sutton, T. C. Whitmore, and A. C. Chadwick. Blackwell Scientific, Oxford. pp 25-41.

Janisch, J., and M. Harmon. 2002. Successional changes in live and dead wood carbon stores: Implications for net ecosystem productivity. Tree Physiol. 22: 77-89.

Kaspari, M., M. N. Garcia, K. E. Harms, M. Santana, S. J. Wright, and J. B. Yavitt. 2008. Multiple nutrients limit litterfall and decomposition in a tropical forest. Ecol. Lett. 11: 35-43.

Kaspari, M., K. A. Roeder, B. Benson, M. D. Weiser, and N. J. Sanders. 2017. Sodium co-limits and catalyzes macronutrients in a prairie food web. Ecol. 98: 315-320.

Kaspari, M., S. P. Yanoviak, R. Dudley, M. Yuan, and N. A. Clay. 2009. Sodium shortage as a constraint on the carbon cycle in an inland tropical rainforest. Proc. Natl. Acad. Sci. 106: 19405-19409.

Kaye, J. P., and S. C. Hart. 1997. Competition for nitrogen between plants and soil microorganisms. Trends Ecol. Evol. 12: 139-143.

Keller, M., M. Palace, G. P. Asner, R. Pereira, and J. N. M. Silva. 2004. Coarse woody debris in undisturbed and logged forests in the eastern brazilian amazon. Glob. Change Biol. 10: 784-795.

Kimmey, J. W. 1955. Rate of deterioration of fire-killed timber in California. Volume 962, Department of Agriculture, Washington D.C., United States.

Kitagawa, N., M. Brook, and E. J. Workman. 1962. Continuing currents in cloud-to-ground lightning discharges. J. Geophys. Res. 67: 637-647.

Knight, D. H. 1987. Parasites, lightning, and the vegetation mosaic in wilderness landscapes. In Landscape heterogeneity and disturbance (ed. MG Turner), pp. 59-83. New York, USA: Springer-Verlag.

Komarek, E. V. 1964. The natural history of lightning. Proc. Tall Timbers Fire Ecol. Conf. 3: 139-183.

Král, K., D. Janík, T. Vrška, D. Adam, L. Hort, P. Unar, and P. Šamonil. 2010. Local variability of stand structural features in beech dominated natural forests of central europe: Implications for sampling. Forest Ecol. Mgmt. 260: 2196-2203.

Král, K., M. Valtera, D. Janík, P. Šamonil, and T. Vrška. 2014. Spatial variability of general stand characteristics in central european beech-dominated natural stands–effects of scale. Forest Ecol. Mgmt. 328: 353-364.

Kurzel, B. P, S. A. Schnitzer, and W. P. Carson. 2006. Predicting liana crown location from stem diameter in three Panamanian lowland forests. Biotropica 38: 262-266.

Kuznetsova, A., P. B. Brockhoff, and R. H. Bojesen. 2016. LmerTest: tests in linear mixed effects models. Version 2.0.

Lang, G. E., and D. H. Knight. 1979. Decay rates for boles of tropical trees in panama. Biotropica. 11: 316-317.

Larjavaara, M., and H. C. Muller-Landau. 2010. Comparison of decay classification, knife test, and two penetrometers for estimating wood density of coarse woody debris. Can. J. For. Res. 40: 2313-2321.

Leigh Jr., E. G., A. S. Rand, and D. M. Windsor. 1996. The Ecology of a Tropical Forest. Second ed. Washington, DC, USA: Smithsonian Institution.

Leigh, E. G., Jr. 1999. Tropical forest ecology: A view from barro colorado island. Oxford University Press, Oxford, England, UK. pp. 245.

Liski, J., T. Palosuo, M. Peltoniemi, and R. Sievänen. 2005. Carbon and decomposition model yasso for forest soils. Ecol. Model. 189: 168-182.

Magnusson, W. E, A. P. Lima, and O. de Lima. 1996. Group lightning mortality of trees in a neotropical forest. J. Trop. Ecol. 12: 899-903.

Mäkelä, A., J. Mäkelä, J. Haapalainen, and N. Porjo. 2016. The verification of lightning location accuracy in Finland deduced from lightning strikes to trees. Atmos. Res. 172: 1-7.

Mäkelä, J., E. Karvinen, N. Porjo, A. Mäkelä, and T. Tuomi. 2009. Attachment of natural lightning flashes to trees: preliminary statistical characteristics. J. Lightning Res. 1: 9-21.

Malhi, Y., C. Doughty, and D. Galbraith. 2011. The allocation of ecosystem net primary productivity in tropical forests. Phil. Trans. R. Soc. B. 366: 3225-3245.

Malhi, Y., et al . 2014. The productivity, metabolism and carbon cycle of two lowland tropical forest plots in south-western amazonia, peru. Plant Ecol. Divers. 7: 85-105.

Marvin, D. C., and G. P. Asner. 2016. Branchfall dominates annual carbon flux across lowland amazonian forests. Environ. Res. Lett. 11: 94027.

Mascaro, J., G. P. Asner, H. C. Muller-Landau, M. van Breugel, J. Hall, and K. Dahlin. 2011. Controls over aboveground forest carbon density on Barro Colorado Island, Panama. Biogeosciences. 8: 1615-1629.

McDowell, N., et al. 2018. Drivers and mechanisms of tree mortality in moist tropical forests. New Phytol. Available Online.

Meakem, V., A. J. Tepley, E. B. Gonzalez-Akre, V. Herrmann, H. C. Muller-Landau, S. J. Wright, S. P. Hubbell, R. Condit, and K. J. Anderson-Teixeira. 2017. Role of tree size in moist tropical forest carbon cycling and water deficit responses. New Phytol. Available Online.

Meerts, P. 2002. Mineral nutrient concentrations in sapwood and heartwood: a literature review. Ann. For. Sci. 59: 713-722.

Metcalfe, D., P. Meir, L. E. O. C. Aragão, A. da Costa, S. Almeida, A. Braga, P. Gonçalves, J. Athaydes, Y. Malhi, and M. Williams. 2008. Sample sizes for estimating key ecosystem characteristics in a tropical terra firme rainforest. Forest Ecol. Mgmt. 255: 558-566.

Mooshammer, M., W. Wanek, S. Zechmeister-Boltenstern, and A. Richter. 2014. Stoichiometric imbalances between terrestrial decomposer communities and their resources: mechanisms and implications of microbial adaptations to their resources. Front. Microbiol. 5: 22.

Muzika, R. M., R. P. Guyette, M. C. Stambaugh, and J. M. Marschall. 2015. Fire, drought, and humans in a heterogeneous Lake Superior landscape. J. Sustainable For. 34: 49-70.

Nottingham, A.T., H. Griffiths, P. M. Chamberlain, A. W. Stott, and E. V. J. Tanner. 2009. Soil priming by sugar and leaf-litter substrates: A link to microbial groups. Appl. Soil Ecol. 42: 183-190.

Oberle, B., K. R. Covey, K. M. Dunham, E. J. Hernandez, M. L. Walton, D. F. Young, and A. E. Zanne. 2017. Dissecting the effects of diameter on wood decay emphasizes the importance of cross-stem conductivity in Fraxinus americana. Ecosystems, 1-13.

Oberle, B., K. M. Dunham, A. M. Milo, M. I. Walton, D. F. Young, and A. E. Zanne. 2014. Progressive, idiosyncratic changes in wood hardness during decay: implications for dead wood inventory and cycling. Forest Ecol. Manag. 323: 1-9.

O'Brien, S. T., S. P. Hubbell, P. Spiro, R. Condit, and R. B. Foster. 1995. Diameter, height, crown, and age relationship in eight neotropical tree species. Ecol. 76: 1926-1939.

Odum, H. T. 1970. Summary: An emerging view of the ecological system at el verde. *In* A tropical rain forest. A study of irradiation and ecology at el verde, puerto rico. *Edited by* H. T. Odum and R. F. Pigeon. U.S. Atomic Commission, Oak Ridge.

Oksanen, J., et al. 2007. The vegan package. Community ecology package, ver. 2.9.

Orville, R. E. 1968. Photograph of a close lightning flash. Science 162: 666-667.

Ovington, J., and H. Madgwick. 1959. Distribution of organic matter and plant nutrients in a plantation of scots pine. For. Sci. 5: 344-355.

Palace, M., M. Keller, and H. Silva. 2008. Necromass production: Studies in undisturbed and logged amazon forests. Ecol. Appl. 18: 873-884.

Palace, M., M. Keller, G. Hurtt, and S. Frolking. 2012. A review of above ground necromass in tropical forests. *In* Tropical forests. *Edited by* P. Sudarshana, M. Nageswara-Rao, and J. R. Soneji. Intech, Rijeka, Croatia. pp 215–252.

Palace, M., M. Keller, G. P. Asner, J. N. M. Silva, and C. Passos. 2007. Necromass in undisturbed and logged forests in the brazilian amazon. Forest Ecol. Mgmt. 238: 309-318.

Pan, Y., R. A. et al. 2011. A large and persistent carbon sink in the world's forests. Science 333: 988-993.

Parton, W., W. L. Silver, I. C. Burke, L. Grassens, M. E. Harmon, W. S. Currie, J. Y. King, E. C. Adair, L. A. Brandt, and S. C. Hart. 2007. Global-scale similarities in nitrogen release patterns during long-term decomposition. Science 315: 361-364.

Pinheiro, J., and D. Bates. 2000. Mixed-Effects Models in S and S-plus. Springer-Verlag, New York, United States.

Plummer, F. G. 1912. Lightning in relation to forest fires. Washington, DC: US Department of Agriculture, Forest Service.

Přívětivý, T., D. Janík, P. Unar, D. Adam, K. Král, and T. Vrška. 2016. How do environmental conditions affect the deadwood decomposition of european beech (*Fagus sylvatica* l.)? Forest Ecol. Mgmt. 381: 177-187.

Putz, F. E. 1984. The natural history of lianas on Barro Colorado Island, Panama. Ecol. 65: 1713-1724.

R Core Team. 2017. R: A language and environment for statistical computing. Foundation for Statistical Computing, Vienna, Austria.

Rakov, V. A., and M. A. Uman. 2003. Lightning: Physics and Effects. Cambridge, UK: Cambridge University Press.

Reynolds, R. R. 1940. Lightning as a cause of timber mortality. Southern Forestry Notes No. 31. Southern Forest Experimental Station, New Orleans, Louisiana: US Department of Agriculture, Forest Service.

Rice, A.H., et al. 2004. Carbon balance and vegetation dynamics in an old-growth Amazonian forest. Ecol. Appl. 14: 55-71.

Romps, D. M., J. T. Seeley, D. Vollaro, and J. Molinari. 2014. Projected increase in lightning strikes in the United States due to global warming. Science 346: 851-854.

Rüger, N., A. Huth, S. P. Hubbell, and R. Condit. 2009. Response of recruitment to light availability across a tropical lowland rain forest community. J. Ecol. 97: 1360–1368.

Sayer, E. J., and L. F. Banin. 2016. Tree nutrient status and nutrient cycling in tropical forests - lessons from fertilization experiments. Tropical tree physiology (eds G. Goldstein and L.S. Santiago), pp. 275-279. Springer International Publishing, Switzerland.

Sayer, E. J., and E. V. J. Tanner. 2010. A new approach to trenching experiments for measuring root-rhizosphere respiration in a lowland tropical forest. Soil Biol. Biogeochem. 42: 347-352.

Sayer, E. J., and E. V. J. Tanner. 2010. Experimental investigation of the importance of litterfall in lowland semi-evergreen tropical forest nutrient cycling. J. Ecol. 98: 1052-1062.

Sayer, E. J., E. V. J. Tanner, and A. L. Lacey. 2006. Effects of litter manipulation on early-stage decomposition and meso-arthropod abundance in a tropical moist forest. Forest Ecol. Manag. 229: 285-293.

Sayer, E. J., et al. 2012. Variable responses of lowland tropical forest nutrient status to fertilization and litter manipulation. Ecosystems, 15, 387-400.

Schnitzer, S. A., et al. 2012 Liana abundance, diversity, and distribution on Barro Colorado Island, Panama. PLoS ONE 7: e52114.

Schnitzer, S. A., and F. Bongers. 2011. Increasing liana abundance and biomass in tropical forests: Emerging patterns and putative mechanisms. Ecol. Lett. 14: 397-406.

Sellin, A. 1994. Sapwood–heartwood proportion related to tree diameter, age, and growth rate in Piceaabies. Can. J. For. Res. 24: 1022-1028.

Sharples, A. 1933. Lightning storms and their significance in relation to diseases of (1) *Cocos nucifera* and (2) *Hevea brasiliensis*. Annal. Appl. Biol. 20: 1-22.

Sheldrake, M., et al. 2017a. Arbuscular mycorrhizal fungal community composition is altered by long-term litter removal but not litter addition in a lowland tropical forest. New Phytol. 214: 455-467.

Sheldrake, M., N. P. Rosenstock, D. Revillini, P. A. Olsson, S. J. Wright, and B. L. Turner. 2017b. A phosphorus threshold for mycoheterotrophic plants in tropical forests. P. R. Soc. B. 284: 20162093.

Shugart, H. H. 1987. Dynamic ecosystem consequences of tree birth and death patterns. Bioscience. 37: 596-602.

Sierra, C. A., et al. 2007. Total carbon stocks in a tropical forest landscape of the porce region, colombia. Forest Ecol. Mgmt. 243: 299-309.

Smith, K. T., and R. O. Blanchard. 1984. Cambial electrical resistance related to the number of vascular cambial cells in balsam fir. Can. J. For. Res. 14: 950-952.

Song, Z., C. Dunn, X.-T. Lü, L. Qiao, J.-P. Pang, and J.-W. Tang. 2017. Coarse woody decay rates vary by physical position in tropical seasonal rainforests of SW China. Forest Ecol. Mgmt. 385: 206-213.

Spetich, M. A., S. R. Shifley, and G. R. Parker. 1999. Regional distribution and dynamics of coarse woody debris in midwestern old-growth forests. For. Sci. 45: 302-313.

Stamm, A. J. 1927. The electrical resistance of wood as a measure of moisture content. Ind. Eng. Chem. 19: 1021-1025.

Stephenson, N. L., P. J. van Mantgem, A. G. Bunn, H. Bruner, M. E. Harmon, K. B. O'Connell, D. L. Urban, and J. F. Franklin. 2011. Causes and implications of the correlation between forest productivity and tree mortality rates. Ecol. Mongr. 81: 527-555.

Stevens, G. C. 1987. Lianas as structural parasites: the *Bursera simaruba* example. Ecology 68: 77-81.

Stone, G. E. 1914. Electrical injuries to trees. Bull. Mass. Agric. Exp. Stn. 156: 123-264.

Stone, G. E., and G. H. Chapman. 1912. Electrical resistance of trees. 24th Annu. Rep. Mass. Agri. Exper. Sta. No. 31: 144-176.

Swift, M., I. Healey, J. Hibberd, J. Sykes, V. Bampoe, and M. Nesbitt. 1976. The decomposition of branch-wood in the canopy and floor of a mixed deciduous woodland. Oecologia. 26: 139-149.

Swift, M.J. (1977) The ecology of wood decomposition. Science Progress (1933-). 64: 175-199.

Taylor, A. R. 1964. Lightning damage to forest trees in Montana. Weatherwise 17: 61-65.

Taylor, A. R. 1974. Ecological aspects of lightning in forests. Proc. Tall Timbers Fire Ecol. Conf. 13: 455-482.

Taylor, A. R. 1977. Lightning and trees. In Lightning (ed. RH Golde), pp. 831-849. New York, USA: Academic Press.

Taylor, A. M., B. L. Gartner, and J. J. Morrell. 2002. Heartwood formation and natural durability-a review. Wood Fiber Sci. 34: 587-611.

Thornton, P. E. 1998. Regional ecosystem simulation: Combining surface-and satellite-based observations to study linkages between terrestrial energy and mass budgets. University of Montana, Missoula.

Uman, M. A. 2001. The lightning discharge, New York, USA: Dover Publications.

Uman, M. A. 2008. The art and science of lightning protection, Cambridge, UK: Cambridge University Press.

van der Heijden, G. M. F., J. S. Powers, and S. A. Schnitzer. 2015. Lianas reduce carbon accumulation and storage in tropical forests. Proc. Natl. Acad. Sci. 112: 13267-13271.

van der Heijden, G. M., S. A. Schnitzer, J. S. Powers, and O. L. Phillips. 2013. Liana impacts on carbon cycling, storage and sequestration in tropical forests. Biotropica. 45: 682-692.

van der Wal, A., E. Ottosson, and W. de Boer. 2015. Neglected role of fungal community composition in explaining variation in wood decay rates. Ecol. 96: 124-133.

van Geffen, K. G., L. Poorter, U. Sass-Klaassen, R. S. P. van Logtestijn, and J. H. C. Cornelissen. 2010. The trait contribution to wood decomposition rates of 15 neotropical tree species. Ecol. 91: 3686-3697.

Wakasa., S. A., S. Nishimura, H. Shimizu, and Y. Matsukura. 2012. Does lightning destroy rocks?: Results from a laboratory lightning experiment using an impulse high-current generator. Geomorphology 161-162: 110-114.

Weedon, J. T., W. K. Cornwell, J. H. Cornelissen, A. E. Zanne, C. Wirth, and D. A. Coomes. 2009. Global meta-analysis of wood decomposition rates: A role for trait variation among tree species? Ecol Lett. 12: 45-56.

Wieder, R. K., and S. J. Wright. 1995. Tropical forest litter dynamics and dry season irrigation on Barro Colorado Island, Panama. Ecol. 76: 1971-1979.

Williams, E. R. 2005. Lightning and climate: a review. Atmos. Res. 76: 272-287.

Woldendorp, G., R. J. Keenan, S. Barry, and R. D. Spencer. 2004. Analysis of sampling methods for coarse woody debris. Forest Ecol. Mgmt. 198: 133-148.

Wright, S. J., et al. 2011. Potassium, phosphorus, or nitrogen limit root allocation, tree growth, or litter production in a lowland tropical forest. Ecol. 92: 1616-1625.

Yanoviak, S. P, E. M. Gora, J. Fredley, P. M. Bitzer, R-M. Muzika, and W. P. Carson. 2015. Direct effects of lightning in temperate forests: a review and preliminary survey in a hemlock-hardwood forest of the northern United States. Can. J. For. Res. 45: 1258-1268.

Yanoviak, S. P. 2013. Shock value: are lianas natural lightning rods? In Treetops at risk: challenges of global forest canopies (eds. M Lowman, S Devy, T Ganesh), pp. 147-154. New York, USA: Springer.

Yanoviak, S. P., E. G. Gora, J. M. Burchfield, P. M. Bitzer, and M. Detto. 2017. Quantification and identification of lightning damage in tropical forests. Ecol. Evol. 7: 5111-5122.

Yavitt, J.B., K. E. Harms, M. N. Garcia, M. J. Mirabello, and S. J. Wright. 2011. Soil fertility and fine root dynamics in response to 4 years of nutrient (N, P, K)

fertilization in a lowland tropical moist forest, Panama. Austral Ecol. 36: 433-445.

Zanne, A. E., B. Oberle, K. M. Dunham, A. M. Milo, M. L. Walton, and D. F. Young. 2015. A deteriorating state of affairs: How endogenous and exogenous factors determine plant decay rates. J. Ecol. 103: 1421-1431.

Zimmerman, J.K., et al. 1995. Nitrogen Immobilization by Decomposing Woody Debris and the Recovery of Tropical Wet Forest from Hurricane Damage. Oikos 72: 314-322.

APPENDIX I – Supplement for Chapter II

SUPPLEMENTARY METHODS

PHOTOGRAMMETRY METHODS

To test the accuracy and precision of our photogrammetry measurements, we performed a pilot study of 48 branches that were measurable by hand. This method of diameter estimation was both accurate (average difference from real diameter = 0.44 cm) and precise (SD of difference between real and estimated diameters = 0.2 cm) for stems >5cm in diameter ($F_{1,46}$ = 3368, $p < 0.001$, $r^2 = 0.99$). The relationship between estimated and real diameter was consistent regardless of distance between the camera and branch (up to 35m; $F_{1,46}$ = 2.40, p = 0.13) and across a range of branch diameters (5-65cm; $F_{1,46}$ = 1.03, p = 0.32).

We used the Law of Cosines to estimate branch length. We measured distance to both ends of the branch or branch subsection, and estimated the angle between the two measurements using a protractor and plumb line. We then calculated branch length as follows,

$$L_b = d_a^2 + d_b^2 - 2d_a d_b \cos C$$

Where L_b is the length of the branch, d is the distance to each end of the branch (subscripts a and b denote each measurement), and C is the angle between the distance measurements.

CALCULATIONS OF MASS AND VOLUME

We summed squared diameter and cross-sectional area to estimate volume and mass of downed woody debris, respectively. We estimated total volume of downed coarse and fine woody debris from transect data assuming circular cross sections,

$$V = \frac{\pi^2}{8*L} \sum D_i^2$$

Where V is volume of woody debris per area (m^3 per m^{-2}), L is the total length of transects (m), and D_i is diameter (m) of the i^{th} piece of wood encountered ({De Vries, #3932}). We estimated the mass of downed woody debris with individual density estimates and used cross-section mass to account for void space and wood heterogeneity,

$$M = \frac{\pi}{2*L} \sum C_i$$

Where M is mass of woody debris per area (kg m^{-2}), L is the total length of transect (m), and C_i is the cross section mass (kg m^{-1}) for the i^{th} piece of wood. Cross-section mass equals mass divided by the length of the sample, or equivalently the product of cross-section area and dry density (kg m^{-3}) as estimated via disk sampling or penetrometer penetration ({Larjavaara, 2011 #3933}). Equations 2 and 3 include a random angle

correction ($\pi/2$) to account for the orientation of diameter measurements relative to the piece of CWD rather than the transect itself.

EXPONENTIAL DECAY

We estimated decomposition constants of individual pieces of CWD. The decomposition constant was calculated using an exponential decay model:

$$k_i = \ln\left(\frac{c_{i,0}}{c_{i,t}}\right) * \frac{1}{t}$$

where k_i is the decomposition constant of CWD piece i, $c_{i,0}$ and $c_{i,t}$ are its initial and final cross-section mass, and t is time elapsed (years). Cross-section mass was replaced by volume, mass, or cross-section area when applicable.

MINIMUM SAMPLE SIZE CALCULATION

We used a simple variance-based equation to calculate the minimum sample size needed to estimate a statistic with the desired accuracy and precision:

$$SS = \frac{t^2 CV^2}{D^2}$$

Where t is the student's t statistic at a chosen alpha probability level (0.05 in this study), CV is the observed coefficient of variation among samples, and D is the desired proximity to the tree mean, as a percent of the true mean (10% in this study). That is, the result is the estimated minimum sample size to estimate the true mean value within 10% confidence limits with 95% probability. We performed this calculation using the mean observed CV and as well as using the upper limit and lower limit of the 95% confidence interval calculated for the CV.

BIAS IN ESTIMATING THE PROPORTION OF ELEVATED WD

Estimates of the elevated proportion of downed WD differed substantially between the two methods used in this study. These two datasets differed in both the parts of the landscape that were sampled and in sampling procedures, and both differences could contribute to differences in the estimated proportion elevated.

In terms of location, the 2017 long transects were conducted on the 50 ha plot forest dynamics plot, whereas the 2015 short transects were distributed across all of BCI. The 50 ha plot is located on a plateau that is relatively flat and has an unusually high amount of human traffic as workers monitor the forest dynamics plot. The flat topography means that few topographical features elevate sections of downed WD ({Přívětivý, 2016 #3733}). Additionally, the normal tendency of a careful field technician is to step on dead logs to avoid encounters with animals (e.g., venomous snakes), often collapses sections of elevated WD (pers. obs., E.M. Gora). In a relatively well-trafficked area such as a forest dynamics plot, this will cause faster-than-normal rates of collapsing for sections of elevated WD. For these reasons, the 2017 long transects are likely to underestimate the proportion of woody debris that is elevated. In contrast, the 2015 short transects were distributed across BCI, covering a topographically more complex landscape that on average is less well-trafficked.

The two datasets also differed in sampling procedures. For the 2017 long transects, each piece was scored based on whether it was elevated at the point where it encounters the transect. Thus, these data enable straightforward estimation of the proportion of all woody debris mass or volume that is elevated. In contrast, for the 2015 short transects, each piece was followed over all connected subunits, and the proportion of its total mass that was elevated was assessed. The mean overall proportion elevated was calculated as the weighted mean across pieces encountered, weighting by the mean cross-section mass of each piece. This is a nonstandard sampling procedure and the relationship of the resulting estimated mean proportion elevated to the true landscape proportion elevated is unclear. There was no correlation between cross-sectional area (the scaling parameter to correct for the size of encountered pieces of WD) and the proportion of WD volume that is elevated ($t_{175} = 1.57$, $p = 0.12$). However, the proportion of WD that was elevated was weakly positively correlated with WD piece length ($t_{175} = 2.86$, $p = 0.004$, $R = 0.21$), which could contribute to overestimation of the proportion of downed WD that is elevated considering that longer pieces are more likely to be encountered.

SUPPLEMENTARY RESULTS

MASS AND DENSITY MEASUREMENTS

Based on destructive sampling, average density of disks extracted from CWD was 0.271 g cm^{-3} (SD = 0.171 g cm^{-3}) and penetrometer penetration was predictive of wood density ($F_{1,136} = 68.27$, $p < 0.01$, $r^2 = 0.34$; Fig. S7). Wood density decreased with increasing CWD diameter ($F_{1,133} = 15.94$, $p < 0.001$), but this relationship was extremely weak ($r^2 = 0.1$). Consequently, we multiplied volume by average CWD density when necessary. As for CWD pools, standing CWD inputs were substantially denser (mean ± SD = 0.350 ± 104 g m^{-3}) than downed CWD inputs (mean ± SD = 0.283 ± 104 g m^{-3}; $t = 9.85$, $df = 699$, $p < 0.001$), suggesting that standing inputs were less decomposed than downed inputs. This likely explained why the volume of downed CWD was substantially larger than standing CWD, but the mass of downed and standing inputs were similar (Fig. 3 and S3.

We compared mass estimates using average density and CWD-specific penetration across 6 years in the 40x40m plots. The mass estimates differed for standing and downed CWD, but the magnitude of this difference was small and the direction was inconsistent. Standing CWD mass was greater when estimated with a penetrometer (dAIC = 9.77, $X^2_1 = 11.77$, $p < 0.001$), whereas downed CWD mass was greater when estimated with average density (dAIC = 7.77, $X^2_1 = 9.77$, $p = 0.002$; Table S2). Because penetrometer-based estimates account for real variation in density, we reported penetrometer-based mass estimates when they are available and average density-based estimates when they were not (Table 1). Disk-extraction estimates of mass were consistent with the other approaches (Table S3).

DIFFERENCES IN THE SIZE DISTRIBUTION OF CWD

CWD inputs are ca. 50% greater than standing CWD inputs, whereas downed CWD stocks are nearly 300% greater than standing CWD stocks (Figs. 2, 3, and S3). This occurs because standing CWD rapidly transitions into downed CWD, and no pools of dead wood transition into standing CWD (Fig. 2). We compared the size distribution of downed and standing CWD inputs to the size distribution of living trees (>20cm DBH) by fitting truncated Weibull distributions ({de Lima, 2015 #3853}). We found that the size distribution of standing CWD inputs (Weibull distribution: $\beta = 0.86$, $\eta = 172.3$) was right-skewed with more frequent large inputs relative to the size distribution of downed CWD inputs (Weibull distribution: $\beta = 0.62$, $\eta = 60.97$).

SUPPLEMENTARY FIGURES

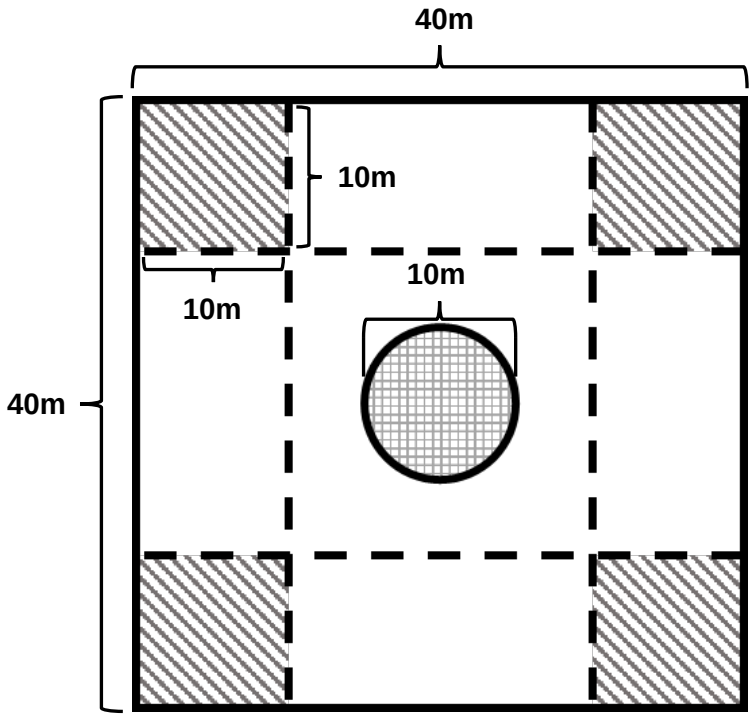

FIGURE S1. The layout of each 40x40m plot surveyed during the course of this study. Dashed lines represent transects for monitoring downed CWD. Diagonally hashed squares represent sub-plots for quantifying suspended WD volume (area = 100 m^2), whereas the circular cross-hashed area represents the sub-plot for recording standing FWD (area = 78.5 m^2). Standing CWD was recorded throughout the entire 40x40m plot (area = 1600 m^2).

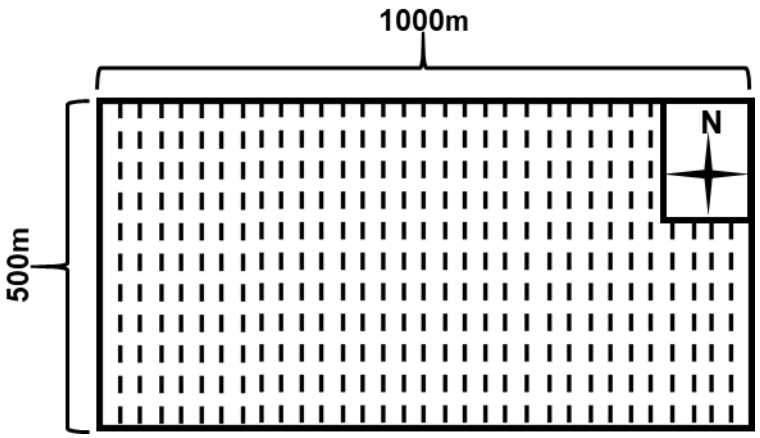

FIGURE S2. An example of long transects distributed within the 50 ha forest dynamics plot. The dashed lines represent transects from the 2010 long transects surveys. Surveys in 2014 were similar in orientation, but offset by 10m. The North-to-South transects in 2017 were also accompanied by transects running West-to-East.

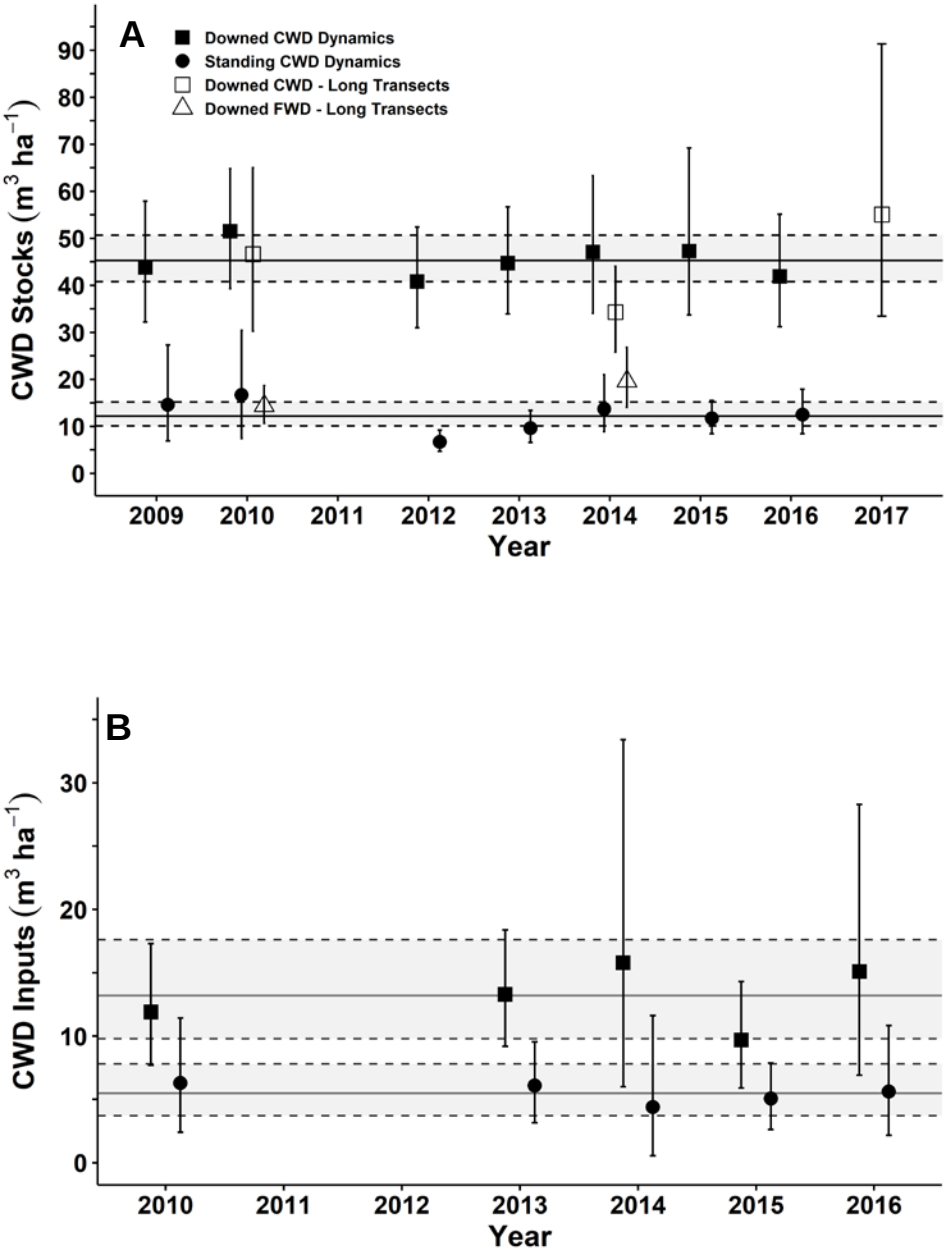

FIGURE S3. Estimated downed and standing CWD stocks (A) and inputs (B) as mass (Mg ha^{-1}) with 95% confidence intervals based on data from the 40x40m dynamics plots in individual years (filled symbols) and estimated stocks from the long transects in 2010, 2014, and 2017 (open symbols). The shaded regions represent the mean volume (±95% CI) of downed CWD and standing CWD as calculated across all years in the dynamics plots.

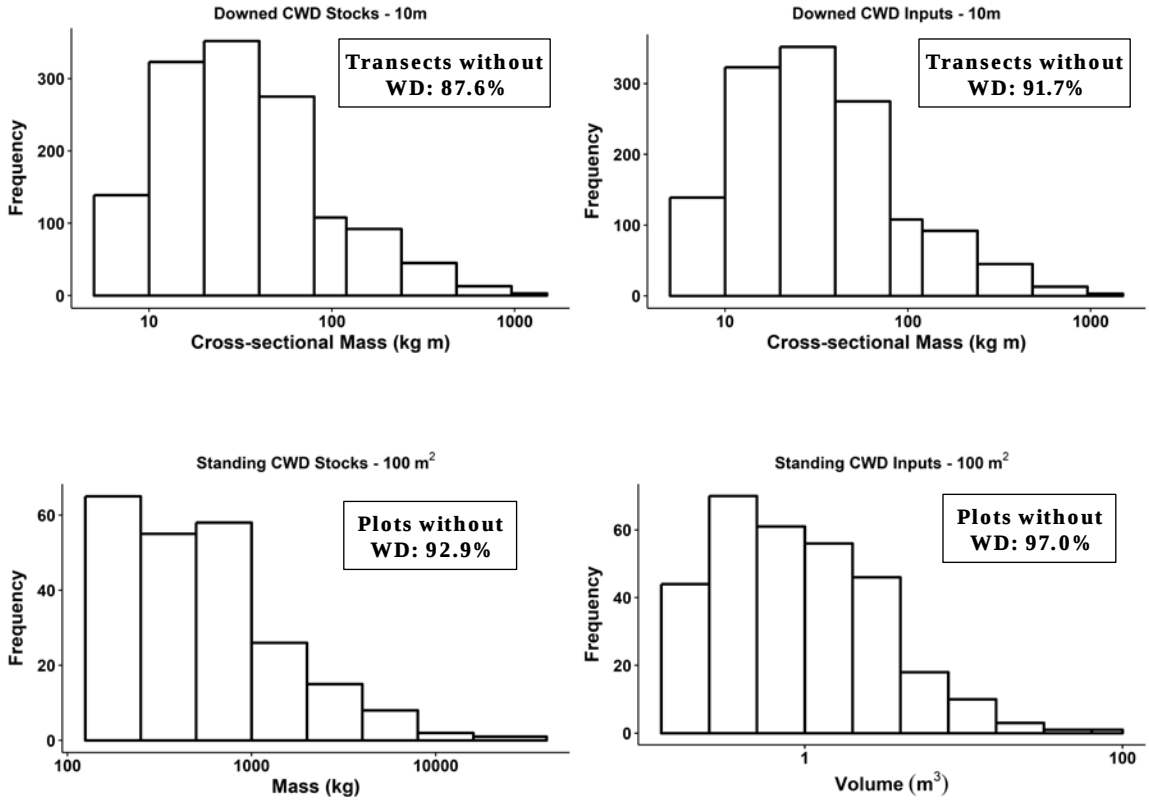

FIGURE S4. Histograms of the cross-sectional mass of downed CWD stocks and inputs, as well as mass of standing CWD stocks and inputs, across all years of the CWD dynamics plot surveys. Bin size doubles with each increasing increment (0.05 m^3, 0.1 m^3, 0.2 m^3, etc.; 5 kg m, 10 kg m, 20 kg m, etc). The histograms only include transects with WD.

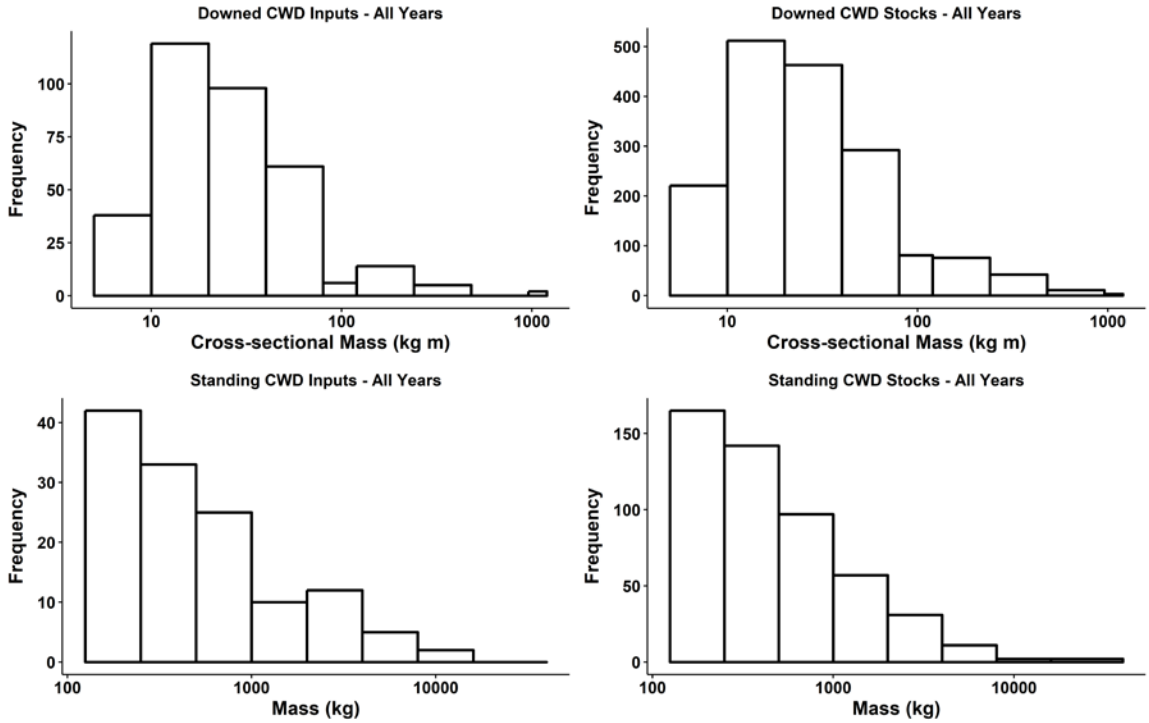

FIGURE S5. Histograms of the squared diameter, cross-sectional mass, volume, and mass of individual pieces of downed and standing CWD stocks and inputs.

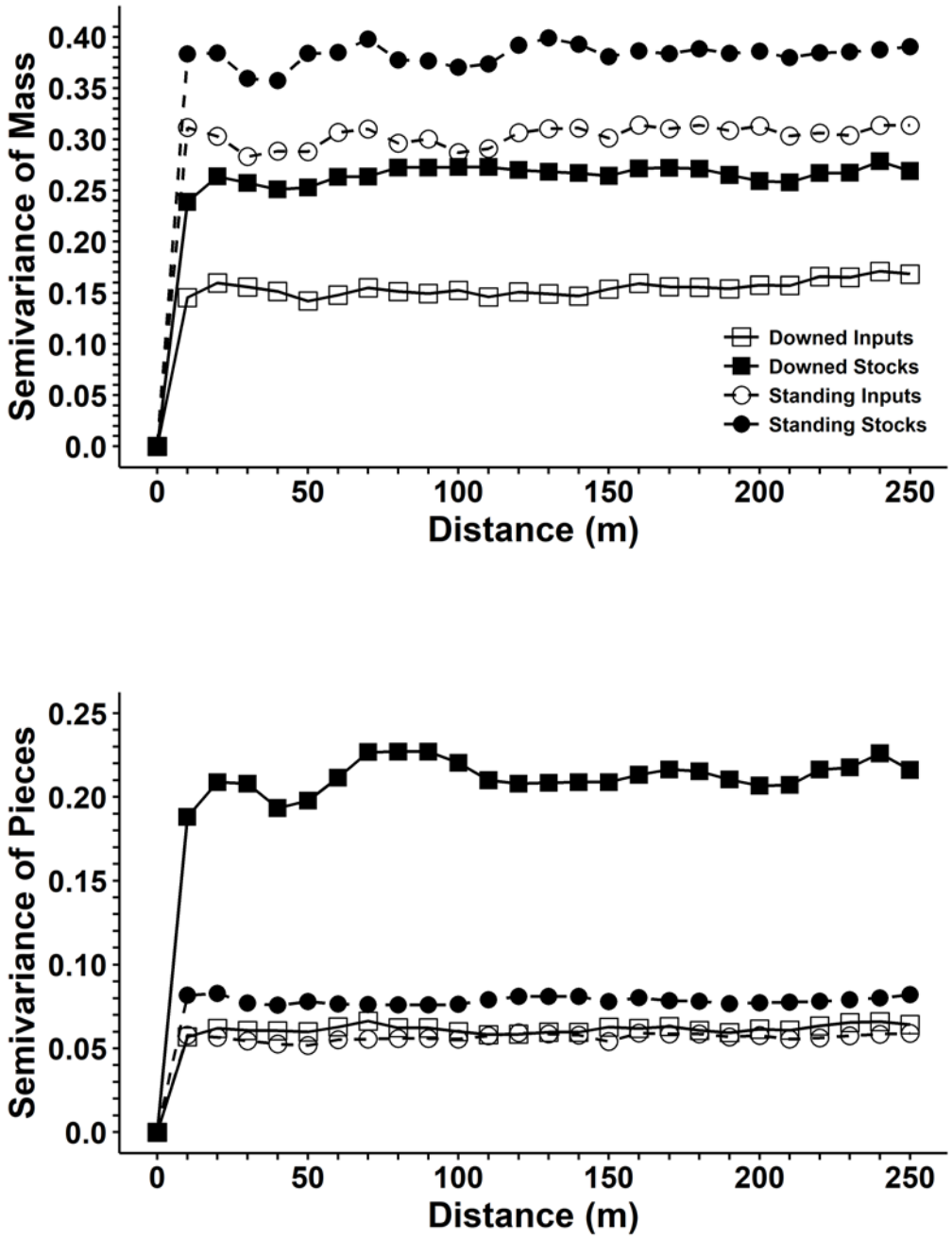

FIGURE S6. Semivariogram of stocks (filled points) and inputs (hollow points) of downed and standing CWD mass and CWD pieces. Each point represents the mean over annual semivariograms calculated for 5 or 7 years for inputs and stocks, respectively.

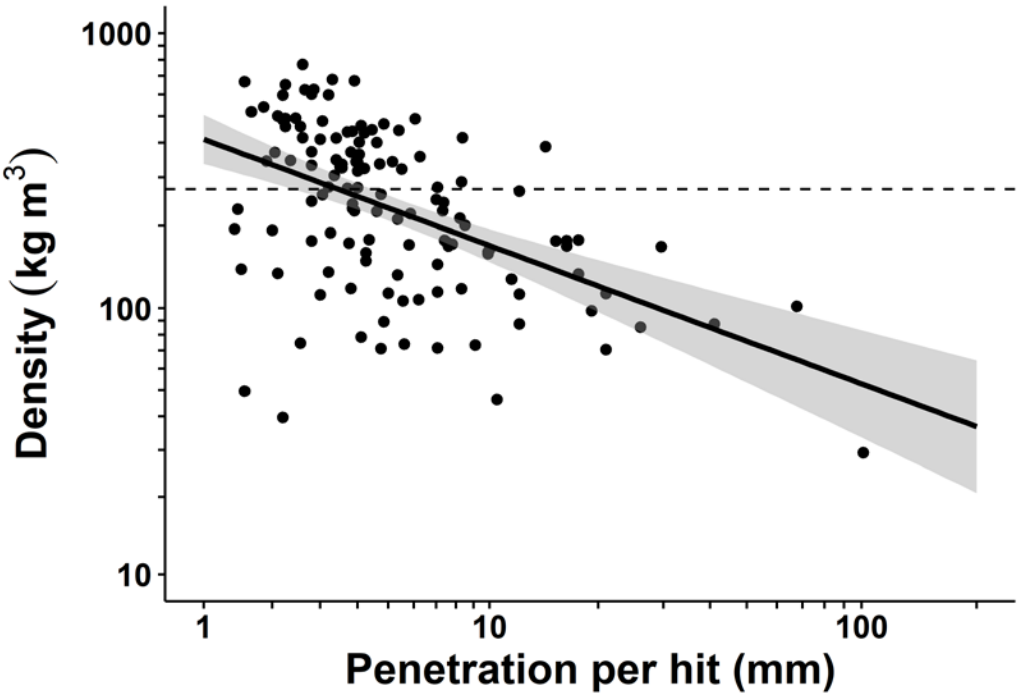

FIGURE S7. Regression and 95% confidence interval of CWD dry density (kg m^3, calculated using extracted disks) and penetrometer penetration (mm per hit). The dashed line represents average density across all samples (271 kg m^3).

TABLE S1. Estimated residence times (means with 95% CI from individualized residence times) of downed and standing CWD under different assumptions regarding the density and diameter at the final census of pieces of CWD that fell below the measurement threshold at the final census (and thus were not remeasured).

CWD pool	Assumed density at final census	Assumed diameter at final census	Estimated residence time (years)
Downed CWD	100%	199 mm	2.10 (1.97, 2.24)
	100%	100 mm	1.03 (0.97, 1.09)
	50%	199 mm	1.38 (1.30, 1.46)
	100%	1 mm	0.23 (0.22, 0.25)
	1%	199 mm	0.47 (0.44, 0.49)
	1%	1 mm	0.16 (0.15, 0.17)
Standing CWD	100%	199 mm	1.28 (1.19, 1.38)
	100%	100 mm	0.60 (0.56, 0.64)
	50%	199 mm	0.91 (0.85, 0.97)
	100%	1 mm	0.14 (0.13, 0.15)
	1%	199 mm	0.35 (0.33, 0.37)
	1%	1 mm	0.1 (0.09, 0.11)

TABLE S2. Estimates of downed CWD, standing CWD, standing FWD, suspended CWD, and suspended FWD pools based on data from the dynamics plots from 2009 to 2016, with 95% confidence intervals from bootstrapping over sampling units, together with information on the total number of pieces encountered and the proportion of samples without any pieces encountered. Sampling units are 10-m transect sections for downed WD, 10x10 m subplots for standing and suspended WD, and 5m radius plots for standing FWD.

Pool	Year	Total WD pieces	Samples without WD (%)	Volume (m^3 ha^{-1})	Mass, penetrometer (Mg ha^{-1})	Mass, average density (Mg ha^{-1})
Downed CWD	2009	230	88.7	43.8 (32.2, 57.9)	11.7 (8.5, 15.6	11.9 (8.7, 15.7)
	2010	258	87.6	51.5 (39.3, 64.8)	12.7 (9.4, 16.3)	13.9 (10.7, 17.6)
	2012	242	87.7	40.8 (31.0, 52.4)	10.6 (8.2, 13.0)	11.1 (8.4, 14.2)
	2013	272	86.5	44.7 (33.9, 56.7)	11.6 (9.0, 14.7)	12.1 (9.2, 15.4)
	2014	260	87.4	47.1 (34.1, 63.3)	11.6 (8.7, 15.0)	12.8 (9.2, 17.2)
	2015	254	87.4	47.3 (33.7, 69.2)	11.7 (9.4, 14.7)	12.8 (9.1, 18.7)
	2016	255	87.5	41.9 (31.2, 55.1)	11.0 (8.3, 14.2)	11.4 (8.5, 14.9)
	All years	1766	87.5	45.3 (40.8, 50.7)	11.5 (10.3, 12.7)	12.3 (11.1, 13.7)
Standing CWD	2009	93	94.6	14.6 (6.9, 27.3)	5.9 (2.6, 11.9)	4.0 (1.9, 7.4)
	2010	120	93.2	16.7 (7.4, 30.4)	5.2 (2.8, 8.7)	4.5 (2.0, 8.2)
	2012	97	94.2	6.7 (4.7, 9.2)	2.2 (1.5, 3.2)	1.8 (1.3, 2.5)
	2013	123	92.9	9.6 (6.6, 13.4)	3.3 (2.2, 4.7)	2.6 (1.8, 3.6)
	2014	143	91.7	13.7 (8.9, 21.0)	4.7 (2.9, 7.5)	3.7 (2.4, 5.7)
	2015	143	91.9	11.7 (8.4, 15.5)	4.1 (2.9, 5.5)	3.2 (2.3, 4.2)
	2016	136	92.3	12.5 (8.4, 17.9)	4.7 (2.9, 6.8)	3.4 (2.3, 4.9)
	All years	855	93	12.2 (10.1, 15.2)	4.3 (3.5, 5.4)	3.3 (2.7, 4.1)

Suspended CWD	2015	22	90	0.23 (0.12, 0.37)	N/A	0.06 (0.03, 0.10)
Suspended FWD	2015	234	42.5	0.62 (0.48, 0.78)	N/A	0.17 (0.13, 0.21)
Standing FWD	All years	97	87	0.004 (0.003, 0.01)	N/A	0.001 (0.001, 0.002)

TABLE S3. The volume and three different mass estimates (penetrometer, average density, and extracted disk methods, ±95% CI) of downed CWD and FWD from long transects on BCI (20m sub-transects). Pools of woody debris are separated by their diameter at the point where they intersect the transect.

Year	Pool	Total WD pieces	Samples without WD (%)	Volume (m^3 ha^{-1})	Mass, penetrometer (Mg ha^{-1})	Mass, average density (Mg ha^{-1})	Mass, extracted disk (Mg ha^{-1})
2010	FWD (<20cm)	176	85.3	14.39 (10.69, 18.68)	N/A	3.90 (2.90, 5.06)	3.41 (2.24, 4.77)
	CWD (>20cm)	137	87.1	46.64 (30.24, 65.00)	11.78 (7.28, 17.41)	12.63 (8.20, 17.62)	11.64 (6.55, 18.83)
2014	FWD (<20cm)	161	87.1	19.64 (14.05, 26.80)	N/A	5.32 (3.81, 7.26)	N/A
	CWD (>20cm)	136	87.5	34.31 (25.81, 44.05)	8.25 (6.30, 10.47)	9.29 (6.99, 11.94)	N/A
2017	FWD (<10cm)	329	71.7	10.59 (8.77, 12.68	N/A	2.87 (2.38, 3.44)	N/A
	CWD (>10cm)	561	44.3	60.45 (37.37, 97.62)	N/A	16.38 (10.13, 26.46)	N/A
	CWD (10-20cm)	314	71.2	5.38 (4.61, 6.16)	N/A	1.46 (1.25, 1.67)	N/A
	CWD (>20cm)	247	75.7	55.07 (33.46, 91.34)	N/A	14.92 (9.07, 24.75)	N/A

TABLE S4. Annual inputs of downed and standing CWD volume, penetrometer mass, and average density-based mass (±95% CI) from the dynamics plots from 2009 to 2016. The majority of inputs occurred during the year identified below, but pieces of CWD were not surveyed until the first two months of the subsequent year. Input values were either calculated as intact inputs using equations for total woody biomass or corrected to account for mass and volume lost between the time that woody debris was input and the time it was first recorded.

Pool	Year	Total WD pieces	Samples without WD (%)	Volume (m^3 ha^{-1})	Mass, penetrometer (Mg ha^{-1})	Mass, average density (Mg ha^{-1})
Downed	2009	75	96.3	11.9 (7.7, 17.3)	2.9 (1.8, 4.1)	3.2 (2.1, 4.7)
	2013	95	95.1	13.3 (9.2, 18.4)	4.0 (2.7, 5.3)	3.6 (2.5, 5)
	2014	63	97	15.8 (6.0, 33.4)	3.6 (1.5, 6.7)	4.3 (1.6, 9.1)
	2015	59	96.8	9.7 (5.9, 14.3)	2.9 (1.7, 4.4)	2.6 (1.6, 3.9)
	2016	67	96.6	15.1 (6.9, 28.3)	4.2 (2.0, 8.0)	4.1 (1.9, 7.7)
	All years	359	96.4	13.2 (9.8, 17.6)	3.5 (2.6, 4.5)	3.6 (2.7, 4.8)
Standing, Corrected	2010	46	97.2	6.3 (2.4, 11.4)	2.4 (0.9, 4.2)	1.7 (0.7, 3.1)
	2013	61	96.3	6.1 (3.2, 9.5)	2.2 (1.2, 3.6)	1.6 (0.9, 2.6)
	2014	53	96.7	4.4 (0.6, 11.6)	1.6 (0.2, 4.6)	1.2 (0.1, 3.1)
	2015	56	96.8	5.1 (2.6, 7.9)	1.9 (1, 2.9)	1.4 (0.7, 2.1)
	2016	35	97.9	5.6 (2.2, 10.8)	2.3 (0.9, 4.6)	1.5 (0.6, 2.9)
	All years	307	96.3	5.5 (3.7, 7.8)	2.1 (1.5, 2.9)	1.5 (1, 2.1)
Standing, Intact	2010	46	97.2	11.4 (4.8, 21.2)	4.1 (1.7, 7.6)	3.1 (1.3, 5.7)
	2013	61	96.3	15.2 (6.7, 26.9)	4.9 (2.5, 8.1)	4.1 (1.8, 7.3)
	2014	53	96.7	10.3 (1.6, 22.9)	3.5 (0.5, 8.2)	2.8 (0.4, 6.2)
	2015	56	96.8	8.5 (5.0, 12.7)	3.0 (1.8, 4.4)	2.3 (1.3, 3.4)
	2016	35	97.9	9.3 (4.1, 15.9)	3.5 (1.5, 6.3)	2.5 (1.1, 4.3)
	All years	307	96.3	11.0 (7.5, 14.8)	3.8 (2.6, 5.1)	3.0 (2.0, 4.0)

TABLE S5. The sample size, mass, and volume (±95% CI) of downed WD inputs separated into branchfall and treefall. Estimates for 2015 and 2016 were based on inputs of CWD into the dynamics plots, with mass calculated using penetrometer measurements, whereas 2017 estimates were based on the volume of WD stocks characterized using long transects. These are the only datasets that separated branchfall and treefall inputs.

Year	Woody Debris Pool	Branchfall			Treefall			Treefall WD (%)	
		N	m^3 ha^{-1} (95% CI)	Mg ha^{-1} (95% CI)	N	m^3 ha^{-1} (95% CI)	Mg ha^{-1} (95% CI)	Volume	Mass
2015	>20cm inputs	14	1.37 (0.36, 3.06)	0.50 (0.10, 1.36)	43	6.39 (3.45, 9.84)	1.76 (0.95, 2.73)	82 (64, 95)	78 (54, 95)
2016	>20cm inputs	10	0.62 (0.23, 1.13)	0.20 (0.07, 0.34)	52	10.89 (4.18, 21.58)	2.99 (1.23, 5.73)	95 (85, 98)	94 (83, 98)
2015-2016	>20cm inputs	24	1.00 (0.42, 1.81)	0.35 (0.13, 0.71)	95	8.64 (4.69, 14.19)	2.38 (1.36, 3.79)	90 (78, 96)	87 (72, 96)
2017	2-10cm stocks	210	6.47 (5.03, 8.06)	N/A	26	1.68 (0.94, 2.51)	N/A	21 (12, 30)	N/A
2017	>10cm stocks	191	4.75 (3.76, 6.00)	N/A	343	53.59 (31.28, 86.48)	N/A	92 (87, 95)	N/A
2017	>2cm stocks	401	11.22 (9.4, 13.16)	N/A	369	55.27 (33.95, 89.83)	N/A	83 (74, 89)	N/A

TABLE S6. The sample size, mass, and volume (±95% CI) of downed CWD *treefall* inputs separated into branch wood and trunk wood. Estimates from 2015 and 2016 were based on inputs of CWD into the dynamics plots, with mass was calculated using penetrometer measurements, whereas 2017 estimates are based on the volume of WD stocks characterized using long transects.

Year	Woody Debris Pool	Branch wood			Trunk wood			Trunk wood (% of total treefall)	
		N	m^3 ha^{-1} (95% CI)	Mg ha^{-1} (95% CI)	N	m^3 ha^{-1} (95% CI)	Mg ha^{-1} (95% CI)	Volume	Mass
2015	>20cm inputs	5	0.34 (0.06, 0.72)	0.09 (0.02, 0.18)	35	5.88 (3.16, 9.59)	1.62 (0.83, 2.59	95 (87, 99)	95 (89, 99)
2016	>20cm inputs	17	1.32 (0.40, 2.64)	0.48 (0.14, 0.94)	35	9.58 (3.29, 20.03)	2.50 (0.79, 5.22)	88 (65, 96)	84 (59, 96)
2015-2016	>20cm inputs	22	0.83 (0.35, 1.47)	0.29 (0.11, 0.50)	70	7.73 (3.93, 13.62)	2.06 (1.04, 3.55)	90 (80, 96)	88 (75, 95)
2017	2-10cm stocks	3	0.41 (0.0, 0.97)	N/A	22	1.26 (0.64, 1.91)	N/A	4.0 (2, 5)	N/A
2017	>10cm stocks	80	3.59 (2.13, 5.28)	N/A	263	50.0 (27.87, 89.54)	N/A	93 (88, 97)	N/A
2017	>2cm stocks	83	4.0 (2.31, 6.06)	N/A	285	51.26 (29.18, 86.1)	N/A	93 (87, 96)	N/A

TABLE S7. The coefficient of variation (CV, with 95% CI) and the overdispersion "size" parameter of the negative binomial distribution (±SE). Scale represents the sampling unit used for each estimate (10 m or 100 m^2) and samples without WD denotes the percent of 10 m transects or 100 m^2 plots without a piece of CWD. The CV is the percent of the standard deviation over the mean of total volume or mass per transect, whereas the overdispersion parameter is based on the number of CWD pieces encountered per transect.

Pool or flux	Inputs or Stocks	Scale	Samples without WD (%)	Coefficient of variation		Overdispersion parameter
				Mass	Volume	
Downed CWD	Stocks	10m	87.6	550 (450, 660)	600 (470, 770)	0.4 (0.02)
		20m	77.3	390 (320, 470)	430 (320, 550)	-
		40m	65.5	320 (260, 390)	350 (270, 440)	-
		160m	22.2	160 (130, 200)	180 (160, 190)	-
	Inputs	10m	97.4	1220 (570, 1900)	1370 (550, 2310)	0.11 (0.02)
		20m	95.1	860 (420, 1370)	970 (420, 1600)	-
		40m	91.7	680 (300, 1080)	760 (310, 1300)	-
		160m	73.7	420 (190, 680)	320 (190, 820)	-
Standing CWD	Stocks	100m^2	92.9	1190 (640, 1870)	1210 (600, 1830)	1.1 (0.27)
		200m^2	86.8	840 (450, 1350)	860 (430, 1280)	-
		400m^2	75.6	600 (320, 930)	600 (320, 930)	-
		1600m^2	32.0	300 (170, 460)	310 (150, 470)	-
	Inputs	100m^2	97.0	1550 (870, 2450)	1580 (860, 2580)	0.77 (0.36)
		200m^2	94.2	1100 (630, 1800)	1110 (630, 1770)	-
		400m^2	88.9	770 (420, 1240)	790 (430, 1310)	-
		1600m^2	64.3	410 (240, 670)	410 (220, 690)	-

APPENDIX II – Supplement for Chapter III

TABLE S1. The original diameter at breast height (DBH, mm), density (g cm^{-3}), and cross-sectional mass (g m^{-2}, ± standard error) of boles retained in our study compared with boles that were excluded. We compared these values using a mixed effect linear model with treatment as a fixed effect and plot as a random grouping factor. Lowercase letters denote similar values of DBH (a or b) and density (x or y), as determined with a post-hoc Tukey test. Many excluded boles were removed because they lacked species identification and therefore could not be assigned densities. Consequently, the sample size "N (with density)" is only for the number of excluded boles with known density (and thus known cross-sectional mass) within each treatment. Similarly, the other sample size of excluded boles [N (with DBH)] specifies the number of boles within each treatment with known diameter-at-breast height.

	Boles retained				Boles excluded				
Litter treatment	N	DBH (mm)	Density (g cm^3)	Cross-sectional mass (g m^2)	N (with DBH)	N (with density)	DBH (mm)	Density (g cm^3)	Cross-sectional mass (g m^2)
Control	67	769[a] (50)	0.536[x] (0.019)	460 (30)	23	1	464[b] (47)	0.675[y] (N/A)	242 (N/A)
Addition	62	893[a] (55)	0.489[x] (0.020)	346 (18)	35	12	519[b] (44)	0.628[y] (0.043)	494 (83)
Removal	85	764[a] (42)	0.552[x] (0.018)	407 (27)	42	14	534[b] (55)	0.637[y] (0.042)	421 (78)

Trees omitted from this study had smaller DBH ($\chi^2_1 = 37.08$, $p < 0.001$) and were denser ($\chi^2_1 = 11.30$, $p < 0.001$) than those retained in the dataset. However, DBH and density did not differ among litter treatments (DBH: $\chi^2_2 = 2.36$, $p = 0.31$; Density: $\chi^2_2 = 3.38$, $p = 0.185$). The cross-sectional mass of boles did not differ ($\chi^2_1 = 2.64$, $p = 0.104$) between groups (i.e., retained or excluded) or among litter treatments ($\chi^2_2 = 2.74$, $p = 0.25$). Furthermore, there were no interactions between the characteristics of boles in the litter treatments and whether they were retained or omitted (DBH: $\chi^2_2 = 3.32$, $p = 0.19$; Density: $\chi^2_2 = 0.69$, $p = 0.71$; cross-sectional mass: $\chi^2_2 = 3.26$, $p = 0.20$), indicating that the effects of these omissions were similar across litter treatments

TABLE S2. The distribution of boles among different classifications of dead wood including standing, downed, suspended, and completely decomposed boles. Classifications with two components indicate that two separate sections of the tree were concurrently classified as different types of CWD.

CWD classification	Control (N)	Addition (N)	Removal (N)
Down	23	14	19
Completely decomposed	31	35	33
Snag	10	11	27
Snag/suspended	1	0	3
Snag/down	2	0	1
Suspended	0	2	2
Totals	67	62	85

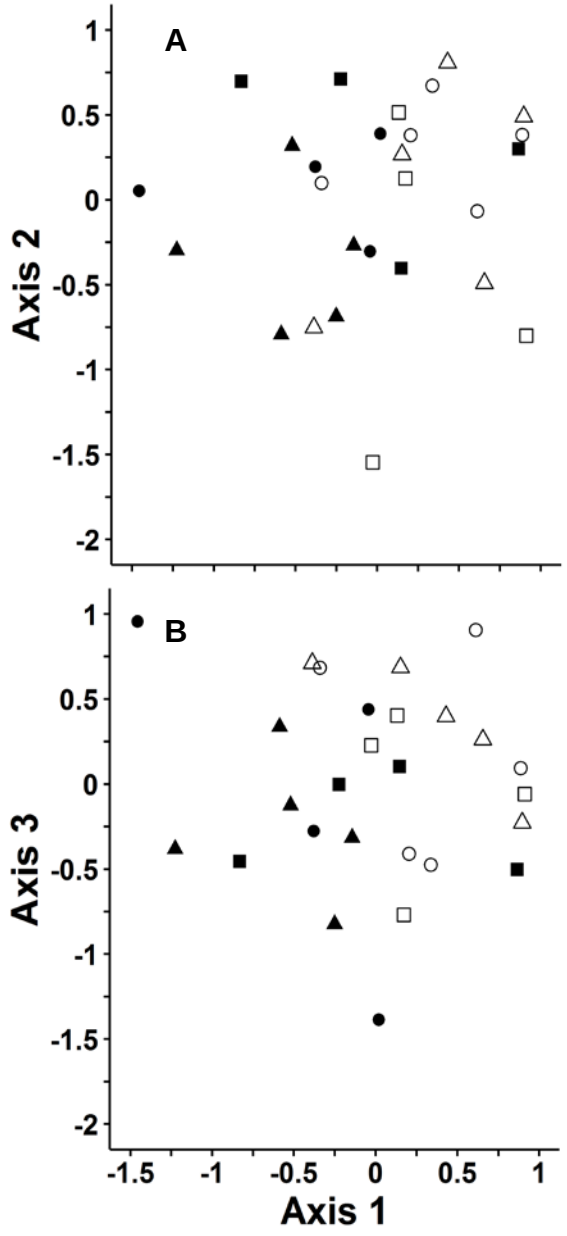

FIGURE S1. Ordination of tree species composition of completely decomposed trees (hollow points; *n* = 14) and dead trees that are still identifiable in 2016 (filled points; *n* = 13). Each point represents either the decomposed or remaining boles of a single plot. Panel A depicts NMS axes 1 and 2, whereas panel B depicts NMS axes 1 and 3. Circles represent litter addition treatment plots (*n* = 9), triangles represent litter removal plots (*n* = 10), and squares represent control plots (*n* = 8).

APPENDIX III – Supplement for Chapter IV

RESULTS WITH COMPLETE STATISTICAL ANALYSES

FUNGAL COMMUNITIES

Although fungal diversity was relatively consistent (Table 1), fungal community composition differed among most vertical positions (pseudo-$F_{4,35}$ = 2.82, $p < 0.001$; Fig. 1; Table S3). Community composition in the canopy was similar to both the emergent and subcanopy vertical positions ($t < 1.29$, $p < 0.073$). However, fungal composition differed among all other vertical positions ($t > 1.35$, $p < 0.033$) and among individual trees (pseudo-$F_{9,35}$ = 1.16, $p = 0.003$; Fig. 1, Table 2). By contrast, fungal sequence richness (mean ± SD; 123 ± 30) did not differ among vertical positions (dAIC = 0.65, X^2_4 = 7.35, $p = 0.118$; Table 1). Beta diversity was greater in the litter than the subcanopy, canopy, and emergent vertical positions (pseudo-$F_{4,44}$ = 3.38, $p = 0.043$; $t > 3.07$, $p < 0.014$), but was similar among all other vertical positions ($t < 1.33$, $p > 0.201$).

Similar to community composition, vertical positions supported different compositions of fungal functional groups (pseudo-$F_{4,35}$ = 3.38, $p = 0.001$) but similar functional diversity (Table 1). Functional group composition in the understory was similar to the subcanopy and emergent vertical positions ($t < 1.32$, $p > 0.139$) and only marginally significantly different from the canopy level ($t = 1.68$, $p = 0.034$). Functional group composition differed among all other vertical positions ($t > 1.67$, $p < 0.024$). However, functional group beta diversity (pseudo-$F_{4,44}$ = 0.98, $p = 0.612$) and Shannon-Weiner diversity (dAIC = 0.5, X^2_4 = 8.5, $p = 0.075$) did not differ among vertical positions (Table 1). Unlike community composition, the functional composition of fungal communities did not differ among trees (pseudo-$F_{9,35}$ = 0.93, $p = 0.594$).

Differences in the composition of fungal communities were primarily caused by a shift from saprotrophs to biotrophs with increasing height (Tables 2-3). There were also severe differences between the litter and understory vertical positions. The relative abundance of Basidiomycota was greater in the litter than the understory, but Ascomycota were relatively more abundant in the understory (Table 2). Similarly, litter and soil saprotrophs (primarily Agaricales) were most abundant in the litter, whereas

soft rot fungi and wood saprotrophs were most abundant in the understory (Pleosporales) and subcanopy (Pleosporales and Polyporales; Tables 2-3, Table S3). Endophytes, fungal parasites (specifically Tremelles), and plant pathogens were most abundant in the canopy and/or emergent vertical positions. Contrary to my expectations, there were no differences in the relative abundance of known lichens (Table 3).

BACTERIAL TAXA AND COMMUNITIES

The phylogenetic structure of bacteria indicated differences in the strength of environmental and competitive filtering (Fig. 2). The phylogenetic evenness of bacterial communities in the leaf litter was not different from random, but evenness in the litter was significantly greater than all other vertical positions (dAIC = 19.2, $X^2_4 = 27.2$, $p < 0.001$; $z > 4.1$, $p < 0.001$). By contrast, phylogenetic structure was similar among communities above the forest floor and they exhibited phylogenetic clustering typically associated with strong environmental filtering ($z = 0.88$, $p = 0.91$).

Bacterial community composition was strongly positively correlated with fungal community composition (Mantel test: $r = 0.74$, $p < 0.001$), and their community compositions followed similar patterns among vertical positions (Figs. 1 and 3). Specifically, the community composition of bacterial colonizers differed among all vertical positions (pseudo-$F_{4,35} = 3.74$, $p < 0.001$; Fig. 3, Table 4). The magnitude of differences among the subcanopy, canopy, and emergent vertical positions ($t_{range} = 1.3$-1.39, $p_{range} = 0.034$-0.046) was substantially smaller than that between the leaf litter and understory ($t = 1.94$, $p = 0.001$). Additionally, the two lowest vertical positions differed from the three highest vertical positions ($t > 1.74$, $p < 0.005$). Apart from the effects of vertical positions, bacterial communities within a single tree were more similar than expected at random (pseudo-$F_{9,35} = 1.13$, $p = 0.004$).

Bacterial richness generally decreased with increasing height (dAIC = 42.6, $X^2_4 = 50.55$, $p < 0.001$), but diversity did not differ among vertical positions (Table 1). Bacterial richness did not differ between the understory and subcanopy ($z = 0.98$, $p = 0.86$) or between the canopy and emergent vertical positions ($z = 0.55$, $p > 0.98$). Richness was greater in the leaf litter than all higher vertical positions ($z > 4.42$, $p < 0.001$), greater in the understory than the emergent level ($z = 3.13$, $p = 0.015$), and marginally significantly greater in the understory than in the canopy ($z = 2.5$, $p = 0.09$). Similarly, richness in the subcanopy was greater than in the canopy or emergent layers of

the forest ($z > 3.44$, $p < 0.005$). Bacterial beta diversity, as estimated by dispersion from the group centroid, was similar among vertical positions (pseudo-$F_{4,44} = 1.56$, $p = 0.28$).

The relative abundance of many orders was greater above the forest floor, particularly in the canopy and emergent vertical positions (Table 4; Table S4). Actinomycetales and Rhizobiales accounted for ca. 25% of sequences for all aboveground vertical positions, but only 13% of sequences in the leaf litter. Acidobacteriales and two orders of primarily phototrophic Cyanobacteria (Chlorophyta and Nostrocales) were most abundant at the emergent layer, accounting for an additional 23% of sequences. Sphingomonadales composed 22% of canopy-level sequences and 10-14% of sequences in the understory, subcanopy, and emergent layers, but only 2.3% of sequences in the leaf litter. The genus *Sphingomonas* dominated this order, composing 1.2%, 6.7%, 10.7%, 17.4%, and 10.8% of relative abundance from the litter, understory, subcanopy, canopy, and emergent vertical positions, respectively. The most abundant OTU in this study, *Sphingomonas wittichii*, represented ca. 20% of this genus and 3.2% of all the sequences above the forest floor.

Individual bacterial orders exhibited lower relative abundance in the leaf litter and fewer differences among lower vertical positions. Of the most abundant orders, only Mycoccocales was more common in the leaf litter (8% of sequences) than all other vertical positions (Table 4). Apart from Mycoccocales and Rhizobiales, the three most abundant orders of bacteria colonizing wood in the leaf litter (Gemmentales, Saprospirales, and Xanthomonadales) were similarly abundant in the understory and/or subcanopy (Table 4).

ARCHAEA

Archaea were exceedingly rare in this study. In total, Iisolated only 41 archaeal sequences distributed among Nitrososphaerales (25 sequences) and the candidate orders WCHD3-30 (2 sequences) and YLA114 (14 sequences). Archaea were concentrated on wood sticks in the leaf litter (80% of sequences) and, to a lesser degree, the understory (10%). Only 4 sequences were isolated from higher vertical positions, and zero archaeal sequences were found at the emergent level of the forest.

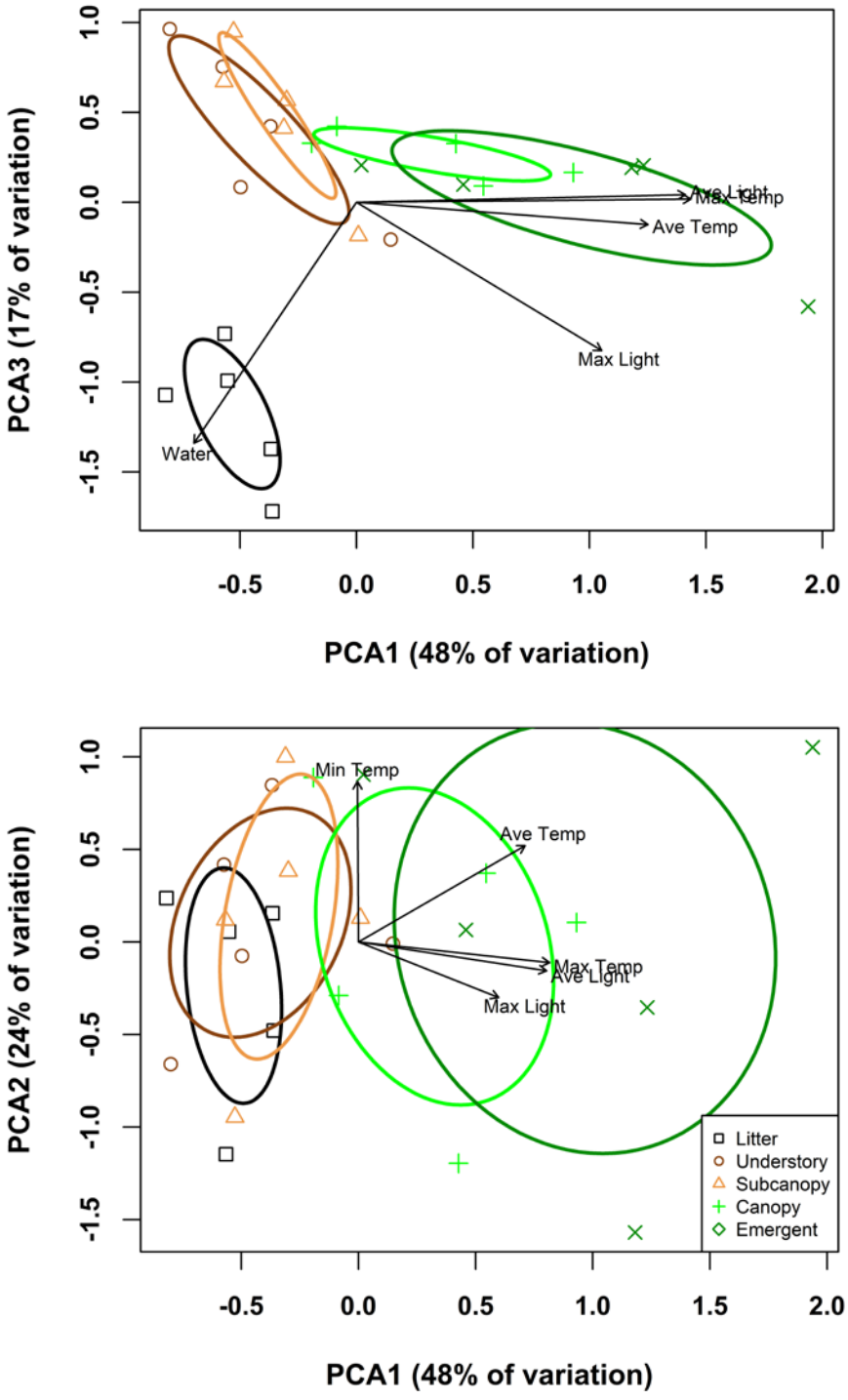

FIGURE S1. Principle components analysis of the dry season microclimate with sampling locations separated by relative vertical position. Ellipses depict the location of the centroid for each level with 95% confidence and the vectors indicate the strength of the correlations between each environmental variable and the axes. The maximum temperature and average light intensity vectors overlap in both ordinations.

TABLE S1. The sampling intensity of all measured variables within each season and year. Forest floor, understory and subcanopy are abbreviated as “For. Floor”, “Under.”, and “Subcan.,” respectively.

Sample Type	Year	Dry Season Sample Size					Wet Season Sample Size				
		For. Floor	Under.	Subcan.	Canopy	Emergent	For. Floor	Under.	Subcan.	Canopy	Emergent
Cellulose Decomposition	2015	5	5	5	5	4	10	10	10	10	10
	2016	9	8	9	7	7	8	9	9	9	5
Cellulose Moisture	2015	4	5	5	5	4	0	9	10	9	9
	2016	3	8	9	7	7	-	-	-	-	-
Wood Decomposition	2015	5	5	5	4	4	10	10	10	9	9
	2016	9	8	9	8	5	9	9	9	9	4
Wood Moisture	2015	5	5	5	4	5	10	10	10	9	9
	2016	9	8	9	8	5	-	-	-	-	-
Temp/Light (HOBO)	2015	5	5	5	5	5	10	10	10	10	10
	2016	-	-	-	-	-	-	-	-	-	-
Prokaryotes and Fungi	2015	-	-	-	-	-	10	10	10	9	10
	2016	-	-	-	-	-	-	-	-	-	-
Respiration	2015	-	-	-	-	-	-	-	-	-	-
	2016	-	-	-	-	-	8	9	9	9	4

TABLE S2. The location of each tree, its species, tree diameter at breast height, the orientation of litter bags on that tree, and the height of the three upper vertical positions.

Tree ID	GPS N	GPS W	litter bag orientation (°)	diameter (cm)	Height, Subcanopy (m)	Height, Canopy (m)	Height, Emergent (m)	species
1	9.16145	79.83743	250	104.5	10.5	15.4	19.9	*Pseudobombax septenatum*
2	9.16118	79.8371	228	140.5	9.3	16.2	21.9	*Pseudobombax septenatum*
3	9.15805	79.83433	208	164	9.3	13.2	19.1	*Pseudobombax septenatum*
4	9.15838	79.83408	290	94.2	6.4	12.3	15.3	*Pseudobombax septenatum*
5	9.16375	79.84052	238	210.5	6	17.1	26.7	*Cavanillesia platanifolia*
6	9.16151	79.83833	122	156.4	6.8	17.5	20.2	*Pseudobombax septenatum*
7	9.15719	79.84219	6	96.9	10.9	18	24.7	*Pseudobombax septenatum*
8	9.15018	79.83631	302	103.3	7.8	17.4	22.8	*Pseudobombax septenatum*
9	9.15023	79.83624	286	77.5	7.7	17	24.3	*Pseudobombax septenatum*
10	9.15064	79.83562	338	66.5	9.6	17.8	22.9	*Pseudobombax septenatum*

TABLE S3. Significant correlations between fungal NMS axes and the 11 most common fungal orders. The axis components are provided as NMS1, NMS2, and NMS3. The R^2 value is proportion to the length of the vector. Only vectors with significant p-values were plotted on Figure 1.

Functional Group	Fungal NMS axes 1 and 2				Fungal NMS axes 1 and 3			
	NMS1	NMS2	R2	p-value	NMS1	NMS3	R2	p-value
Soft Rot	-0.05	1	0.4	<0.001	-0.18	-0.98	0.02	0.70
White Rot	0.79	-0.62	0.06	0.24	0.8	0.59	0.05	0.29
Brown Rot	0.56	-0.83	0.02	0.63	0.29	-0.96	0.04	0.34
General Saprotroph	-0.97	-0.24	0.05	0.32	-0.34	0.94	0.15	0.02
Wood Saprotroph	-0.14	0.99	0.18	0.01	-0.44	0.9	0.02	0.71
Litter Saprotroph	-0.82	-0.57	0.16	0.02	-0.62	0.79	0.19	0.01
Soil Saprotroph	-0.96	-0.27	0.22	<0.001	-0.79	0.62	0.25	<0.001
Undefined Saprotroph	-0.8	-0.6	0.04	0.36	-0.36	0.93	0.1	0.09
Lichenized	-0.91	-0.4	0.05	0.32	-0.52	-0.85	0.08	0.15
Arbuscular Mycorrhizal	-0.71	-0.7	0.14	0.03	-0.4	0.92	0.23	<0.001
Ectomycorrhizal	0.59	-0.81	0.05	0.35	0.78	0.63	0.03	0.51
Plant Pathogen	0.74	0.67	0.08	0.13	0.35	0.94	0.18	0.01
Animal Pathogen	0.27	0.96	0.2	0.01	0.78	0.63	0.03	0.48
Endophyte	0.96	0.28	0.15	0.02	0.46	0.89	0.3	<0.001
Richness	-0.19	0.98	0.29	<0.001	-0.87	-0.49	0.02	0.61
Fungal Parasites	0.99	0.13	0.23	<0.001	0.64	0.77	0.32	<0.001

TABLE S4. Significant correlations between bacterial NMS axes and the 14 most common bacterial orders. The axis components are provided as NMS1 and NMS2, and the R^2 value is proportion to the length of the vector. Only vectors with significant p-values were plotted on Figure 3.

Abundant Orders	NMS1	NMS2	R^2	p-value
Chthoniobacterales	0.67	-0.75	0.2	**0.003**
Saprospirales	0.47	-0.88	0.51	**0.001**
Acidobacteriales	-0.61	0.8	0.7	**0.001**
Actinomycetales	-0.34	-0.94	0.38	**0.001**
Burkholderiales	-0.89	0.46	0.17	**0.016**
Caulobacterales	-0.71	0.7	0.46	**0.001**
Chlorophyta	-0.35	0.94	0.40	**0.001**
Gemmatales	0.95	0.33	0.5	**0.001**
Myxococcales	0.98	0.19	0.55	**0.001**
Nostocales	-0.74	-0.67	0.11	0.056
Rhizobiales	-0.8	-0.61	0.16	**0.022**
Rhodospirillales	0.1	1.0	0.23	**0.002**
Solirubrobacterales	-0.43	-0.91	0.08	0.135
Sphingomonadales	-0.6	-0.8	0.59	**0.001**
Xanthomonadales	0.99	-0.17	0.45	**0.001**

TABLE S5. Average number of sequences (±SE) in each functional group, along with statistical results of comparisons. Superscript letters denote similar abundances. Idid not run analyses for functional groups with fewer than 100 total sequences, with the exception of soil saprotrophs. Some sequences were categorized into multiple functional groups (e.g., soft rot and wood saprotrophs).

Functional type	Functional Group	Litter	Understory	Subcanopy	Canopy	Emergent	dAIC	X^2	p-value
Decomposition type	White Rot	24.1 (3.7)	10.9 (1.4)	38.4 (7.8)	36 (7.5)	64 (7.6)	-5.0	3.0	0.558
	Soft Rot	3.5 (0.4)^{ab}	59.5 (5.1)^{c}	24.8 (4.2)^{b}	9.7 (2.3)^{ab}	1.5 (0.2)^{a}	27.1	35.2	< 0.001
	Brown Rot	0.4 (0.1)	0.2 (0)	3 (0.9)	0.3 (0.1)	0.6 (0.1)	-	-	-
Saprotrophs	Wood Saprotroph	32.8 (4.3)^{ab}	86.9 (6.7)^{a}	35.4 (4)^{ab}	14.6 (2.3)^{b}	27.4 (6.4)^{b}	9.3	17.3	0.002
	Litter Saprotroph	20 (3.7)^{a}	0.6 (0.1)^{b}	0.5 (0.1)^{b}	1.4 (0.2)^{b}	0.1 (0)^{b}	14.4	22.4	< 0.001
	Soil Saprotroph	2.4 (0.3)^{a}	0.5 (0.1)^{b}	0.5 (0.1)^{b}	0.8 (0.1)^{ab}	0.1 (0)^{b}	6.6	14.6	0.006
	Dung Saprotroph	0.3 (0.1)	0.1 (0)	0.1 (0)	0.2 (0)	0.2 (0)	-	-	-
	Undefined Saprotroph	338.1 (18.9)	259.1 (7.8)	302 (11.4)	244.9 (12)	279.3 (12.3)	-4.6	3.4	0.488
Pathogens, parasites, and symbionts	Plant Pathogen	47.7 (4.5)^{a}	62.1 (3.8)^{ab}	47.6 (6)^{a}	143.8 (12.8)^{b}	47.1 (3.9)^{ab}	7.6	15.7	0.004
	Fungal Parasite	3.2 (0.5)^{a}	7.9 (1.1)^{ab}	15.8 (0.9)^{bc}	55.9 (5)^{c}	24.5 (2.7)^{c}	25.6	33.7	< 0.001
	Animal Pathogen	3.9 (0.6)^{a}	69.7 (8)^{b}	39.2 (2.3)^{b}	67.9 (10.4)^{b}	14.5 (1.9)^{ab}	12.6	20.6	< 0.001
	Endophyte	5.5 (0.6)^{a}	35 (4.7)^{a}	20.1 (4.4)^{ab}	90.3 (10.4)^{b}	23.1 (2.2)^{ab}	14.7	22.7	< 0.001
	Epiphyte	0 (0)	0 (0)	0.3 (0.1)	0 (0)	0.3 (0)	-	-	-
	Arbuscular Mycorrhizal	4.2 (0.8)	0.1 (0)	0.2 (0.1)	0.9 (0.3)	0.3 (0)	-	-	-
	Ectomycorrhizal	1 (0.1)	0.2 (0)	0.7 (0.1)	0.3 (0.1)	21.4 (6.6)	-	-	-
Lichens	Lichenized	2.4 (0.5)	1.4 (0.3)	0.5 (0.1)	1.7 (0.4)	0.7 (0.1)	-6.7	1.3	0.853

TABLE S6. The PCA axis loadings for the wet season microclimate PCA along with values for the vectors fit on these ordinations for visualization. The PCA loadings for each axis are presented together. The strength of the relationship between each vector and the ordination are depicted separately for the plot of PCA axes 1 and 2, and for the plot of PCA axes 1 and 3.

PCA variables	PCA Loadings			PCA Axes 1 and 2		PCA Axes 1 and 3	
	PC1	PC2	PC3	R^2	P-value	R^2	P-Value
Average light intensity	1.52	-0.45	0.33	0.87	<0.001	0.84	<0.001
Maximum light intensity	1.27	-0.55	0.8	0.67	<0.001	0.79	<0.001
Average Temperature (˚C)	1.28	0.99	-0.14	0.92	<0.001	0.58	<0.001
Maximum Temperature (˚C)	1.54	-0.09	-0.12	0.83	<0.001	0.83	<0.001
Minimum Temperature (˚C)	0.54	1.53	0.02	0.92	<0.001	0.1	0.071
Water content (% of total mass)	-0.99	0.58	1.18	0.46	<0.001	0.83	<0.001

CURRICULUM VITAE

Evan M. Gora

139 Life Sciences Building
Department of Biology
University of Louisville
Louisville, KY, 40292

Email: emgora22@gmail.com
Alt. email: evan.gora@louisville.edu
Website: evanmgora.net

EDUCATION

PH.D. ECOLOGY, University Of Louisville, 4.0 GPA 2014-2018

Advisor: Dr. Stephen Yanoviak

Post-Baccalaureate, University of Louisville, 4.0 GPA 2014

B.S. Biology, University of Pittsburgh, *Cum Laude*: 3.63 GPA 2009-2013

Honors in Biology, **Major** in Economics

Advisor: Dr. Walter Carson

Thesis: "Patterns of coarse woody debris volume among 18 late-successional and mature forest stands in Pennsylvania"

RESEARCH INTERESTS

I am a quantitative ecologist interested in how community assembly and abiotic processes shape ecosystem function. Specifically, my research focuses on tree communities, microbial decomposers, and nutrient cycling. I use lightning as a model phenomenon for understanding tree community assembly and the ramifications of disturbance in tropical forests. I also explore how local

environment, biogeochemistry, and microbial community assembly influence decomposition.

PUBLICATIONS

***Denotes mentored undergraduate author**

Gora, E.M., E.J. Sayer, B.L. Turner, and E.V.J. Tanner. 2018. Decomposition of coarse woody debris in a long-term litter manipulation experiment: a focus on nutrient availability. Funct. Ecol. 32(4): 1128-1138. doi: 10.1111/1365-2435.13047.

Gora, E.M., P.M. Bitzer, J.C. Burchfield, S.A. Schnitzer, and S.P. Yanoviak. 2017. Effects of lightning on trees: a predictive model based on *in situ* electrical resistivity. Ecol. Evol. doi: 10.1002/ece3.3347.

Lucas, J.M., **E.M. Gora**, and A. Alonso. 2017. A view of the global conservation job market and how to succeed in it. Conserv. Biol. 31(6): 1223-1231. doi: 10.1111/cobi.12949.

Yanoviak, S.P., **E.M. Gora**, J.M. Burchfield, P.M. Bitzer, and M. Detto. 2017. Quantification and identification of lightning damage in tropical forests. Ecol. Evol. 7(14): 5111-5122. doi: 10.1002/ece3.3095.

Gora, E.M., N. Gripshover*, and S.P. Yanoviak. 2016. Orientation at the water surface by the carpenter ant Camponotus pennsylvanicus (De Geer, 1773) (Hymenoptera: Formicidae). Myrmecol. News 23: 33-39.

Gora, E.M. and S.P. Yanoviak. 2015. Electrical properties of temperate forest trees: a review and quantitative comparison with vines. Can. J. Forest Res. 45(3): 236-245, 10.1139/cjfr-2014-0380.

Yanoviak, S.P., **E.M. Gora**, J. Fredley*, P.M. Bitzer, R.M. Muzika, and W.P. Carson. 2015. Direct effects of lightning in temperate forests: a review and preliminary survey

in a hemlock-hardwood forest of the northern United States. Can. J. For. Res. 45(10): 1258-1268. 10.1139/cjfr-2015-0081.

Gora, E.M., L.L. Battaglia, H. Schumacher, and W.P. Carson. 2014. Patterns of coarse woody debris volume among 18 late-successional and mature forest stands in Pennsylvania. J. Torrey Bot. Soc. 141(2): 151-160, 10.3159/TORREY-D-13-00066.1.

GRANTS AND AWARDS

Graduate Research Internship, NSF – 2017-18 $5,000

Award Recipient, Carl C. Cornett Entomological Fund - 2016 $2,500

Research Grant, Graduate Network in Arts and Sciences – 2016 $100

Graduate Research Fellowship, NSF - 2015-18 $138,000

Young Explorer's Grant, National Geographic Society – 2015-16 $4,750

Short-term Fellowship, Smithsonian Tropical Research Institute – 2015-16 $8,000

Beechmont Garden Club Award, University of Louisville – 2015 $1,000

Research Grant, Graduate Student Council – 2015 $280

Graduate Student Publication Award, University of Louisville – 2015 $150

Graduate Fellowship, University of Louisville – 2014, 2018 (declined) $72,000

Award Recipient, Carl C. Cornett Entomological Endowment Fund – 2014 $2,500

Honorable Mention, NSF Graduate Research Fellowships Program – 2014

Honors degree in Biology granted by Departmental Honors Committee – 2013

PROFESSIONAL PRESENTATIONS

Gora, E. M., P. M. Bitzer, J. C. Burchfield, and S. P. Yanoviak. 2017. Lightning is the primary cause of large tropical tree mortality. Ecological Society of America Annual Meeting, Portland, Oregon.

Gora, E. M., P. M. Bitzer, J. C. Burchfield, and S. P. Yanoviak. 2017. Lightning on BCI: Observations and quantification of effects on trees. Forest Ecology Working Group, Smithsonian Tropical Research Institute. Gamboa, Panama.

Gora, E. M., P. M. Bitzer, J. C. Burchfield, and S. P. Yanoviak. 2016. Why does lightning only kill some trees? A model-based approach. Ecological Society of America Annual Meeting, Fort Lauderdale, Florida.

Gora, E. M. 2016. Dead wood stocks, fluxes, and patterns of decomposition. Forest Ecology Working Group, Smithsonian Tropical Research Institute. Gamboa, Panama.

Gora, E. M., P. M. Bitzer, J. C. Burchfield, and S. P. Yanoviak. 2016. Lightning on Barro Colorado Island: Tree characteristics influence lightning-tree interactions. Smithsonian Tropical Research Institute, Bambi Seminar Series. Barro Colorado Island, Panama.

Gora, E. M., N. D. Gripshover and S. P. Yanoviak. 2015. Orientation at the water surface by the carpenter ant *Camponotus pennsylvanicus*. Kentucky Academy of Science 2015 Annual Meeting. Newport, Kentucky.

Gora, E. M., and S. P. Yanoviak. 2015. Lightning's impact on forest ecology. Society of Integrative Comparative Biology Meeting. Palm Beach, Florida.

Gora, E. M., and S. P. Yanoviak. 2014. Lightning disturbance in forests. Smithsonian Tropical Research Institute, Bambi Seminar Series. Barro Colorado Island, Panama.

Gora, E. M. and S. P. Yanoviak. 2014. Lightning ecology and electrical resistivity of trees. Kentucky Academy of Science (third place in graduate competition). Lexington, Kentucky.

Gora, E. M. and S. P. Yanoviak. 2014. The Ecology of Lightning in a Northern Forest. Midwest Ecology and Evolution Conference (> 70 in attendance). Dayton, Ohio.

Gora, E. M., S. P. Yanoviak, and M. Feil. 2013. Resistivity of trees and vines. Kentucky Academy of Science 2013 Annual Meeting. Lexington, Kentucky.

Gora, E. M., 2013. Patterns of coarse woody debris volume among 18 late-successional and mature forest stands in Pennsylvania. University of Pittsburgh, Honors Research Symposium.

INVITED SEMINARS AND PRESENTATIONS

Gora, E. M. and S. P. Yanoviak. 2018. Wood decomposition in a tropical forest: vertical patterns, microbial colonization, and the role of lightning. Ecology and Evolutionary Biology Seminar Series, University of Pittsburgh, Pittsburgh, PA.

Gora, E. M., P. M. Bitzer, J. C. Burchfield, and S. P. Yanoviak. 2017. Real-time location and quantification of lightning in a neotropical forest. Invited presentation for the Xishuangbanna Scientific Delegation. Barro Colorado Island, Panama.

Gora, E. M. and S. P. Yanoviak. 2016. Lightning and its impact in a tropical forest. Seminar Series, Smithsonian Center for Sustainability and Conservation. Washington, D.C.

Gora, E. M. 2015. Effects of lightning on a tropical forest. Invited presentation for Matt Larson, the Director of the Smithsonian Tropical Research Institute, and guest Meghan Lamson. Barro Colorado Island, Panama.

PRESENTATIONS BY MENTORED STUDENTS

Kneale, R., **E. M. Gora**, S. P. Yanoviak. 2018. The role of ground contact in colonization and decomposition of dead wood. Kentucky Organization of Field Stations Annual meeting. Horse Cave, Kentucky.

Gripshover, N. D., **E. M. Gora**, and S. P. Yanoviak. 2017. Swimming mechanisms of temperate forest ants (*Camponotus pennsylvanicus* and *Formica subsericea*). Posters-at-the-Capitol Annual Meeting. Frankfurt, Kentucky. (Poster)

Gripshover, N. D., **E. M. Gora**, and S. P. Yanoviak. 2017. Swimming mechanisms of temperate forest ants (*Camponotus pennsylvanicus* and *Formica subsericea*). ACC Undergraduate Research Meeting of the Minds Conference. (Poster)

Kneale, R., **E. M. Gora**, S. P. Yanoviak. 2016. Factors influencing colonization of woody debris by saproxylic insects. Kentucky Academy of Sciences. Louisville, Kentucky. (Poster)

Gripshover, N. D., **E. M. Gora**, and S. P. Yanoviak. 2016. Biomechanics of water surface locomotion in temperate ants. Kentucky Academy of Science 2016 Annual Meeting. Louisville, Kentucky.

Gripshover, N. D., **E. M. Gora**, and S. P. Yanoviak. 2016. Biomechanics of water surface locomotion in temperate ants. Summer Research Opportunity Program symposium. Louisville, Kentucky.

TEACHING EXPERIENCE

Guest Lecturer, Organization for Tropical Studies Field Course 2016

Teaching Assistant, Biology 244 2015

Course Consultant, R statistical programming 2015

Guest Lecturer, Graduate-level Experimental Design and Analysis 2015

Guest Lecturer, Graduate-level Conservation Biology 2014

University of Pittsburgh Athletic Department Tutor 2012-2013

SERVICE AND SOCIETY MEMBERSHIP

Invited Moderator, Round Table Discussion of Conservation Biology Jobs 2018

Invited Presenter, ACCelerate Creativity and Innovation Festival	2017
Outreach Lecture, UCSB Smithsonian Scholars	2017
Granting Review Committee, Biology Graduate Student Association	2015-2018
Administrative Researcher Representative, Barro Colorado Island	2015-2016
Barro Colorado Island Journal Club, Co-founder/Co-president	2016
Outreach Lecture, Guides Program, STRI	2016
Science Fair Judge, Kentucky State Middle School Competition	2016
Departmental liaison with CDS Fleet Repairs, Inc.	2014-2015
Field trip organizer, Jefferson Country Public Schools	2014
Graduate Student Union representative from the Department of Biology	2014
Ecological Society of America- Student member	2013-present
Kentucky Academy of Science- Student member	2013-present
Biology Graduate Student Association –Student member	2013-present
Habitat for Humanity	2007-2014